Institut für Nutzpflanzenwissenschaften und Ressourcenschutz (INRES)

Subcellular localization of Glutathione peroxidase-like enzymes (GPXLs) in *Arabidopsis thaliana* and characterization of GPXL3 deficient mutants

Inaugural-Dissertaion zur
Erlangung des Grades
Doktorin der Agrarwissenschaften
(Dr. agr.) der
Landwirtschaftlichen Fakultät der
Rheinische Friedrich-Wilhelms-Universität Bonn

von

Safira Attacha

aus Malakand, Pakistan

Bonn
2017

Referent: Prof. Dr. Andreas Meyer
Koreferent: Prof. Dr.Frank Hochholdinger
Tag der Mündlichen Prüfung: 22. März 2017

Contents

List of abbreviations

$^1O_2$	singlet oxygen
$^3O_2$	triplet oxygen
ACT	actin
AOX	alternative oxidase
APS	ammonium per sulfate
APX	ascorbate peroxidase
AsA	ascorbate
Basta	glufosinate ammonium
CaMV35S	cauliflower mosaic virus 35S promoter
CLSM	confocal laser scanning microscopy
Col-0	Arabidopsis wild-type ecotype Columbia-0
CT	cytoplasmic tail
CytP450	cytochrome P450
DHA	dehydroascorbate
DHAR	dehydroascorbate reductase
ECM	extra cellular matrix
ER	endoplasmic reticulum
ERO-	ER thiol oxidase
ETC	electron transport chain
FP	fluorescent protein
GPX	glutathione peroxidase
GPXL	glutathione peroxidase-like enzyme
GSH	reduced glutathione
GSSG	glutathione disulfide
H_2O_2	hydrogen peroxide
HO_2	hydroperoxyl radical
HOCl	hypochlorous acid
LOX	lipooxygenase
MDA	monodehydroascorbate
MDAR	monodehydroascorbate reductase
MLS	mitochondrial localization sequence
NMT	N-myristoyl transferase
$NO^{\cdot}$	nitric oxide

NTR	NADPH dependent thioredoxin reductase
$O_2^{\cdot-}$	superoxide anion
O_3	ozone
OH	hydroxyl radical
PAT	palmitoyl acyl transferase
POXs	pH dependent peroxidase
PSI	photosystem I
PSII	photosystem II
PTOX	plastid terminal oxidase
RBOHs	respiratory burst oxidase homologue
RNS	reactive nitrogen species
RO_2	peroxyl radical
ROS	reactive oxygen species
Rubisco	ribulose-1, 5 bisphosphate carboxylase-oxygenase
SRP	signal recognition particle
TCHQD	tetrachlorohydroquinone dehalogenase
TMD	transmembrane domain
TRX	thioredoxin
UV	ultraviole

1 Zusammenfassung/Summary

1.1 Zusammenfassung

Ein gemeinsames Merkmal von Pflanzen, die verschiedenen Formen von Umweltbelastungen ausgesetzt sind, ist die verstärkte Bildung reaktiver Sauerstoffspezies (ROS) sowohl bei der Photosynthese als auch bei der Atmung. Bildung von ROS ist jedoch nicht auf die Elektronentransportketten beschränkt (ETC), sondern tritt auch in erheblichen Mengen an der Plasmamembran über NADPH Oxidasen, in den Peroxisomen im Verlauf mehrerer Stoffwechselwege und im ER während oxidative Proteinfaltung auf. Wenn nicht entgiftet, können ROS biologische Moleküle wie Nukleinsäuren, Aminosäuren und Proteine direkt schädigen. Die schädlichste Wirkung ist der Beginn der autokatalytischen Lipidperoxidation, die zu einer schweren Membranschädigung führt. Um sich vor schweren Schädigungen zu schützen, entwickelten sich mehrere Entgiftungssysteme zur effizienten Entfernung von H_2O_2 und Phospholipid-Hydroperoxiden. Neben der Wirkung als schädlich Toxine, werden Peroxide auch als wesentliche Elemente von Signalwegen in Stressreaktionen und dem koordinierte Auftreten von Abwehrmechanismen beteiligt betrachtet. Entgiftung von Peroxiden erfolgt mittels Katalase in Peroxisomen, über Ascorbat Peroxidasen (APX) und den Ascorbat-Glutathion (Asa-GSH) Zyklus im Cytosol, in Plastiden, in Mitochondrien und Peroxisomen, via Peroxiredoxinen (PRXs) und über Glutathion-S-Transferasen (GSTs). Eine weitere Klasse von Proteinen, die an der Peroxidentgiftung beteiligt sind, sind Glutathionperoxidasen (GPXs). Pflanzliche GPXen unterscheiden sich von tierischen GPXen dadurch, dass einige der tierischen GPXen Selenoproteine sind und ein Selenocystein (SeCys) an der katalytischen Stelle enthalten, während die pflanzlichen GPXen ausschließlich Cystein in ihrem katalytischen Zentrum besitzen. Darüber hinaus verwenden die tierischen Secys-GPx bevorzugt GSH als reduzierendes Substrat, während pflanzliche GPX das reduzierte Thioredoxin (TRX) als Reduktionsmittel bevorzugen und vergleichsweise geringe Aktivitäten mit GSH zeigen. Basierend auf ihrer Aktivität wurde auch vorgeschlagen, dass Pflanzen-GPX eine separate Gruppe funktioneller PRX-Homologe darstellen. Um Verwechslungen von Proteinnamen, die nur auf Sequenzhomologie beruht und somit stark eine funktionelle Verbindung zu Glutathion vorschlagen, zu vermeiden, werden acht Isoformen der GPX Familie in Arabidopsis in dieser Arbeit als GPX-like (GPXL) bezeichnet.

Das Isoenzym GPXL3 wurde in der Vergangenheit als Schlüsselenzym in der stressbedingten H_2O_2-Signalisierung in Arabidopsis insbesondere bei Dürre-Reaktionen beschrieben. In dieser Arbeit werden nun jedoch ergebnisse vorgestellt, die zeigen, dass *gpxl3* T-DNA Insertions mutanten und GPXL3 Überexpressionslinien keinen offensichtlichen Phänotyp unter Mannit oder Dürrestressbedingungen aufweisen. Die Bestimmung der Lokalisation von GPXLs ist für das Verständnis ihrer physiologischen Funktion bei der Entgiftung von H_2O_2oder Lipidhydroperoxiden wesentlich. Es gibt verschiedene Vorhersagen für die Lokalisierung der Proteine dieser Genfamilie, aber die genaue subzelluläre Lage der meisten GPXL-Proteine in Arabidopsis war zu Beginn dieser Arbeit noch unbekannt. Unter Verwendung der konfokalen Laserscanningmikroskopie (CLSM) wurden die intrazellulären Verteilungsmuster von mit roGFP markierten GPXL-Proteinen in zwei unterschiedlichen Expressionssystemen über transiente und stabile Transformationsverfahren untersucht. Um die Lokalisation von jedem GPXL zu untersuchen, wurden C- und N-terminale Fusionen der meisten Isoformen erzeugt und durch CLSM analysiert. Unsere Ergebnisse bestätigen, dass GPXL1 und GPXL7 auf Plastiden gerichtet sind und dass GPXL2 und GPXL8 cytosolische/nukleäre Proteine sind. Die Ergebnisse zeigen auch unerwartete neue Lokalisierungen für GPXL3 im Sekretorischen Weg,

überwiegend dem Golgi und für GPXL4 und GPXL5 spezifisch an der Plasmamembran. Diese Ergebnisse bestätigen und ergänzen das derzeitige Wissen über die Lokalisierung von GPXLs in Arabidopsis. Die neue Information kann helfen, die Rolle von GPXLs in Kulturen besser zu verstehen und letztlich ihre Eigenschaften bei der Züchtung von stressresistenten Nutzpflanzen zu nutzen.

1.2 Summary

A common feature of plants being exposed to diverse forms of environmental stress is the increased formation of reactive oxygen species (ROS) in both photosynthesis and respiration. Formation of ROS, however, is not restricted to the electron transport chains (ETC) but also occurs in significant amounts at the plasma membrane via NADPH oxidases, in peroxisomes in the course of multiple metabolic pathways and in the ER during oxidative protein folding. If not detoxified, ROS may directly damage biological molecules such as nucleic acids, amino acids and proteins. The most damaging effect is the onset of autocatalytic lipid peroxidation leading to severe membrane damage. To protect themselves from severe damage, plants evolved multiple detoxification systems for efficient removal of H_2O_2 and phospholipid hydroperoxides. Besides acting as damaging toxins, peroxides are also considered as essential elements of signalling pathways involved in stress sensing and coordinated onset of defence pathways. Detoxification of peroxides occurs via catalase in peroxisomes, via ascorbate peroxidases (APX) and the ascorbate-glutathione (Asa-GSH) cycle in the cytosol, plastids, mitochondria, peroxisomes, via peroxiredoxins (PRXs), and via glutathione-S transferases (GSTs). Another class of proteins involved in peroxide detoxification are glutathione peroxidases (GPXs). Plant GPXs are distinct from animals GPxs as some of the animal GPxs are selenoproteins containing a selenocysteine (Secys) at the catalytic site, whereas the plant GPXs rather possess a cysteine in their catalytic centre. Moreover, the animal Secys-GPxs preferentially use GSH as the reducing substrate while plant GPXs prefer reduced thioredoxin (TRX) as a reductant and show comparatively low activities with GSH. Based on their activity, plant GPX homologues have also been suggested to constitute functional PRXs. To avoid confusion resulting from protein names that are named only on homology and thus strongly suggest a functional link to glutathione, the Arabidopsis GPX family consisting of eight genes for clarity is called GPX-like (GPXL) in this work.

The isoenzyme GPXL3 has been implicated in stress-related H_2O_2 signalling in Arabidopsis and particularly in drought responses. However, results presented in this thesis demonstrate that *gpxl3* T-DNA insertion mutants and GPXL3 overexpression lines did not display any obvious phenotype under mannitol or drought stress conditions. Determination of localization of GPXLs is essential for understanding their physiological function in the detoxification of H_2O_2 or lipid hydroperoxides. There are various predictions for the localization of this gene family, but the precise subcellular location of most GPXL proteins in Arabidopsis was still unknown at the beginning of this work. Using confocal laser scanning microscopy (CLSM), the intracellular distribution patterns of roGFP2-tagged GPXL proteins were examined in two different expression systems via transient and stable transformation methods. In order to study the localization of each GPXL, C- and N-terminal fusions of most of the isoforms were generated and analysed by CLSM. Our findings validate that GPXL1 and GPXL7 are targeted to plastids, and that GPXL2 and GPXL8 are cytosolic/nuclear proteins. The results also show novel unexpected localizations for GPXL3 in the secretory pathway, predominantly the Golgi, and for GPXL4 and GPXL5 being specifically anchored to the plasma membrane. These findings substantiate and complement current knowledge on the localization of GPXLs in Arabidopsis. The novel information may help to better understand the role of GPXLs in crops and ultimately exploit their features in breeding of more stress-resistant plants.

2 Introduction

Plants being sessile organisms cannot simply escape from adverse conditions such as biotic stresses like insects, pathogens infection and abiotic stresses like drought, nutrient deficiency, temperature extremes, salinity, heavy metals toxicity, UV-B radiations and ozone, etc. These stresses may affect plants by generating ROS, thus limiting crop yields and value which have negative impacts on human well-being. The scenario gets more aggravated by the predicted forthcoming global changes in climate and continuous increase of world population. All these changes emphasize the importance of developing stress-resistant crops that are able to sustain growth and productivity in stressful environments (Ambrosone *et al.*, 2008). Various abiotic and biotic stresses in plants may lead to a situation called oxidative stress which is characterized by the formation of ROS. ROS are deleterious chemical entities capable of inducing cellular damage by degrading proteins and inactivating enzymes and interfering with several metabolic pathways. Even though ROS are regarded to impart negative impact on plants, they are now also considered to be important in regulating key cellular functions (Choudhury *et al.*, 2013).

The most abundant ROS produced during stress is hydrogen peroxide (H_2O_2). This compound is not only an oxidant but also a signal generated from superoxide ions through the action of superoxide dismutases (SOD) (Laloi *et al.*, 2004). It is important that H_2O_2 levels are properly controlled under stress or normal conditions, and this is regulated by the orchestrated participation of a range of different enzymatic and non-enzymatic antioxidant systems. The anti-oxidant and repair system of plants is considerably enhanced and diversified compared to bacterial or animal systems. Because plants in addition to the mitochondrial ETC also have to cope with a second source of ROS from chloroplasts (Rouhier *et al.*, 2008).

Plants tolerate abiotic stresses by modulating multiple genes and by coordinating the action of various genes from different pathways or systems (Ahuja *et al.*, 2010). A thorough understanding of biochemical and molecular responses of plants to various stresses and the interaction of different molecular pathways is, therefore, essential for a holistic perception of plant resistance mechanisms under stressful conditions (Chen *et al.*, 2004; Hossain *et al.*, 2009).

2.1 Formation of ROS

ROS is the cluster term used to describe a variety of molecules and free radicals (chemical species with one unpaired electron) derived from molecular oxygen. Such ROS include oxygen radicals such as superoxide ($O_2^{\cdot-}$), hydroxyl ($OH^{\cdot}$), peroxyl ($RO_2^{\cdot}$), and hydroperoxyl ($HO_2^{\cdot}$) radicals, and certain non-radical oxidizing agents, such as H_2O_2, hypochlorous acid (HOCl), and ozone (O_3), that can be converted easily into radicals (Bayr, 2005) (Figure 2.1). H_2O_2 is one of the ROS compounds that received most of the attention of the scientific community in the last decade. Hydrogen peroxide is formed as the result of a two-step reduction of molecular oxygen (the first step leading to superoxide radical) and has a relatively long lifespan in comparison to other ROS. The long half-life (1 ms) of H_2O_2 and its small size allow it to traverse cellular membranes and migrate in different compartments, which facilitates its signalling functions (Bienert *et al.*, 2006; Petrov & Van Breusegem, 2012). $O_2^{\cdot-}$ may also react with other radicals including nitric oxide ($NO\cdot$) in a reaction controlled by the rate of diffusion of both radicals. The oxidants derived from $NO\cdot$ are called reactive nitrogen species (RNS) (Turrens, 2003).

ROS are produced in plants via different cellular processes in various subcellular compartments. These include non-enzymatic mechanisms such as electron transfer to molecular oxygen during photosynthesis and respiration in chloroplasts and mitochondria respectively. They are also produced as by-products of enzymes such as glycolate oxidase in peroxisomes, amine oxidase and oxalate oxidase in the apoplast and xanthine oxidase and enzymes of fatty acid oxidation in peroxisomes (Desikan *et al.*, 2005; Gill & Tuteja, 2010; Luis *et al.*, 2006; Navrot *et al.*, 2007). ROS are also deliberately generated by enzymatic complexes such as class III peroxidases, oxalate oxidases, amine oxidases, lipoxygenases, quinone reductases and plant NADPH oxidases (Marino *et al.*, 2012; Nanda *et al.*, 2010; O'Brien *et al.*, 2012). As a result of any kind of disturbances, intracellular levels of ROS may rapidly rise leading into a situation termed oxidative stress. As ROS can cause serious damage to lipids, DNA and proteins which ultimately results in cell death, the equilibrium between production and scavenging of ROS should be strictly controlled. Under steady state conditions the ROS molecules are detoxified by different antioxidative defence components that are often confined to particular compartments (Apel & Hirt, 2004).

On one hand, plants need to control the levels of ROS because of their harmful nature, but on the other hand, they also use ROS as signalling molecules especially in response to various stresses such as pathogen attacks, or abiotic stress components. ROS can thus act as messengers to trigger protein deactivation, or induce gene transcription (Desikan *et al.*, 2001; Navrot *et al.*, 2007). The action of ROS as damaging, protective or signalling molecules depends on the delicate equilibrium between ROS production and scavenging at the proper site and time (Gill & Tuteja, 2010; Gratão *et al.*, 2005).

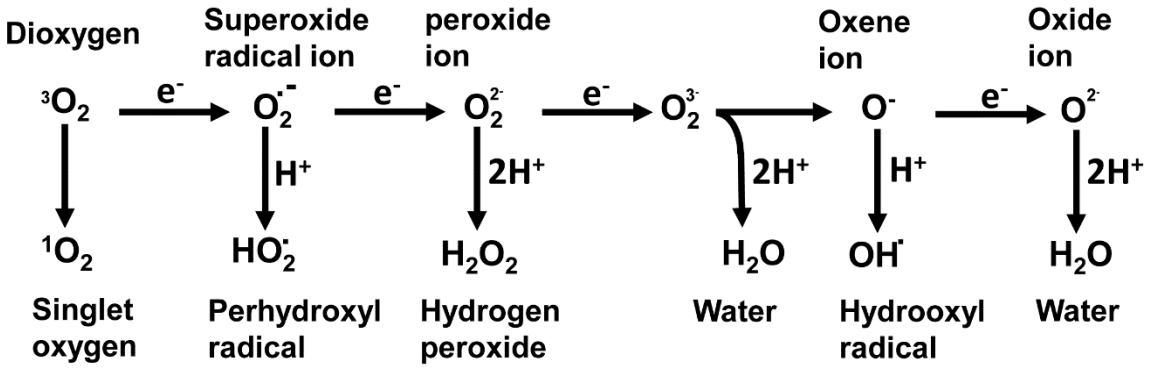

Figure 2.1: Generation of ROS by energy transfer or sequential univalent reduction of ground state triplet oxygen. Figure adopted from (Apel & Hirt, 2004).

2.2 Chemistry of ROS

2.2.1 Singlet oxygen ($^1O_2$)

Singlet oxygen is a singular ROS that is the first excited electronic state of molecular oxygen and it is not related to electron transfer to O_2. It is an infrequent ROS that can exist as an excited state for a short period of time only, before returning to the ground state by energy dissipation to the solvent. The life time of $^1O_2$ in a cell has been measured to be approximately 3 µs. $^1O_2$ can diffuse over considerable distances of several hundred nanometres. It can last for nearly 4 µs in H_2O and 100 µs in polar solvent. $^1O_2$ is produced constitutively in plant leaves in light via chlorophylls that act as photosensitizers. It can also be produced by phytotoxins during plant-pathogen interactions. $^1O_2$, is an oxidizing agent for a wide range of biological molecules and can react with proteins, pigments, nucleic acids and lipids and may trigger cell death (Triantaphylidès & Havaux, 2009).

2.2.2 Superoxide radicals (O_2^-)

The single electron reduction of O_2 results in the generation of the O_2^-. At low pH, dismutation of O_2^- is unavoidable, with one O_2^- giving up its added electron to another O_2^- and then with protonation resulting in the generation of H_2O_2. Furthermore, O_2^- can be protonated to form the HO_2. Additionally, in the presence of transition metals such as copper and iron, further reactions take place, e.g. through the Haber-Weiss mechanism or the Fenton reaction to generate $OH^{\cdot}$, which is the most reactive chemical species in the biological world (Gill & Tuteja, 2010).

2.2.3 Hydrogen peroxide (H_2O_2)

The major source of H_2O_2 comes from the dismutation of $O_2^{\cdot -}$. H_2O_2 is moderately reactive and has relatively long half-life (1 ms) whereas, other ROS such as $O_2^{\cdot -}$, $OH^{\cdot}$ and $^1O_2$, have much shorter half-life (2-4 μs) (Bhattacharjee, 2005). H_2O_2 may inactivate enzymes by oxidizing their thiol group. H_2O_2 plays a dual role in plants: at low concentrations, it acts as a signal molecule and, at high concentrations, it leads to programmed cell death (PCD) (Asada, 2006; Gechev & Hille, 2005). H_2O_2 has also been shown to play a key role in the regulation of many physiological processes, such as, photorespiration, photosynthesis, senescence, cell cycle, stomatal movement, and growth and development (Gill & Tuteja, 2010). Because of its longer half-life H_2O_2 can migrate from the site of its synthesis to neighbouring compartments or cells. The chemical and physicochemical properties of H_2O_2 are close to those of H_2O. Hence it can use water channels, the aquaporins, to cross the cell membrane more rapidly than by simple diffusion. Specific aquaporins facilitate the diffusion of H_2O_2 across membranes, which is why they are also referred to as peroxiporins (Sies, 2014).

2.2.4 Hydroxyl radicals ($OH^{\cdot}$)

OH. is among the most highly reactive ROS known. In the presence of suitable transitional metals, especially Fe, OH. can also be produced from O_2^- and H_2O_2 at neutral pH and ambient temperatures by the iron-catalysed, O_2^- driven Fenton reaction. Due to its reactivity $OH^{\cdot}$ is thought to be largely responsible for mediating oxygen toxicity *in vivo*. $OH^{\cdot}$ can potentially react with all biological molecules like DNA, proteins, lipids, and almost any constituent of cells and ultimately leads to cell death. Cells do

not possess enzymatic mechanism to detoxify $OH^{\cdot}$ and rely on mechanisms that prevent their formation (Mittler *et al.*, 2004).

2.2.5 Generation of ROS due to biotic stress

Oxidative burst characterized by the rapid production of ROS is a well-known defence response to pathogen attack (Figure 2.2). The ROS that have been detected in plant pathogen interactions are O_2^{-}, ($HO_2^{\cdot}$), H_2O_2, and $OH^{\cdot}$. Various potential sources of these ROS include apoplastic amine, diamine, and polyamine oxidase-type enzymes, a cell wall localized peroxidase that directly forms H_2O_2 and a plasma membrane localized NADPH oxidases. The product of NADPH oxidase activity is very likely O_2^{-}, which is converted to the more stable ROS forms of H_2O_2 and O_2 spontaneously or by a SOD reaction (Mithöfer *et al.*, 2004).

2.2.6 Generation of ROS due to abiotic stresses

ROS are produced at several subcellular locations such as chloroplasts, mitochondria, plasma membranes, peroxisomes, apoplast, ER, and cell walls as a result of normal cellular activities or under stressed conditions (Figure 2.2). Production and removal of ROS must be strictly controlled. However, the equilibrium between production and scavenging of ROS may be perturbed by a number of adverse abiotic stress factors such as high light, drought, low or high temperature, and mechanical stress (Apel & Hirt, 2004)

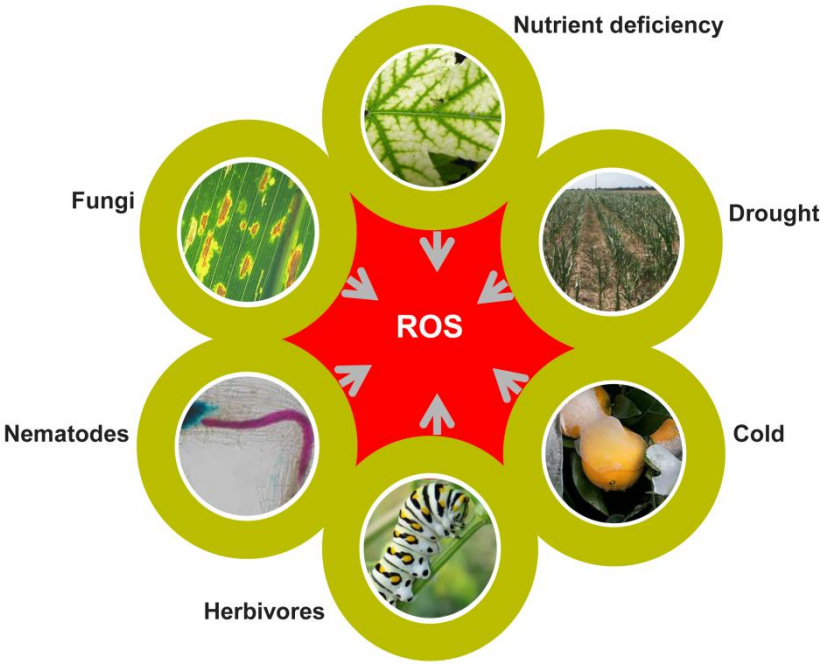

Figure 2.2: Various abiotic and biotic sources of ROS. ROS are produced in the cell as a result of various biotic and abiotic stresses. Biotic stresses comprise infection by a pathogen or attack by an insect or pests and abiotic stresses include nutrients deficiency, water stress and extreme temperatures. Figure courtesy of Andreas Meyer.

2.2.7 ROS production in different organelles

Photosynthesizing organisms are at greater risk of oxidative damage, because of their oxygenic conditions and the abundance of the photosensitizers and polyunsaturated fatty acids (PUFA) in the chloroplast envelope (Gill & Tuteja, 2010). The main sources of ROS in light are the chloroplasts and peroxisomes while mitochondria appear to be the main ROS producers in the dark (Foyer & Noctor, 2003).

2.2.7.1 Chloroplasts

Photosynthesis is a characteristic of higher plants and algae, which takes place in chloroplasts, containing a highly organized thylakoid membrane system that harbours all constituents of the light-capturing photosynthetic apparatus (Pfannschmidt, 2003). Photosynthetic electron transport continuously produces oxygen which is removed from chloroplasts by reduction and assimilation (Gill & Tuteja, 2010). Therefore, the presence of three types of oxygen-consuming processes closely associated with photosynthesis: (a) the oxygenase reaction of ribulose-1,5 bisphosphate carboxylase-oxygenase (Rubisco), and (b) direct reduction of molecular oxygen by photosystem I (PSI) electron transport, make chloroplasts a major site of ROS production (Apel & Hirt, 2004; Asada, 2006).

2.2.7.2 Mitochondria

It has been assessed that about 1% of mitochondrial O_2 consumption leads to H_2O_2 production in plants (Møller, 2001). However, ROS production in mitochondria can be enhanced in response to various biotic and abiotic stress conditions. Complex I and III of mitochondrial ETC are the most eminent sites of $O_2^{\cdot -}$ production. Most of the superoxide ions produced are efficiently converted to H_2O_2 by SOD dismutation (Gill & Tuteja, 2010; Quan *et al.*, 2008; Sweetlove & Foyer, 2004). The ROS molecules targets high-molecular mass molecules, such as membrane lipids or mitochondrial DNA, with the formation of lipid or nucleotide peroxides, especially at the level of thymine (Cullis *et al.*, 1987; Navrot *et al.*, 2007). The plant mitochondrial ETC also contains alternative oxidase as well as two rotenone-insensitive, non-proton-pumping NAD(P)H

dehydrogenases on each side of the inner membrane: external rotenone-insensitive NADPH dehydrogenase (NDex) on the outer surface and internal rotenone-insensitive NADPH dehydrogenase (NDin) on the inner surface. The alternative oxidase and possibly NDin(NADH) function to limit mitochondrial ROS production by keeping the ETC relatively oxidized. The removal of ROS in mitochondria is carried out by several enzymes together with small antioxidants such as glutathione. During stress conditions the defence responses may be overwhelmed, which can lead to the production of oxidative stress in mitochondria (Møller, 2001).

2.2.7.3 Peroxisomes

Peroxisomes are the hot spots of H_2O_2 production. Like mitochondria and chloroplasts, peroxisomes produce $O_2^{\cdot-}$ radicals as a consequence of their normal metabolism. There are at least two sites of $O_2^{\cdot-}$ generation in peroxisomes: the first one is in the organelle matrix, where xanthine oxidase (XOD) catalyses the oxidation of xanthine and hypoxanthine to uric acid. The second site is in the peroxisome membranes which is dependent on NAD(P)H where a small ETC is composed of a flavoprotein NADH and cytochrome b, and here $O_2^{\cdot-}$ is produced by the peroxisome ETC (Luis *et al.*, 2002). Other metabolic processes responsible for the generation of H_2O_2 in different types of peroxisomes are the photorespiratory glycolate oxidase reaction, the fatty acid β-oxidation, the enzymatic reaction of flavin oxidases, and the disproportionation of $O_2^{\cdot-}$ radicals. Formation of $NO^{\cdot}$ radicals have also reported in peroxisomes (Gill & Tuteja, 2010; Luis *et al.*, 2002; Luis *et al.*, 2006). Peroxisomes have been considered to generate and release important signal molecules such as $O_2^{\cdot-}$, H_2O_2 into the cytosol, which can contribute to a more integrated communication system among cell compartments (Corpas *et al.*, 2001). The amount of ROS in peroxisomes is regulated by a delicate balance between production and scavenging.

2.2.7.4 Other sources of ROS generation in plants

Plasma membrane: The NADPH oxidase, also known as the respiratory burst oxidase homologues (RBOHs), localized at the plasma membrane mediate the production of ROS during plant-microbe interactions. RBOHs catalyses the formation of the $O_2^{\cdot-}$ by transferring an electron from intracellular NADPH to an apoplastic molecule of oxygen (O_2) (Sagi & Fluhr, 2006). $O_2^{\cdot-}$ dismutates to produce H_2O_2 and O_2 (Noirot *et al.*, 2014).

Cell wall and apoplast: Cell walls are also regarded as active sites for ROS production. Various ROS like $OH^{\cdot}$, $O_2^{\cdot -}$, H_2O_2, and $^1O_2$ are produced by cell wall-localized lipoxygenase (LOX) during stress, which results in hydroperoxidation of PUFA. Cell wall located enzymes have been shown to be responsible for the production of ROS at apoplast. pH-dependent peroxidases (POXs), cell wall-linked oxidases, germin-like oxalate oxidases and polyamine oxidases, all are the main sources of H_2O_2 in the apoplast (Sharma *et al.*, 2012).

ER: The NADPH-mediated electron transport involving $CytP_{450}$ anchored on the outer surface of the ER generates $O_2^{\bullet -}$ into cytosol. (Höfer *et al.*, 2008; Werck-Reichhart & Feyereisen, 2000). The formation of a free radical intermediate (Cyt P_{450} R^-) occurs by interaction of an organic substrate, RH, with the $CytP_{450}$ followed by the reduction of a flavoprotein. An oxygenated complex (Cyt P_{450}-ROO^-) is formed by the prompt reaction of this intermediate with triplet oxygen ($^3O_2$). The complex may rarely decompose to Cyt P_{450}-RH by generating $O_2^{\bullet -}$ as a by-product (Das & Roychoudhury, 2014).

2.2.8 Antioxidant system in plants

To counteract stress-induced ROS accumulation, plants have evolved an efficient antioxidant system consisting of mainly two components; the non-enzymatic and enzymatic antioxidant system. These include a variety of scavengers such as SOD, APX, GPX, GST, PRXs and CAT and non-enzymatic low molecular metabolites, such as ascorbate, GSH, α-tocopherol, carotenoids and flavonoids (Gill & Tuteja, 2010; Mittler *et al.*, 2004).

2.2.8.1 Non enzymatic ROS scavenging mechanism

Non-enzymatic antioxidants include compounds of intrinsic antioxidant properties such as ascorbate, tocopherol, glutathione (GSH), flavonoids, alkaloids and carotenoids. GSH is oxidized by ROS forming the oxidized form glutathione disulfide (GSSG), ascorbate is oxidized to monodehydroascorbate (MDA) and dehydroascorbate (DHA). Through the AsA-GSH cycle (Figure 2.3 (III)), GSSG, MDA, and DHA can be reduced regenerating GSH and ascorbate (Sharma *et al.*, 2012).

2.2.8.2 Enzymatic ROS scavenging mechanism

Enzymatic ROS scavenging component in plants include SOD, APX, GPX, CAT, PRX, GST and enzymes of AsA-GSH cycle (Figure 2.3).

SOD: Under environmental stresses, SOD forms the first line of defence against ROS-induced damages (Figure 2.3 (I)). SODs are classified into three isozymes based on the metal ion it binds, Mn-SOD (localized in mitochondria), Fe-SOD (localized in chloroplasts), and Cu/Zn-SOD (localized in cytosol, peroxisomes, and chloroplasts) (Mittler *et al.*, 2004).

CAT: Catalase, which degrades H_2O_2 into water and oxygen, is one of the major antioxidant enzymes. It is a predominant peroxisomal enzyme, but it also exists in the mitochondria and cytoplasm (Yang & Poovaiah, 2002). In plants, catalase scavenges H_2O_2 generated during mitochondrial electron transport, β-oxidation of the fatty acids, and most importantly photorespiratory oxidation.

PRXs: Peroxiredoxins are abundant thiol peroxidases located in distinct cell compartments including the nucleus, cytosol, plastids and mitochondria, Thiol peroxidases catalyse the reduction of H_2O_2 and organic hydroperoxides. They are grouped into four clans based on their structural and biochemical properties: 1-Cys PRX, 2-Cys PRX, PRX II, PRXQ. The catalytic centre contains a cysteinyl residue that reduces diverse peroxides and is regenerated via intramolecular or intermolecular thiol-disulfide-reactions and finally by electron donors such as TRXs and glutaredoxins (GRXs). PRXs react with peroxides with higher molar efficiency than other protein containing SH-groups. In addition to their role in antioxidant defence in photosynthesis, respiration, and stress response, they may also be involved in modulating redox signalling during development and adaptation (Dietz, 2003).

GSTs: Plant Glutathione-S-transferases (GSTs) form a complex superfamily composed of a number of discrete classes. They can be divided into seven classes, phi, tau, theta, zeta, lambda, DHAR, tetrachlorohydroquinone dehalogenase (TCHQD), and microsomal (Dixon & Edwards, 2010). In addition to the classical conjugation activity involved in the detoxification of xenobiotics by generating an S-glutathionylated reaction product that is then rapidly sequestered to the vacuole and degraded, certain GSTs can function as glutathione peroxidases. In this reaction, GSTs use electrons from GSH to reduce organic hydroperoxides of fatty acids and nucleic acids, thus preventing permanent oxidative damage of these components (Edwards & Dixon, 2005).

Enzymes of AsA-GSH cycle: Enzymes that operate in AsA-GSH cycle are as follows:
APX: Ascorbate peroxidase an integral component of AsA-GSH cycle, plays an

important role in the metabolism of H_2O_2 in higher plants. APX isoenzymes are distributed in different compartments of plant cells such as chloroplasts, mitochondria, microbody (including glyoxysome and peroxisome) and cytosol (Caverzan *et al.*, 2012). One of the most characteristic properties of APX is its instability in the absence of ascorbate. Under conditions where the concentration of ascorbate is lower than 20 μM, APX activity is rapidly lost. In plants, APX uses the reduced form of ascorbate as a reductant in the first step of the AsA-GSH cycle, to reduce H_2O_2 to water with the concomitant generation of monodehydroascorbate (MDHA) (Shigeoka *et al.*, 2002) (Figure 2.3 (III)(i)).

MDAR: MDHA is either directly reduced back to ascorbate by monodehydroascorbate reductase (MDAR) or undergoes non-enzymatic disproportionation to ascorbate and dehydroascorbate (DHA) (Chew *et al.*, 2003) (Figure 2.3 (III)(ii)).

DHAR: Dehydroascorbate reductase (DHAR) reduces dehydroascorbate (DHA) to ascorbate using reduced glutathione (GSH) as an electron donor (Chew *et al.*, 2003) (Figure 2.3 (III)(i)).

GR: Glutathione reductase (GR) is a flavoprotein oxidoreductase which uses NADPH as a reductant to reduce GSSG to GSH. Reduced glutathione (GSH) is used up to regenerate ascorbate from MDHA and DHA, and as a result is converted to its oxidized form (GSSG). GR converts oxidized glutathione (GSSG) to reduced glutathione (GSH) thus helps in maintaining high ratio of GSH/GSSG under various abiotic stresses. GR, a crucial enzyme of AsA-GSH cycle catalyses the formation of a disulfide bond in glutathione disulfide to maintain a high cellular GSH/GSSG ratio. It is predominantly found in chloroplasts with small amounts occurring in the mitochondria and cytosol (Gill *et al.*, 2013).

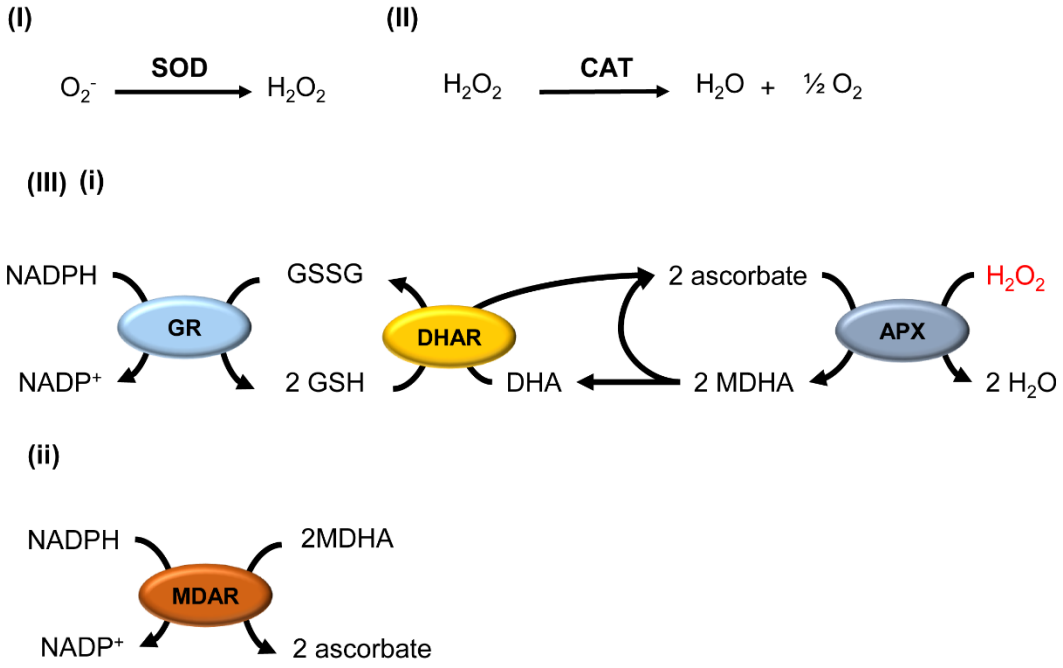

Figure 2.3: The principal modes of enzymatic ROS scavenging by SOD, CAT, the AsA-GSH cycle. SOD converts superoxide into H_2O_2. CAT converts H_2O_2 into water. Hydrogen peroxide is also converted into water by the AsA-GSH cycle.

The thioredoxin/thioredoxin reductase (TRX-NTR) system: TRXs are key components of cellular redox balance, regulating many target proteins through thiol/disulfide exchange reactions. These are small proteins with a redox active disulfide bridge present in the characteristic active site sequence -Trp-**Cys**-Gly-Pro-**Cys**- (Schürmann & Jacquot, 2000). TRX catalyse the reduction of disulfide bridges in target proteins via a dithiol mechanism requiring two cysteine residues, the catalytic and the resolving cysteine. Depending on their intracellular location, TRXs are reduced by a different electron donor system. TRXs in non-photosynthetic tissue and in the cytosol of photosynthetic cells are reduced with electrons from NADPH via the NADP/TRX system, whereas the chloroplast TRXs of plants and eukaryotic algae and the TRXs of oxygenic photosynthetic prokaryotes are reduced via the ferredoxin/TRX system with electrons provided by photosynthetic electron transport (Balmer *et al.*, 2004). The major types are TRXf, TRXh, TRXm, TRXo, TRXx, TRXy, TRXz, CDSP32 and Lilium. TRX are present in the cytosol, plastids/mitochondria and have also been proposed in the nucleus (Meyer *et al.*, 2008).

Glutathione peroxidases

Glutathione peroxidase is the general name for the family of enzymes that catalyse the reduction of H_2O_2 or organic hydroperoxides to water or the corresponding alcohols using GSH/TRX as a reducing substrate. They are generally considered as one of the key players in the enzymatic defence system of plants. In this system, SODs convert O_2^- into H_2O_2, whereas GPXs and CATs convert H_2O_2 into water (Racchi, 2013). The active site of these enzymes forms a tetrad consisting of selenocysteine/cysteine, glutamine, and tryptophan (Tosatto *et al.*, 2008). Half of the animal GPxs are selenoproteins with a selenocysteine at the catalytic site, whereas the plant enzymes contain cysteine rather than selenocysteine (Herbette *et al.*, 2007) (Figure 2.4). Moreover, in *Saccharomyces cerevisiae*, the GPX-like enzyme Orp1 (syn. Gpx3) has been reported to act as hydroperoxide sensor that promotes the oxidation of Yap1 to its intra-molecular disulfide bond (Delaunay *et al.*, 2002). This relay mechanism has been exploited for the development of genetically encoded H_2O_2-sensors (Gutscher *et al.*, 2009).

In mammals, eight glutathione peroxidases (GPx1-GPx8) have been identified so far. Mammalian GPx1-4 are selenoproteins with a selenocysteine (Sec) in the catalytic center. GPx6 is a selenocysteine only in humans but not in rats (Brigelius-Flohé & Maiorino, 2013). GPx7 and GPx8 are distinctly different from the “real” glutathione peroxidases of mammals, the Sec GPxs, as the Sec residue is replaced by a Cys. They also differ from the 2-Cys-GPxs of bacteria/invertebrates/plants, as there is no C_R (resolving Cysteine) residue within the Cys block. Being reduced by PDI and located within the ER, these enzymes have been involved in oxidative protein folding (Maiorino *et al.*, 2015). Mammalian GPXs with selenocysteine prefer glutathione as an electron donor while plant GPXLs do not rely on GSH as reductant but prefer so-called redoxins characterized by a CxxC motif, from which Trxs are most commonly used (Brigelius-Flohé & Maiorino, 2013; Herbette *et al.*, 2007)(Figure 2.6). Based on the substrates specificities these homologues have been referred to as phospholipid hydroperoxide glutathione peroxidases (PHGPX), TRX peroxidases, or GPX-type enzymes (Bela *et al.*, 2015; Maiorino *et al.*, 2015; Schlecker *et al.*, 2005). The biochemical evidence for plant GPX homologues indicates a strong preference for the TRX system instead of GSH as electron donor (Iqbal *et al.*, 2006; Navrot *et al.*, 2006). To avoid confusion resulting from protein names that are based on homology and thus

misleadingly suggest a functional link to glutathione, the nomenclature GPX-like (GPXL) was adopted in this thesis for the Arabidopsis isoforms.

The plant GPXLs have been shown to be present in different plant tissues, compartments and developmental stages (Bela *et al.*, 2015). At present, GPXL genes from several plant species, such as *Nicotiana sylvestris* (Criqui *et al.*, 1992), *Citrus sinensis* (Holland *et al.*, 1994), *Avena fatua* (Johnson *et al.*, 1995), *Arabidopsis thaliana* (Sugimoto & Sakamoto, 1997), *Brassica campestris* (Eshdat *et al.*, 1997), *Spinacia oleracea* (Sugimoto *et al.*, 1997), *Helianthus annuus* (Roeckel-Drevet *et al.*, 1998), *Pisum sativum* (Mullineaux *et al.*, 1998), *Lycopersicon esculentum* (Depège *et al.*, 1998), *Oryza sativa* (Li *et al.*, 2000), *Triticum aestivum* (Zhai *et al.*, 2013), *Camellia sinesis* (Fu, 2014), *Thellungiella salsuginea* (Gao *et al.*, 2014) and *Panax ginseng* (Kim *et al.*, 2014) have been isolated and characterized. Gene expression analysis of several GPXLs revealed that the steady state level of GPXLs increase with several stress conditions such as pathogen infections (Criqui et al., 1992), high salt and metal concentration (Sugimoto and Sakamoto, 1997), mechanical stimulation (Depège *et al.*, 1998), Aluminium toxicity (Milla *et al.*, 2002), photooxidative stress (Chang *et al.*, 2009), oxidative stress (Gaber *et al.*, 2012), salinity and osmotic stress (Gao *et al.*, 2014). Several reports have indicated that GPXLs could be used to develop plants with enhanced traits under stress conditions. Overexpression of a *GPXL* gene from *Nelumbu nucifera* enhanced salt tolerance in rice plants (Diao *et al.*, 2014). Overexpression of a eukaryotic *GPXL* (*GPXL5*) in tomato plants modifies specifically gene expression and leads to modification of photosynthetic regulation processes (Herbette *et al.*, 2005).

GPX(L)s may also act as H_2O_2 sensors enabling the transfer of the primary oxidation from the peroxidatic Cys in the active site to specific target proteins with a regulatory or signalling role (Delaunay *et al.*, 2002). This relay mechanism has been exploited for the development of genetically encoded H_2O_2-sensors (Gutscher *et al.*, 2009) . A role in stress-related H_2O_2 signalling has also been implicated for Arabidopsis GPXL3. Miao and colleagues reported *gpxl3* null mutants as drought-sensitive and GPXL3 overexpressor lines as drought-tolerant (Miao *et al.*, 2006). Based on this observation the authors hypothesized that GPXL3 might be involved in drought stress signalling in guard cells through interference with the type 2C Ser/Thr phosphatases ABI1 and ABI2 during the ABA response. To support their hypothesis, Miao *et al.* provided data

indicating physical interaction of GPXL3 with ABI1 and ABI2 in both yeast-two-hybrid and pull-down assays as well as bimolecular fluorescence complementation for GPXL3 and ABI2 fused with YFP-fragments complementing each other in the cytosol. Based on these results and on transient expression of GFP-fusions in protoplasts, the authors proposed that GPXL3 functions as both a cytosolic redox transducer and a scavenger of H_2O_2 in ABA and drought stress responses. The proposed localization of GPXL3 in the cytosol, however, conflicts with annotations based on bioinformatics that predict mitochondrial targeting, and with proteomic data that indicate the presence of GPXL3 in the Golgi or in plastids (Miao *et al.*, 2006; Milla *et al.*, 2003; Nikolovski *et al.*, 2012).

The presence of GPXLs in Arabidopsis was first reported by Sugimoto and Sakamoto in 1997. In Arabidopsis, GPXLs are encoded by a family of eight isoenzymes, GPXL1 to GPXL8 which have been predicted to be localized in different subcellular compartments. While all Arabidopsis isoforms except GPXL7 have been detected by proteomic approaches, localization results are often inconsistent as exemplified above for GPXL3. In the absence of suitable antibodies for immunogold labelling and electron microscopy, the use of fluorescent proteins has been developed as a suitable complementary approach for protein localization studies (Nelson *et al.*, 2007). In Arabidopsis, localization data for expression of GFP fusions are available only for GPXL8 which has been reported to localize to the cytosol and the nucleus (Gaber *et al.*, 2012). Without robust localization data for the entire GPXL family, however, the generation of suitable hypotheses concerning isoform-specific functions and non-redundant roles specific to different subcellular compartments, is hindered. Associated with this is the risk that inappropriate assumptions about the subcellular localization may mislead future research by proposing flawed hypotheses for further functional analysis.

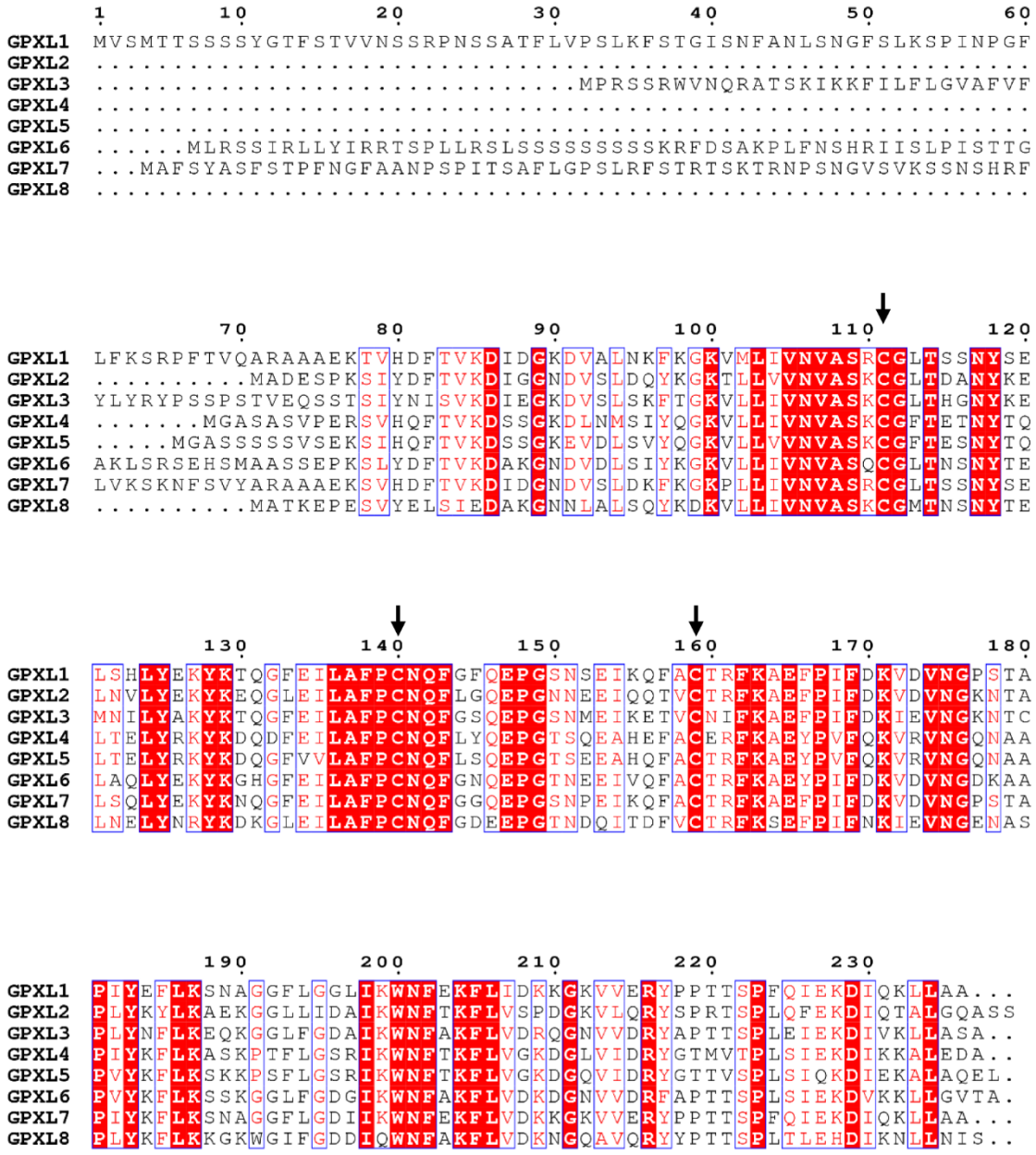

Figure 2.4 Amino acid sequence alignment of GPXLs from Arabidopsis.

Numbering is according to GPXL1. Arrows mark the three conserved cysteines present in *Arabidopsis* GPXLs. Sequences were aligned by Mafft with default settings using JalView. Gaps within the signal peptides until position 70 were removed manually. Highly similar residues (Score >0.8) are framed and coloured in red. 100% similar residues are marked in white letters on red background.

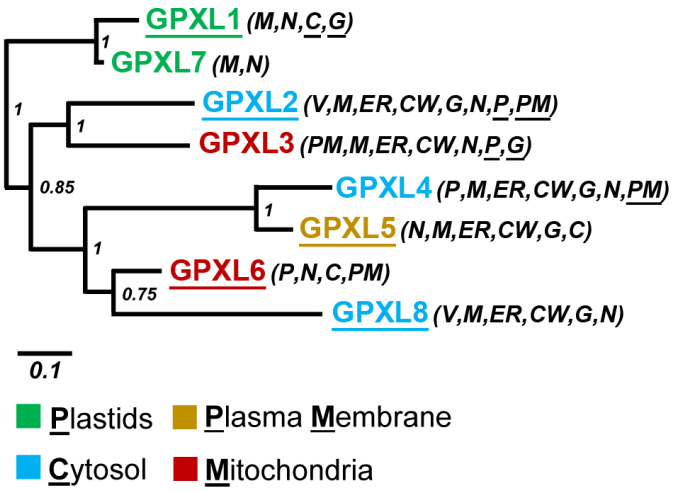

Figure 2.5: Phylogenetic tree of the Arabidopsis GPXL protein family. The unrooted phylogenetic tree based on the core sequence of amino acids 77 to 160 of GPXL1 and the respective homologous sequences from other GPXLs was constructed by MrBayes (Ronquist & Huelsenbeck, 2003). Node values display the probability. Scale bar indicates the expected changes per site. The colour code displays subcellular localizations predicted by SUBAcon (Hooper *et al.*, 2014). Additional localizations for which bioinformatics prediction as documented in SUBA3 (Tanz *et al.*, 2012) exist are indicated in parentheses and compartments for which experimental evidence is available are underlined. V: Vacuole, CW: Cell wall, G: Golgi, N: Nucleus, PM: Plasma membrane, ER. Sequences were aligned by MAFFT (Katoh & Standley, 2013) with default settings using JalView. GPXL1: At2g25080; GPXL2: At2g31570; GPXL3: At2g43350; GPXL4: At2g48150; GPXL5: At3g63080; GPXL6: At4g11600; GPXL7: At4g31870; GPXL8: At1g63460.

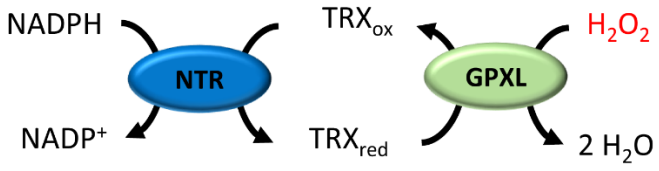

Figure 2.6: Detoxification of H_2O_2 by GPXLs. The GPXLs converts hydrogen peroxide into water using reducing equivalents from TRX. Oxidized TRX is again converted into reduced form by NTR and the reducing agent NAD(P)H.

2.2.9 Protein targeting

All living cells contain proteins that carry out specialized functions within various subcellular compartments. Approximately half of the proteins synthesized in a cell are transported into or across membranes. Proteins embedded in membranes or localized in the aqueous spaces surrounded by membranes give rise to the specialized functions carried out in these compartments. For example nucleus accomplishes the major functions of the cell, including DNA replication, transcription, pre-mRNA splicing and ribosome assembly, the mitochondria are specialized in respiration producing ATP for the cell, the chloroplasts houses the photosynthetic machinery of the cell, the Golgi apparatus contains enzymes that modify sugars attached to exported proteins and the peroxisomes comprise enzymes necessary for fatty acid oxidation and other metabolic activities. Most of the proteins are synthesized in the cytoplasm except for a small number which are encoded by chloroplasts and mitochondria. This raises the question of how proteins are transported from the cytoplasm to other destinations. Proteins are targeted into different compartments by a mechanism that uses targeting sequences and translocation machinery. The proteins are synthesized in the precursor form with a signal peptide that directs the protein into the export pathway (Dalbey & von Heijne, 2002).

2.2.9.1 Chloroplast and mitochondrial targeting

The vast majority of plastid proteins are imported from outside of the organelle as it encodes only about 100 different proteins instead of retaining a functional endogenous genetic system. Over 90% of the ~3000 different proteins present in mature chloroplasts are encoded on nuclear DNA and translated in the cytosol (Keegstra & Cline, 1999; Leister, 2003). Most chloroplast proteins are synthesized in the precursor form and have a cleavable N-terminal extension, the transit peptide. The transit peptide direct proteins into chloroplasts and target them to their final destinations within plastids. The transit peptides do not have a consensus sequence however, they share some common features, such as being rich in serine, possessing a low abundance of acidic amino acids and having lengths ranging from 20 to >100 residuals (Jarvis, 2008). Majority of mitochondrial proteins are synthesized as precursor proteins in the cytosol and are imported preferentially, although not exclusively, by a post-translational mechanism. Cytosolic chaperones are involved in guiding the precursor proteins to receptors on the mitochondrial surface (Wiedemann *et al.*, 2004). In plants,

mitochondrial targeting sequences are about 40 amino acids having a net positive charge (rich in Arg and poor in acidic amino acids) and contain many aliphatic residues such as Leu and Ala. Additionally the plant mitochondrial targeting sequences are particularly rich in serine residues.

2.2.9.2 Targeting of proteins to the plasma membrane

Secretory and plasma membrane proteins as well as proteins retained in the secretory organelles are synthesized in the cytoplasm and are referred to as secretory proteins. All of them cross the rough endoplasmic reticulum membrane (RERM) during transit through the cell. They are targeted to and cross the RERM by the same mechanism irrespective of their final destinations by complicated signal receptor interaction (Pubsley, 2012).

Membrane proteins are anchored to the lipid membranes via a hydrophobic TMD, which consists of ~20 hydrophobic amino acid residues (Kim & Hwang, 2013). Binding and targeting of proteins to membrane is influenced by fatty acylation of proteins. The two most common forms of protein fatty acylation are modification with myristate, a 14-carbon saturated fatty acid, and palmitate, a 16-carbon saturated fatty acid. N-myristoylation occurs when the initiating Met is removed co-translationally by methionine amino-peptidase, and myristate provided by myristoyl Co-A is linked via an amide bond to a terminal Gly becoming exposed after Met cleavage. *N*-myristoylation is catalysed by *N*-myristoyl transferase (NMT) (Resh, 1999). The requirement for Gly at the N-terminus is absolute; no other amino acid will substitute. The consensus sequence for NMT protein substrates is: Met-Gly-X-X-X-Ser/Thr-. But, this is not true for all proteins with an N-terminal Gly and the recognition by NMT depends on the downstream amino acid sequence. Especially Ser or Thr at position 6 and Lys or Arg is preferred at positions 7 and/or 8 (Resh, 2016).

In order to achieve stable membrane binding N-myristoylated proteins employ four types of second signals; polybasic region, hydrophobic residues, another membrane bound binding partner or a second lipid modification myristate inserts hydrophobically into the lipid bilayer, and approximately 10 of the 14 carbons penetrate the hydrocarbon core of the bilayer (Resh, 2016). The positively charged amino acids form electrostatic interactions with the negatively charged phospholipids which are present on the cytoplasmic leaflet of the plasma membrane and many intercellular membranes (Resh, 2013). In the absence of myristate the binding energy from these electrostatic

interactions is not sufficient to anchor a protein to a membrane. However, when both myristate and a basic motif are present within the protein, the hydrophobic and electrostatic forces synergize resulting in strong membrane binding affinity. Myristoylated proteins that lack a polybasic motif can use nearby hydrophobic residues as a second signal. Another alternative mechanism is to utilize protein-protein interaction with a membrane bound binding partner. The second signal for membrane binding proteins can also be an additional lipid modification. Palmitoylated proteins are acylated by attachment of palmitate derived from palmitoyl Co-A through a thioester linkage to the sulfhydryl group of cysteine. S-palmitoylation is catalysed by palmitoyl acyltransferases (PAT). The location of these palmitoylated cysteine residues varies - some are present near the N- or C-termini of proteins, while others are located near TMDs (Resh, 2016).

2.2.9.3 Targeting proteins to secretory pathway - Golgi

The secretory membrane system is made up of distinct organelles including the ER, Golgi complex, plasma membrane and tubulovesicular transport intermediates that mediate intracellular membrane transport between them (Lippincott-Schwartz *et al.*, 2000). Proteins transported across the eukaryotic ER membrane include soluble proteins, such as those ultimately secreted from the cell or localized to the ER lumen, and membrane proteins, such as those in the plasma membrane or in other organelles of the secretory pathway (Rapoport, 2007). Soluble proteins cross the membrane completely and usually have amino-terminal, cleavable signal sequences, the major feature of which is a segment of 7-12 hydrophobic amino acids (Kim & Hwang, 2013). Membrane proteins have different topologies in the lipid bilayer, with one or more transmembrane segments composed of about 20 hydrophobic amino acids; the hydrophilic regions of these proteins either cross the membrane or remain in the cytosol. Both types of proteins are handled by the same machinery within the membrane: a protein-conducting channel. The channel allows soluble polypeptides to cross the membrane and hydrophobic transmembrane segments of membrane proteins to exit laterally into the lipid phase (Rapoport, 2007).

2.2.9.3.1 Signal-based retention of secretory pathway resident proteins via arginine and lysine-based motifs

Two types of coat protein complex I (COPI)-interacting motifs: a dilysine (KKXX) motif and K/HDEL motif at the C-terminus are responsible for membrane retention in the

early secretory pathway of plants: Arg-based motifs (-RR-, -RXR-, and -RRR-) have also been identified as ER retrieval signals in membrane proteins of various topologies and in a variety of positions within the proteins (Michelsen *et al.*, 2005; Uemura *et al.*, 2009).

2.2.9.3.2 The models for Golgi protein retention

Most proteins that have been synthesized in the ER are transported to the Golgi during their biogenesis. In most eukaryotes, the membranes of the Golgi assume a characteristic stacked morphology with cisternae that differ in enzymatic content and activity (Rabouille *et al.*, 1995; Saint-Jore-Dupas *et al.*, 2006). This highly polarized organization defines cis-, medial- and trans-cisternae, with the cis-most cisternae facing the ER (Klumperman, 2000). The trans-most cisternae face the trans-Golgi network (TGN), a tubular vesicular cluster that executes final sorting steps to post-Golgi destinations, exchanges material with the endocytic pathway (Brandizzi & Barlowe, 2013; Strompen *et al.*, 2005; Van Meel & Klumperman, 2008).

Protein aggregation/kin-recognition as a Golgi retention mechanism

The kin-recognition model proposed that the due to aggregation of Golgi resident proteins, they were considered to be too large and were excluded from transport vesicles and hence this resulted in their retention in the Golgi (Nilsson *et al.*, 1994).

Transmembrane domain-mediated Golgi retention

According to this model the TMDs of Golgi membrane proteins, in particular type II proteins, prevent their entry into the sterol enriched and thicker bilayers of Golgi-derived transport vesicles which are destined to the cell surface (Bretscher & Munro, 1993; Klemm *et al.*, 2009). The length and amino acid composition of the TMDs are thought to exclude them from transport vesicles destined to the cell surface. The TMDs of Golgi membrane proteins are normally shorter than plasma membrane counterparts and are typically enriched in amino acids with aromatic side chains (Banfield, 2011).

Golgi membrane lipid composition-based retention

This lipid-based partitioning model postulates that integral membrane proteins rapidly partition into Golgi membrane domains on the basis of the properties of individual membrane compartments. Differences in the ratios of lipids, in particular the ratio of

glycerophospholipids to sphingolipids (which are lowest in the *cis* and highest in the *trans*-Golgi) could account for observed Golgi protein distributions in cells. Integral membrane proteins with different preferences for glycerophospholipid: sphingolipid ratios would be enriched in Golgi subcompartments that contain the preferable lipid composition (Banfield, 2011; Lippincott-Schwartz & Phair, 2010; Patterson *et al.*, 2008).

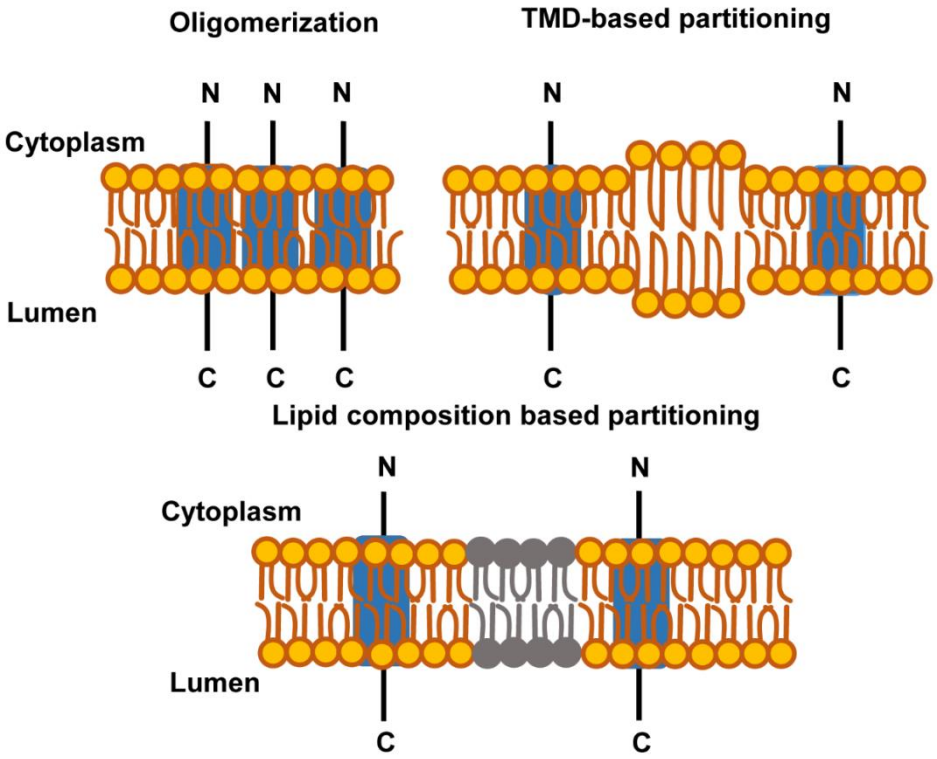

Figure 2.7: The membrane topology of Golgi resident proteins. Models and mechanisms of type II membrane protein retention in the Golgi. Figure adapted from Banfield, 2011.

2.3 Genetically encoded fluorescent reporters

The cellular redox status influences many processes in plants, and a variety of signal transduction pathways (Jiang *et al.*, 2006). In plants E_{GSH} of the subcellular compartments vary from highly reducing in mitochondrial matrix with an E_{GSH} of about -360 mV and cytosol with an E_{GSH} of -320 mV (Schwarzländer *et al.*, 2008) to an E_{GSH} of -240 mV in the ER Lumen (Brach *et al.*, 2009). To analyse dynamic changes in the redox based processes of the cell *in vivo* certain probes are required that facilitate the read out of these changes in living cells. However, conventional techniques for the analysis of changes in cellular redox status either lack well-defined specificity or disrupt

cellular integrity. To overcome these limitations genetically encoded biosensors such as reduction-oxidation-sensitive GFPs (roGFPs) have been created to facilitate *in vivo* redox measurements (Gutscher *et al.*, 2008). These proteins were engineered by substitution of surface-exposed residues on GFP with cysteines in appropriate positions to form disulfide bonds, roGFPs have two fluorescence excitation maxima (at approximately 400 and 475-490 nm) that show rapid and reversible ratiometric changes in their fluorescence in relation to ambient redox status (Hanson *et al.*, 2004; Jiang *et al.*, 2006). Different versions of roGFPs have been generated and tested for their redox-dependent fluorescence. Because of its two excitation peaks, a ratiometric readout of changes in fluorescence intensities can be determined (Meyer & Dick, 2010).The high sensitivity of roGFP2 toward GSSG via GRX enables the use of roGFP2 for monitoring stress-induced redox changes *in vivo* in real time (Meyer *et al.*, 2007).

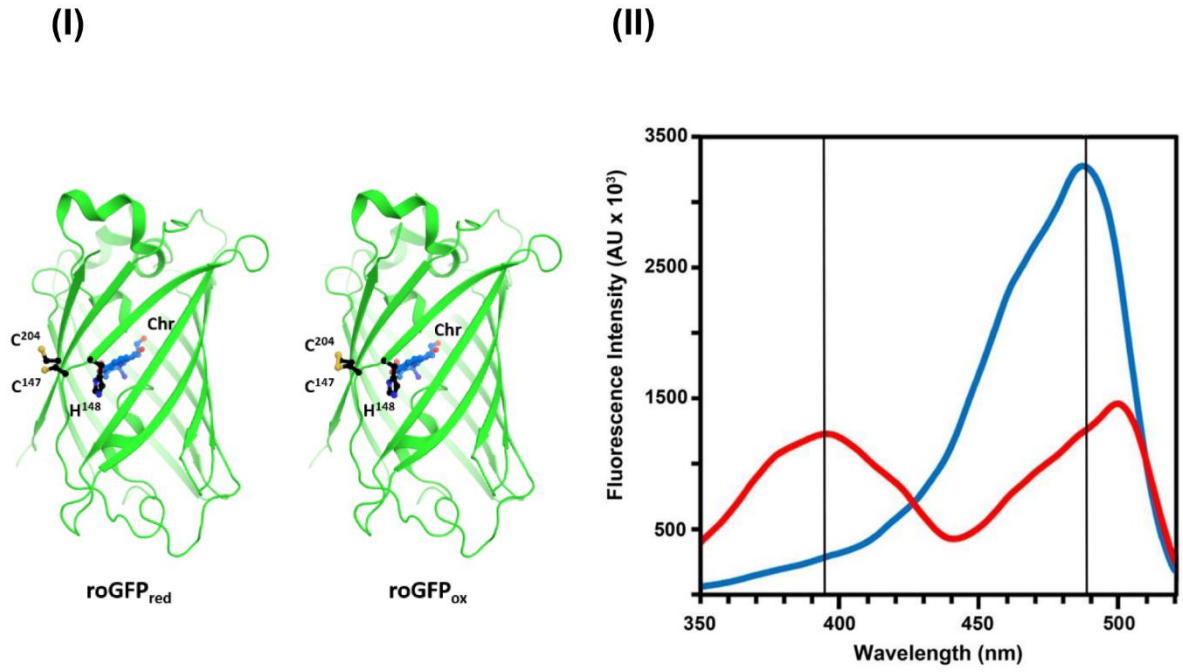

Figure 2.8: Structure and excitation wavelengths of roGFP2. **(I)**: Tertiary structure of reduced (left) and oxidized (right) roGFP2 showing the chromophore and the two cysteines at position 147 (C147) and 204 (C204.) **(II):** Fluorescence excitation spectra of roGFP2 in the fully reduced (blue curve) or fully oxidized (red curve) state. Excitation wavelengths are indicated by vertical lines. Figure adopted from Aller *et al.*,2013.

Aims

Although ROS have been shown to play an important role in signal transduction when cells are exposed to unfavourable conditions, accumulated ROS may result in uncontrolled oxidation of various cellular components, leading to free radical-mediated destruction of the cell structure (Gao *et al.*, 2014). GPXLs reduce H_2O_2 and organic hydroperoxides to water and correspondingly alcohols using TRXs thus inhibiting the ROS-induced damage to membranes and proteins (Navrot *et al.*, 2006). At present, several studies have been reported on the isolation and characterization of GPXL genes from several plant species. These studies revealed that Arabidopsis GPXL family consists of eight isoforms with distinct subcellular location and functions. These enzymes exhibit different tissue-specific expression patterns and environmental stress responses, functioning co-ordinately in ROS scavenging. The potential subcellular locations of GPXL genes are predicted by various computer algorithms however the precise subcellular location of each gene in Arabidopsis is still not clear. Predictions of proteins intracellular location from DNA sequence by computational tools are helpful but not necessarily conclusive. Other techniques such as cell fractionation and protein purification for defining intracellular location is often challenging, and antibody production for immunodetection can be time-consuming and laborious.

The first aim of this work was to study the role of GPXL3 in drought stress responses as *gpxl3* null mutants are reported to be drought-sensitive and GPXL3 overexpressor lines as drought-tolerant (Miao *et al.,* 2006). However, cytosolic localization of GPXL3 reported by Miao *et al*., 2006 conflicted with the annotations based on bioinformatics that predict mitochondrial targeting, and with proteomic data. Therefore, the aim was also to investigate the subcellular localization of GPXL3 with genetically encoded reporter proteins *in vivo* and to re-evaluate the reported drought stress-related phenotypes of the respective mutants and overexpressors.

The next goal was to provide comprehensive information on the subcellular localization of entire GPXLs family in *Arabidopsis* through expression of GFP fusions. For this, GPXLs were fused with roGFP2 as a reporter gene and expressed either heterologously in tobacco or homologously in Arabidopsis and analysed by CLSM.

.

3 Material and Methods

3.1 Technical equipment and materials

3.1.1 Technical Equipment

SONOPULS Ultrasonic Homogenizers HD 2200	Bandelin, www.bandelin.com
Beckman Centrifuge Avanti® J-26-XP	Beckman, www.beckmancoulter.com
Beckman Rotor JA-25.50	Beckman, www.beckmancoulter.com
Beckman Rotor JA-10	Beckman, www.beckmancoulter.com
Micropulser™ electroporator	Bio-Rad, www.bio-rad.com
PowerPac Basic™ power supply	Bio-Rad, www.bio-rad.com
PowerPac™ HC power supply	Bio-Rad, www.bio-rad.com
Mini-PROTEAN® Tetra cell	Bio-Rad, www.bio-rad.com
Mini-PROTEAN® II Multi-casting chamber	Bio-Rad, www.bio-rad.com
Criterion™ Blotter	Bio-Rad, www.bio-rad.com
C1000™ Thermal cycler	Bio-Rad, www.bio-rad.com
C1000™ Thermal cycler Reaction Module 48W	Bio-Rad, www.bio-rad.com
S1000™ Thermal Cycler	Bio-Rad, www.bio-rad.com
S1000™ Thermal Cycler Reaction Module 96W	Bio-Rad, www.bio-rad.com
POLARstar Omega	BMG, www.bmglabtech.com
Canon EOS 1100D EF-S digital camera	Cannon, www.cannon.de
Canon CanoScanLide 700F	Cannon, www.canon.de
A1000 growth chamber	Conviron, www.conviron.com
Precision Balance TP1502	Denver Instrument, www.denverinstrument.com
Analytical Balance Summit Typ SI-234	Denver Instrument, www.denverinstrument.com
Gel documention MF-ChemiBIS2.0	DNR Bio-Imaging Systems, www.dnr-is.com

Eppendorf BioPhotometer Plus	Eppendorf, www.eppendorf.de
Eppendorf Centrifuge 5810 R	Eppendorf, www.eppendorf.de
Eppendorf Centrifuge 5430	Eppendorf, www.eppendorf.de
Eppendorf Thermomixer™ Comfort	Eppendorf, www.eppendorf.de
Labculture® Vertical laminar flow cabinet	ESCO, www.escoglobal.com
Airstream® Class II Biological safety Cabinet	ESCO, www.escoglobal.com
Incubator 37 °C Ecotron Typ ET25-TA-00	INFORSHT, www.infors-ht.com
Incubator 28°C Ecotron Typ ET25-TA-RC	INFORSHT, www.infors-ht.com
ISMATEC Peristaltic pump REGLO digital	Ismatec, www.ismatec.com
Plant growth chambers	Jan Weiler GmbH
Leica M165FC stereomicroscope	Leica, www.leica-microsystems.com
Leica DCF425C camera	Leica, www.leica-microsystems.com
FE20 – FiveEasy™ pH-Meter	Mettler Toledo, www.mt.com
LS-55 Spectralfluorometer	PerkinElmer, www.perkinelmer.de
Vortex mixers	Scientific Industries, www.scientificindustries.com
Nanodrop 2000c	Thermo Scientific, www.thermoscientific.com
TKA LabTower EDI water purification system	Thermo Electron LED, www.tka.de/
Zeiss confocal microscope LSM780	Zeiss, www.zeiss.de
Objective C-Apochromat 40x/1.2 W Corr M27	Zeiss, www.zeiss.de

3.1.2 Consumables

General chemicals were purchased from Applichem (www.applichem.com/home/), Roth (www.carlroth.com), and Sigma-Aldrich (www.sigmaaldrich.com). General plastic ware was purchased from VWR (de.vwr.com/app/Home) and Sarstedt (www.sarstedt.com/php/main.php).

3.1.3 Kits

NucleoSpin® Plasmid	Machery-Nagel, www.mn- net.com
NucleoSpin® RNA II	Machery-Nagel, www.mn-net.com
M-MLV Transcriptase Kit	LifeTech., www.lifetechnologies.com

3.1.4 Software

Adobe Photoshop vCS5.1	Adobe, www.adobe.com
MEGA v5.1 (Tamura *et al.,* 2011)	MEGA, www.megasoftware.net
Microsoft Office 2010	Microsoft, www.microsoft.com
MatLab based ratiometric imaging software	The Mathworks, www.mathworks.de
Serial Cloner v2.6.1	SerialCloner, serialbasics.free.fr
ZEN 2011	ZEISS, www.zeiss.de/ZEN

3.1.5 Enzymes

Gateway® BP clonase II enzyme mix	Invitrogen™, www.thermoscientific.com
Gateway® LR clonase II enzyme mix	Invitrogen™, www.thermoscientific.com
Phusion High-Fidelity DNA Polymerase	ThermoScientific, www.thermoscientific.com
Taq™ DNA Polymeras (5 u/µl)	New England Biolabs, www.neb-online.de
TEV protease (1mg/ml)	

3.1.6 Primers

Table 1: Primer used for genotyping

No.	Primer sequence
2696	gcatggtttgacgattttgtga

2697	TTGACTATAAGAAGCACTTTCCCG

Table 2: Primers for SQ-RT PCR

No.	Primers sequence
2751	ATGCCTAGATCAAGCAGATG
2752	GACGATATCCTTCTCAATTTCAA
364	CAACCGGTATTGTGCTCGATTC
436	aacctcaggacaacggaatctc

Table 3: Primers for Sequencing

plasmid	forward	reverse
pDONR	689	690

Table 4: Primers used for cloning of GPXLs

No.	Primer	Sequence
2558	AtGPX1_F	GGGGACAAGTTTGTACAAAAAAGCAGGCTttATGGTTTCCATGACTACTTCATCT
2560	AtGPX1_C	ggggaccactttgtacaagaaagctgggtcAGCGGCAAGCAACTTCTGGAT
2561	AtGPX2_F	GGGGACAAGTTTGTACAAAAAAGCAGGCTttATGGCGGATGAATCTCCAAAGT
2562	AtGPX2_N	ggggaccactttgtacaagaaagctgggtcTTAAGAAGAGGCCTGTCCCAA
2563	AtGPX2_C	ggggaccactttgtacaagaaagctgggtcAGAAGAGGCCTGTCCCAAC
2412	AtGPX3_fwd	GGGGACAAGTTTGTACAAAAAAGCAGGCTttATGCCTAGATCAAGCAGATGGGTCA
2413	AtGPX3_rev_C	ggggaccactttgtacaagaaagctgggtcAGCAGATGCCAATAGCTTGACGATATC
2628	AtGPX3_rev_N	ggggaccactttgtacaagaaagctgggtcTCAAGCAGATGCCAATAGCTTGA
2564	AtGPX4_F	GGGGACAAGTTTGTACAAAAAAGCAGGCTttATGGGTGCTTCTGCTTCGGTT
2565	AtGPX4_N	ggggaccactttgtacaagaaagctgggtcTCAAGCGTCTTCAAGAGCTTTCT
2566	AtGPX4_C	ggggaccactttgtacaagaaagctgggtcAGCGTCTTCAAGAGCTTTCTTGA
2538	AtGPX5_fw	GGGGACAAGTTTGTACAAAAAAGCAGGCTttATGGGTGCTTCATCATCATCATC
2539	ATGPX5_C	ggggaccactttgtacaagaaagctgggtcCAATTCTTGTGCAAGGGCTTTC

3604	AtGPX5_N	ggggaccactttgtacaagaaagctgggtcTCACAATTCTTGTGCAAGGGCT
2568	AtGPX6_F	GGGGACAAGTTTGTACAAAAAAGCAGGCTttATGCTTCGCTCCTCAATTCGA
2569	AtGPX6_N	ggggaccactttgtacaagaaagctgggtcTTAAGCAGTAACTCCCAACAACTT
2570	AtGPX6_C	ggggaccactttgtacaagaaagctgggtcAGCAGTAACTCCCAACAACTTCT
2571	AtGPX7_F	GGGGACAAGTTTGTACAAAAAAGCAGGCTttATGGCTTTCTCTTACGCATCATT
2573	AtGPX7_C	ggggaccactttgtacaagaaagctgggtcAGCCGCAAGCAACTTCTG
2574	AtGPX8_F	GGGGACAAGTTTGTACAAAAAAGCAGGCTttATGGCGACGAAGGAACCAGA
2575	AtGPX8_N	ggggaccactttgtacaagaaagctgggtcTCAGGAGATATTCAGAAGATTCTTT
2576	AtGPX8_C	ggggaccactttgtacaagaaagctgggtcGGAGATATTCAGAAGATTCTTTATG
2992	GPX3_targ_34AA_rev	ctcctcgcccttgctcacGTATCTGTAGAGGTAGAAGACAAA
3031	GPX3_TP_34AA_fw2	TTTGTCTTCTACCTCTACAGATACgtgagcaagggcgaggag
3032	GPX3_∆34 and ∆12_fw2	GTCAAGCTATTGGCATCTGCTgtgagcaagggcgaggag
3033	GPX3_∆34 and ∆12 _rv1	ctcctcgcccttgctcacAGCAGATGCCAATAGCTTGAC
3034	GPX3_∆34 _fw1	GGGGACAAGTTTGTACAAAAAAGCAGGCTttATGCCTTCTTCGCCATCGAC
3569	3569_AtGPX4_F	GGGGACAAGTTTGTACAAAAAAGCAGGCTttATGGCAGCTTCTGCTTCGGTT
3581	3581_GPX4-ro2_Rv	ctcctcgcccttgctcacAGCGTCTTCAAGAGCTTTCTTG
3582	3582_GPX4-ro2_Fw	CAAGAAAGCTCTTGAAGACGCTgtgagcaagggcgaggag
3570	3570_AtGPX5_F	GGGGACAAGTTTGTACAAAAAAGCAGGCTttATGGCAGCTTCATCATCATCATC
3605	3605_ GPX5-ro2_Rv	ctcctcgcccttgctcacCAATTCTTGTGCAAGGGCTTTC
3584	3584_GPX5-ro2_Fw	GAAAGCCCTTGCACAAGAATTGgtgagcaagggcgaggag
3785	3775_AtGPX6_Oh_r	ctcctcgcccttgctcacAGCCATTGAATGCTCCGATCT
3786	3776_AtGPX6_Oh_f	AGATCGGAGCATTCAATGGCTgtgagcaagggcgaggag
2659	ro2_GW_rev	ggggaccactttgtacaagaaagctgggtcTTActtgtacagctcgtccatg
2725	HDEL_GW	GGGGACCACTTTGTACAAGAAAGCTGGGTCttaaagctcatcatgtctagactt
2993	ro2_HDEL_rv	ttaaagctcatcatgcttgtacagctcgtccatgc
3204	3204_GPX3_TP_fw	ATGACCTCTAAGATTAAAAAATTTATACT
3205	3205_GPX3_TP_GW_f	GGGGACAAGTTTGTACAAAAAAGCAGGCTttATGACCTCTAAGATTAAAAAATTTATAC
2945	GPX3_sig_1	GATGGGTCAATCAGCGAGCTatggtgagcaagggcgagg
2946	GPX3_sig_1	GATGGGTCAATCAGCGAGCTatggtgagcaagggcgagg

2944	attB1_GPX3 truncated	GGGGACAAGTTTGTACAAAAAAGCAGGCTttATGACCTCTAAGATTAAAAAATTTATAC TC
3606	3606_GPX4 TP18_Fw 1	CCGTCCATCAATTCACTGTAAAG gtgagcaagggcgaggag
3607	3607_GPX4TP18_Fw 2	ATGGGTGCTTCTGCTTCGGTT CCCGAGAGATCCGTCCATCAATTCACTGTAAAG
3608	3608_ GPX4-TP18_Rv	CTTTACAGTGAATTGATGGACGGctcctcgcccttgctcac
3609	3609_GPX5 TP18_Fw1	GAGAAATCAATCCATCAATTCACCgtgagcaagggcgaggag
3610	3610_GPX5-TP18_Fw2	ATGGGTGCTTCATCATCATCATCTGTGTCGGAGAAATCAATCCATCAATTCACC

3.2 Plant methods

3.2.1 Plant material

3.2.2 Cultivation of plants

Arabidopsis thaliana [L.] Heynh. ecotype Col-0 was used as wild-type. Additionally, the *gpxl3-1* allele and line SALK_071176 was used.

3.2.2.1 Growth of plants on soil

Soil mixture was composed of Floradur B-seed (Floragard, www.floragard.de) supplemented with perlite (perligran 0-6) and quartz sand mixed in a ratio of 10:1:1. Seeds were sown in pots and stratified for two days at 4°C. Plants were grown in growth chambers under long-day conditions with a diurnal cycle of 16 h light at 22°C and 8 h dark at 18°C or short-day conditions (8h light/16h dark, 22°C/18°C). Humidity of growth chamber was set to 50% and light intensity to 120 µE m^{-2} s^{-1}.

3.2.2.2 *In vitro* growth of Arabidopsis on plates

The seeds were first surface sterilized with 70% ethanol for 3-5 min and then washed 3-4 times with deionized autoclaved water. Then the seeds were germinated on nutrient medium (5 mM KNO_3, 2.5 mM KH_2PO_4 pH 5.6, 2 mM $MgSO_4$, 2 mM $Ca(NO_3)_2$, 10 mM Fe-EDTA, 0.1% (v/v) micronutrient mix, pH adjusted to 5.8 or on half-strength Murashige & Skoog medium including vitamins (Duchefa, www.duchefa-biochemie.nl), solidified with 0.8% (w/v) phytagel (Sigma-Aldrich, www.sigmaaldrich.com) or 1% (w/v) microagar (Duchefa, www.duchefa-biochemie.nl). The seeds were then stratified for two days at 4°C. And the plates were transferred into growth cabinets with a controlled diurnal cycle

(16 h light at 22°C and 8 h dark at 18°C) and light intensities of 75 µE m^{-2} s^{-1}. For microscopic analysis the plates were placed in vertical position and for screening the plates were put in horizontal orientation.

3.2.3 Stress treatments

3.2.3.1 Germination of *Arabidopsis* seeds on mannitol and NaCl

After sterilization, Arabidopsis seeds were plated on ½ MS agar medium supplemented with 0 mM,100 mM, 200 mM, 300 mM and 400 mM mannitol or 0 mM, 50 mM, 150 mM, and 250 mM NaCl and stratified for 2 days at 4°C. Then, the seeds were germinated in long-day conditions in a growth cabinet for seven days and the germination rate was checked on day 8 after plating.

3.2.3.2 Growth of Arabidopsis on soil for drought stress

Seeds of the mutant (*gpxl3)* the complemented line (*gpxl3* cpl *GPXL3*), GPXL3 over expressing lines (Col-0 OE *GPXL3*) and Col-0 were grown on soil for seven days in long day conditions. One plant from each genotype was shifted to a pot such that a single pot contained four genotypes and grown for another ten days. When the plants were 17 days old, water was withheld until complete wilting was observed. After 33 days plants were rewatered. And the plants recovered within three days.

3.2.4 Sterilization of Arabidopsis seeds

For surface sterilization seeds were incubated in 1 ml 70% (v/v) ethanol for 3-5 min and then washed 3-4 times with deionized autoclaved water. Then the seeds were distributed on sterile filter paper for drying. Then seeds were plated separately or disseminated loosely.

3.2.5 Selection of transformed plants and mutant lines

3.2.5.1 BASTA® selection

Arabidopsis T1 plants containing the *BAR* gene (coding for phosphinothricine acetyltransferase) as selection marker were germinated on soil. Plants in two leaf stage were sprayed with a 200 mg/l glufosinate ammonium solution (BASTA®, Bayer

CropScience). The treatment was repeated after one week. The non-transformed plants died off soon and the transformed plants carrying resistance became obvious.

3.2.5.2 Kanamycin selection

Arabidopsis T1 seeds containing kanamycin resistance gene as a selection marker were grown on agar plates supplemented with kanamycin monosulfate at a concentration of 50 µg ml^{-1} (Melford Laboratories Ltd., Ipswich, UK #K0126). Seeds were stratified for 2 d in the dark at 4°C. The seeds were then kept in light for 6 to 8 h in a growth cabinet to induce germination. Then, the plates were wrapped in aluminium foil and kept in the growth cabinet in the dark for 2 days. After unwrapping the plates, they were incubated for another 24-48 h at 22ºC in continuous white light (80-200 µmol m^{-2} s^{-1}). Resistant seedlings exhibited long hypocotyls and green cotyledons; whereas non-resistant seedlings had long hypocotyls but pale cotyledons.

3.2.6 Stable transformation of Arabidopsis

Stable transformation of Arabidopsis plants was performed according to the procedure described in (Clough & Bent, 1998). Agrobacterium strains containing the desired constructs were incubated in 30 ml of selective LB medium for 24 h on a shaker at 28°C and 220 rpm as pre-culture. 400 ml of selective LB medium was inoculated with this pre-culture and incubated for further 24 h under the same conditions. The cells were harvested by centrifugation at 4°C and 7,000 g for 8 min, finally the pellet was resuspended in dip medium (5% sucrose and 0.02% (v/v) Silwett L-77) to an OD_{600} of 0.8 to 1. Flower buds were dipped into the suspension, placed on a tray in horizontal orientation, incubated in humid, dark conditions overnight. Then the plants were grown in long day conditions. In order to increase transformation rate the whole procedure was repeated after one week. After maturation of plants seeds were harvested and pooled for screening.

3.2.7 Transient transformation of tobacco

After electroporation of agrobacteria (as described in section 3.5.4) the cells containing the binary vector were inoculated in 5 ml of selective LB medium supplemented with rifampicin and ampicillin (AGL1 and C58C1) and the appropriate antibiotic selection for

the binary plasmid. The culture was incubated for 2 days on a shaker at 28°C and 220 rpm. The OD_{600} was measured with the aim to achieve an OD_{600} of 0.5-1 for the required culture volume. The cells were harvested by centrifugation at 5,000 g for 2 min, the pellet was washed with the same culture volume of deionized water and finally resuspended in deionized water to an OD_{600} of 0.5-1. *Nicotiana benthamiana* Domin plants used for transformation were well watered before infiltration. The Agrobacterium solution was infiltrated into the leaf through the lower leaf epidermis using a 1 ml syringe without a needle. The expression of the transgene was analyzed 2 to 4 days after the infiltration.

3.2.8 Extraction of genomic DNA

Extraction of genomic DNA from Arabidopsis leaves was done according to the method of (Edwards *et al.*, 1991). Leaves were crushed in a microtube with a small pestle and 400 µl extraction buffer (200 mM Tris-HCl pH 7.5, 250 mM NaCl, 25 mM EDTA, 0.5% SDS).was added to the samples and vortexed. The samples were then centrifuged at 13,000 rpm for 10 min. 350 µl of the supernatant were transferred into a fresh microtube, and the same amount of isopropanol (350 µl) was added and mixed. The samples were centrifuged at 13,000 rpm for 10 min to precipitate the DNA. The supernatant was discarded and the pellet washed with 700 µl of 70% ethanol. The ethanol was discarded and the pellet was left at room temperature for 1 hour to air dry. The DNA was resolved in 40 µl of sterile water, heated for 5 min at 95°C and spun down. 2 µl of the isolated gDNA was used as PCR template.

3.2.9 Genotyping of *Arabidopsis thaliana* mutants through PCR

Extraction of gDNA was performed as described in section 3.2.8. The primer combinations listed in table 5 were used for genotyping of T-DNA insertion mutants. The respective primer sequences are shown in section 3.1.6. Wild-type alleles (genomic) were identified with left and right genomic primers, whereas T-DNA alleles (T-DNA) were identified using the indicated combination of a genomic and the T-DNA left border primer. The PCR was conducted as described in section 3.3.3.2

Table 5: Primer combinations used for identification of Arabidopsis mutant lines

			Primer combination		Fragment size (bp)	
Locus	**Line**	**allele**	**#TDNA**	**#Genomic**	**T-DNA**	**Genomic**
GPXL3	SALK_071176	*gpxl3-1*	2696/309	2696/2697	605	912

3.2.10 Extraction of RNA from leaf tissue

About 100-150 mg leaf tissues were harvested from Arabidopsis and shock-frozen in liquid nitrogen (N_2). Then the frozen leaf tissues were crushed to powder using a mechanical stirrer equipped with a microtube-pestle. RNA was extracted from crushed leaf tissue using the NucleoSpin RNAII Kit according to manufacturer's protocol and resuspended in sterile deionized water. RNA was stored at -80°C.

3.2.11 Extraction of total proteins from leaf tissue

About 150 mg of leaf tissue was harvested, frozen in liquid nitrogen and crushed to powder. 500 µl extraction buffer (50 mM Hepes KOH pH 7.4, 10 mM KCl, 1 mM EDTA, 1 mM EGTA, 10% (v/v) glycerol) supplemented with 10 mM DTT and 0.5 mM PMSF was added to the crushed samples and vortexed vigorously for 15 min at 4°C or room temperature. Then the samples were centrifuged to remove cell debris. The extracts were desalted via PD-Midi Trap G25 columns according to the manufacturer's protocol (www.gelifesciences.com) and eluted in resuspension buffer (100 mM potassium phosphate buffer pH 7.4, 1 mM EDTA). Protein extracts were stored at -80°C.

3.3 Nucleic acid methods

3.3.1 Oligonucleotides

Primers were acquired from MWG (www.eurofinsgenomics.eu/en/dna-rna-oligonucleotides). Lyophilized primers were resuspended in deionized water to working concentration of 20 pmol/µl. Both stock and working solutions were stored at -20°C. Primer sequences are listed in section 3.1.6.

3.3.2 DNA gel electrophoresis

DNA fragments were separated on an agarose gel. 0.8% (w/v) agarose was dissolved in 1x TBE buffer (90 mM Tris-HCl pH 8.0, 90 mM boric acid, 0.5 mM EDTA) by heating. After cooling, ethidium bromide was added to a final concentration of 0.7 µg/ml. The DNA samples were mixed with loading buffer (0.25% bromophenol blue, 0.25% xylene cyanole and 40% glycerol). GeneRuler™ DNA Ladder Mix (www.thermoscientificbio.com) was used as molecular mass standard. DNA was separated by applying a current of 70-140 V in 1x TBE running buffer. Documentation was done using the MF-ChemiBIS2.0.

3.3.3 Polymerase chain reaction (PCR)

Two different types of PCRs were used, one for cloning purposes and the other for genotyping and SQ-RT PCR.

3.3.3.1 PCR for cloning

For cloning purposes DNA fragments were amplified using Phusion High-Fidelity DNA Polymerase. The PCR was carried out in a total volume of 50/20 µl and the programs were run according to the manufacturer's protocol. The salt adjusted primer melting temperatures were defined using an online calculator Oligo Calc (http://www.basic.northwestern.edu/biotools/oligocalc.html).

3.3.3.2 PCR for genotyping

For Genotyping the PCR was performed in a total volume of 20 µl with gDNA isolated from plants as template and using Taq™ DNA Polymerase or homemade/purified Taq (Table 6).

Annealing temperatures were adjusted to primer properties using the Oligonucleotide Properties Calculator (http://biotools.nubic.northwestern.edu/OligoCalc.html) (Table 7).

Table 6: PCR master mix protocols

component	Taq (µl)	Phusion. (µl)	final conc.
deionized H_2O	14.6-16.2	36	-
template	0.5-2	0.5	-
primer forward	0.4	1	2 µM
primer reverse	0.4	1	2 µM
dNTPs	0.4	1	200 µM
buffer	2	2	1x
polymerase	0.1	0.5	2.5 units

The PCR programs were adjusted to the recommended parameters for the respective DNA polymerases:

Table 7: PCR programs

No.	step	temperature		time
		Taq	Phusion	
1	initial denaturation	95°C	98°C	2 min
2	denaturation	95°C	98°C	20 sec
3	annealing	57°C	60°C	20 sec
4	elongation	72°C	72°C	30-60 sec per kb
5	final elongation	72°C	72°C	10 min
Step 2 to 4 was repeated 35 times				

3.3.4 cDNA synthesis and semi-quantitative RT-PCR

cDNA was synthesized from 1 µg of total RNA using M-MLV reverse transcriptase (www.lifetechnologies.com). The reaction was carried out according to the manufacturer's instructions with RNAse free deionised water. PCR was performed on 1 µl of cDNA with the following gene-specific primers: 364 & 436 for *ACTIN7*, 2751 & 2752 for *GPXL3.* cDNA was stored at -20°C. PCR was set up as described in section 3.3.3.2.

3.3.5 DNA purification

PCR samples or DNA fragments from gel electrophoresis were cut out from the gel and purified using the NucleoSpin Gel and PCR clean up kit following the manufacturer's instructions.

3.3.6 RNA purification

About 150 mg leaf material was harvested from Arabidopsis plants. The leaf tissues were frozen in liquid N_2 and crushed to powder form. Total RNA was extracted using the NucleoSpin RNAII Kit according to manufacturer's instructions. The RNA concentration was measured using NanoDrop

3.3.7 Determination of nucleic acid concentration

DNA and RNA concentrations were determined by spectrophotometric analysis using the Nanodrop photometer.

3.4 Gateway Cloning

Gateway® cloning was performed according to the manufacturer's instructions (www.lifetechnologies.com/de/de/home/lifescience/cloning/gatewaycloning/protocols.html). Empty Gateway® vectors used in this study are listed in Table 8

Table 8: Empty Gateway® vectors used for cloning.

Name	Bacterial resistance	Plant resistance	Promoter	Reference/Description
pDONR201	Kan^R		35S	www.lifetechnologies.com
pDONR207	$Gent^R$		-	www.lifetechnologies.com
pSS01	Kan^R	$Basta^R$	-	(diploma thesis S. Soyk, 2008)
pCM01	Kan/Hyg^R	Kan^R	-	(PhD thesis Christopher Müller, 2010)
pB7WG2	$Spec^R$	$Basta^R$	-	Overexpression of gene of interest (Karimi *et al.,* 2005)
pK7WG2	$Spec^R$	Kan^R	-	Overexpression of gene of interest (Karimi *et al.,* 2005)
pETG10A	Amp^R		T7/lacO	Overexpression of recombinant proteins in *E.coli*
pETG41A	Amp^R		T7/lacO	Overexpression of recombinant proteins in *E.coli*

Gateway primers were designed with the *attB* recombination sites listed in section 3.1.6. The total volume of BP and LR reaction was 10 µl each. Incubation time for both reactions was 1 hour at 25°C. Reaction mix was transformed into DH5α for selection on the respective antibiotic. The pDONR entry vectors were checked by PCR for positive clones and confirmed by sequencing. The entry clones generated are listed in Table 9.

3.4.1.1 Generation of C- and N-terminal fusion constructs of GPXLs with roGFP2

To obtain C and N-terminal fusions of full-length GPXLs with roGFP2, roGFP2 was cloned in frame to GPXLs via Gateway Cloning (Invitrogen) by using the vector pSS01 for C-terminal fusion and the vector pCM01 for N-terminal fusion (Brach *et al.*, 2009)(Table 11). Fusion of the truncated constructs ($GPXL_t$) of GPXL3, GPXL4, GPXL5 and GPXL6 was achieved through assembly PCR using nucleotide specific primers (Table 10). In the first round, the nucleotide sequence of $GPXL_t$ was amplified using specific primers. Simultaneously, roGFP2 was amplified in the second round using appropriate primers. The resulting PCR products were mixed in 1:1 ratio and amplified using appropriate primers. The resulting fragments were purified and mixed with pDONR201 for the BP reaction and recombined in the LR reaction with the destination vectors pB7WG2 or pK7WG2 (Karimi *et al.*, 2002).

3.4.1.2 Generation of *GPXL3* Complementation/overexpression construct

GPXL3 full length sequence was amplified by PCR using gateway primers # 2412 and # 2628 for complementation of *GPXL3* in *gpxl3-1* or overexpression of *GPXL3* in Col-0. The resulting PCR product has a length of 621 bp. The product was subcloned into pDONR201 and subsequently sequenced via Sanger sequencing (GATC© Biotech). Expression clone of GPXL3 was generated by gateway cloning of GPXL3-pDONR201 into a destination vector pB7WG2.

Table 9: List of generated entry clones.

Code	Vector name	Primer 1	Primer 2	Description
G1	pDONR207 _GPXL1_C	2558	2560	C-terminal roGFP2 fusion
G2	pDONR207 _GPXL2_C	2560	2562	C-terminal roGFP2 fusion
G3	pDONR201 _GPXL2_N	2560	2561	N-terminal roGFP2 fusion
G4	pDONR201 _GPXL3_C	2412	2413	C-terminal roGFP2 fusion
G5	pDONR201 _GPXL3_N	2412	2628	N-terminal roGFP2 fusion
G6	pDONR207 _GPXL4_C	2564	2566	C-terminal roGFP2 fusion
G7	pDONR201 _GPXL4_N	2564	2565	N-terminal roGFP2 fusion
G8	pDONR207 _GPXL5_C	2538	2539	C-terminal roGFP2 fusion
G9	pDONR201 _GPXL5_N	2538	3604	N-terminal roGFP2 fusion
G10	pDONR207 _GPXL6_C	2568	2570	C-terminal roGFP2 fusion
G11	pDONR201 _GPXL6_N	2568	2569	N-terminal roGFP2 fusion
G12	pDONR201 _GPXL7_C	2571	2573	C-terminal roGFP2 fusion
G13	pDONR207 _GPXL8_C	2574	2576	C-terminal roGFP2 fusion
G14	pDONR201 _GPXL8_N	2574	2575	N-terminal roGFP2 fusion

Table 10: List of truncated entry clones

Code	Vector	PCR	Primer 1	Primer 2	Template
G15	pDONR201_GPXL3 $_{1\text{-}34}$ roGFP2	1	2412	2992	pSS01-GPXL3
	-	2	3031	2659	pCM01-GPXL3
	-	3	2412	2659	1 + 2 (1:1)
G16	pDONR201_GPXL3$_{\Delta 1\text{-}34}$-roGFP2-HDEL	1	3034	3033	pSS01-GPXL3
		2	3032	2993	pCM01-GPXL3
		3	3034	2725	1 + 2 (1:1)
G17	pDONR201_GPXL3 $_{13\text{-}34}$ - roGFP2	1	3204	2992	pSS01-GPXL3
		2	3031	2659	pCM01-GPXL3
		3	3205	2659	1 + 2 (1:1)
G18	pDONR201_GPXL3$_{1\text{-}12}$-roGFP2-HDEL	1	2945	2993	pSS01-GPXL3
		2	2946	2993	PCR1
		3	2412	2725	PCR2

G19	pDONR201_GPXL3$_{\Delta 1\text{-}12}$-roGFP2-HDEL	1	2944	3033	pSS01-GPXL3
		2	3032	2993	pCM01-GPXL3
		3	2944	2725	1 + 2 (1:1)
G20	pDONR201_GPXL3$_{1\text{-}34}$-roGFP2-HDEL	1	2412	2992	pSS01-GPXL3
		2	3031	2993	pCM01-GPXL3
		3	2412	2725	#1 + #2 (1:1)
G21	pDONR201:GPXL3 $_{\Delta 1\text{-}12}$ - roGFP2-	1	2944	3033	pSS01-GPXL3
		2	3032	2659	pCM01-GPXL3
		3	2944	2659	1 + 2 (1:1)
G22	pDONR201_GPXL4 $_{G2A}$ -roGFP2	1	3569	3581	pSS01-GPXL4
		2	3582	2659	pCM01-GPXL4
		3	3569	2659	1 + 2 (1:1)
G23	pDONR201_GPXL5 $_{G2A}$ -roGFP2	1	3570	3605	pSS01-GPXL4
		2	3584	2659	pCM01-GPXL4
		3	3570	2659	1 + 2 (1:1)
G24	pDONR201_GPXL4 $_{1\text{-}18}$ -roGFP2	1	3606	2659	pSS01-GPXL4
		2	3607	2659	PCR1
		3	2564	2659	PCR2
G25	pDONR201_GPXL5 $_{1\text{-}18}$ -roGFP2	1	3609	2659	pSS01-GPXL4
		2	3610	2659	PCR1
		3	2538	2659	PCR2
G26	pDONR201_GPXL6 $_{1\text{-}65}$ -roGFP2	1	3774	3775	pSS01-GPXL4
		2	3776	2659	pCM01-GPXL4
		3	3774	2659	1 + 2 (1:1)

Table 11: List of generated destination vectors

Code	Entry clone	Vector name	Purpose
G27	G1	pSS01-GPXL1	Localization of GPXL1
G28	G2	pSS01-GPXL2	Localization of GPXL2
G29	G3	pCM01-GPXL2	Localization of GPXL2
G30	G4	pSS01-GPXL3	Localization of GPXL3

G31	G5	pCM01-GPXL3	Localization of GPXL3
G32	G6	pSS01-GPXL4	Localization of GPXL4
G33	G7	pCM01-GPXL4	Localization of GPXL4
G34	G8	pSS01-GPXL5	Localization of GPXL5
G35	G9	pCM01-GPXL5	Localization of GPXL5
G36	G10	pSS01-GPXL6	Localization of GPXL6
G37	G11	pCM01-GPXL6	Localization of GPXL6
G38	G12	pSS01-GPXL7	Localization of GPXL7
G39	G13	pSS01-GPXL8	Localization of GPXL8
G40	G14	pCM01-GPXL8	Localization of GPXL8
G41	G15	pB7WG2_GPXL3 $_{1-34}$-roGFP2	Localization of GPXL3 $_{1-34}$-roGFP2
G42	G16	pB7WG2_GPXL3 $_{\Delta 1-34}$-roGFP2	Localization of GPXL3 $_{\Delta 1-34}$-roGFP2
G43	G17	pB7WG2_GPXL3 $_{13-34}$-roGFP2	Localization of GPXL3 $_{13-34}$-roGFP2
G44	G18	pB7WG2_GPXL3 $_{1-12}$ -roGFP2-HDEL	Localization of GPXL3 $_{1-12}$-roGFP2-HDEL
G45	G19	pB7WG2_GPXL3 $_{\Delta 1-12}$-roGFP2-HDEL	Localization of GPXL3 $_{\Delta 1-12}$-roGFP2-HDEL
G46	G20	pB7WG2_GPXL3 $_{1-34}$ -roGFP2-HDEL	Localization of GPXL3 $_{1-34}$-roGFP2-HDEL
G47	G21	pK7WG2_GPXL3 $_{\Delta 1-12}$- roGFP2	Localization of GPXL3 $_{\Delta 1-12}$-roGFP2
G48	G22	pK7WG2_GPXL4 $_{G2A}$-roGFP2	Localization of GPXL4 $_{G2A}$-roGFP2
G49	G23	pB7WG2_GPXL4 $_{G2A}$-roGFP2	Localization of GPXL5 $_{G2A}$-roGFP2
G50	G24	pB7WG2_GPXL4 $_{1-18}$-roGFP2	Localization of GPXL4 $_{1-18}$-roGFP2
G51	G25	pK7WG2_GPXL5 $_{1-18}$-roGFP2	Localization of GPXL5 $_{1-18}$-roGFP2
G52	G26	pB7WG2_GPXL6 $_{1-65}$-roGFP2	Localization of GPXL6 $_{1-65}$-roGFP2
G53	G5	pB7WG2_GPXL3	Complementation of *gpxl3*

G54	G5	pETG10a	Cloning of GPXL3 recombinant protein
G55	G5	pETG41a	Cloning of GPXL3 recombinant protein for antibody production

3.4.2 Sequencing

Sequencing was done by StarSeq GmbH (www.starseq.de/com) and GATC© Biotech (www.gatc-biotech.de/com) with the respective sequencing primers. Samples were prepared according to the company's guidelines. The sequences were analysed with Serial Cloner 2.5.

3.5 Microbiological methods

3.5.1 Bacterial strains

E. coli DH5α	F-, 80lacZdeltaM15 Δ (lacZYA-argF) U169 deoR recA1 endA1 hsdR17 (rK-, mK+) phoA supE44 thi-1 gyrA96 relA1 lambda-(Stratagene)
E. coli DB3.1	F-, gyrA462 endA- Δ (sr1-recA) mcrB mrr hsdS20 (rB-,mB) supE44 ara14 galK2 lacY1 proA2 rpsL20(Sm^R) xyl5 lambda- leu mtl1 (Invitrogen)
A. tumefaciens AGL-1	C58 (Rif^R), RecA, pTiBo542DT- ($Carb^R$) (Lazo *et al.*, 1991)
A. tumefaciens C58C1	C58 (Rif^R), pTiC58 cured, pGV2260 ($Carb^R$) (Deblaere *et al.*, 1985)

3.5.2 Bacterial growth

Bacteria were grown in LB medium (1% tryptone, 0.5% yeast extract, 1% NaCl, pH 7.0 with NaOH) over-night. *E. coli* was incubated at 37°C and *A. tumefaciens* strains at 28°C. Transformed bacteria were selected on LB plates solidified with 1.5% agar containing antibiotics in the following final concentrations: ampicillin/carbenicillin 100 µg/ml; kanamycin 50 µg/ml; rifampicin 50 µg/l; spectinomycin/streptomycin 50 µg/ml and gentamicin 10 µg/ml.

3.5.3 Glycerol stocks

4 ml liquid bacteria culture were grown for 16 hours in LB medium under antibiotic selection pressure. 400 µl of the culture were mixed with 600 µl of 80% (v/v) sterile glycerol, shock-frozen in liquid nitrogen and stored at -80°C.

3.5.4 Transformation of electro competent cells

Electro-competent agrobacteria cells were transformed with a Micropulser™ electroporator according to manufacturer's protocol. For transformation, 1 µl of plasmid was added to cells on ice and transferred to the electroporation cuvette (0.2 mm gap). After incubation for 10 min on ice the cells were pulsed with 2,500 V for approximately 5 ms. Immediately after pulsing, 500 µl of sterile LB medium was added to the bacteria and the solution removed from the cuvette. The bacteria were incubated at 28°C under shaking for 1 hour. Afterwards, the bacteria were plated on agar plates containing the selective antibiotic.

3.5.5 Transformation of chemically competent cells

Chemically competent *E. coli* cells were transformed by heat-shock. For the transformation, 1 µl of plasmid or whole ligation mix were added to the cells preincubated on ice. The mix was heat-shocked at 42°C for 50-60 sec and 400 µl LB directly added to the transformation mix. The transformed cells were incubated at 37°C under shaking conditions for 1 hour and the culture plated on LB plates containing the appropriate selection.

3.5.6 Plasmid isolation

E. coli cells containing the plasmid were grown in 3 ml LB supplemented with the respective antibiotic over-night. The plasmid was extracted with the NucleoSpin Plasmid Kit® according to the manufacturer's protocol.

3.6 Protein methods

3.6.1 Generation of GPXL3 recombinant protein

GPXL3 lacking the signal peptide ($GPXL3_{\Delta 1\text{-}34}$) sequence was amplified by PCR. The forward primer #3093, which possesses a recognition sequence for a TEV protease

cleavage, and the reverse primer #2628 were used for amplification. The resulting PCR product has a length of 519bp. The product was subcloned into pDONR201 (Gateway) and subsequently sequenced via Sanger sequencing (GATC© Biotech). Cloning of GPXL3 into the expression vector pETG10A which contain an N - and C- terminal 6x His was achieved by Gateway® cloning. In order to increase the solubility of GPXL3, the protein was fused to Maltose binding protein (MBP). For this purpose GPXL3 was cloned into the expression vector pETG41A, which has N- terminal MBP and C- terminal His,

3.6.2 Expression of recombinant GPXL3 protein

Recombinant proteins of $GPXL3_{\Delta 1\text{-}34}$ were expressed in Origami DE3 and BL21. The cells were transformed by heat shock and plated on LB plates supplemented with appropriate antibiotic. A pre-culture of 50 ml LB medium containing respective selective antibiotics was incubated overnight shaking at 37°C. 10 ml of the pre-culture was added to 500 ml selective LB medium and grown at room temperature to an OD_{600} of 0.8. The cells were kept at 4°C without shaking for 10 min. 1 ml of the culture was taken as t0 sample. The cells were centrifuged and the pellet was stored at -20°C. Protein expression was induced by addition of IPTG to a final concentration of 1 mM. The culture was further incubated at 19-20°C temperature shaking at 220 rpm for 24 hours. Control samples were taken at 1h, 3h and 24 h according to OD at t0.

e.g $OD_{t0} = 0.6$

t1 = x ml = $\frac{OD_{t0}}{OD_{t1}}$

3.6.3 Purification of GPXL3 recombinant protein by affinity chromatography

$GPXL3_{\Delta 1\text{-}34}$ recombinant proteins were purified using HiTrap™ Chelating HP columns (www.gelifesciences.com). Cells were harvested from expression cultures by centrifugation at 8,000 g for 10 min at 4°C. The resulting sediment was resuspended in 10 ml binding buffer (50 mM Tris-HCl pH 8.0, 250 mM NaCl) supplemented with 0.5 mM PMSF and transferred to a 50 ml falcon tube. After sonication at 40% power on ice for 10 min, the lysate was centrifuged at 25,000 g for 15 min at 4°C in order to pellet cell debris. The supernatant was immediately transferred to a falcon tube and filtered through a 0.45 µm aseptic filter. 100 µl aliquot (crude) was taken for SDS-PAGE. The proteins were circulated over the HiTrap™ Chelating HP column using a peristaltic pump at a flow rate

of 1 ml min^{-1}. The column was preloaded with 5 ml 50 mM $NiCl_2$ and 10 ml binding buffer. After loading of the column with the His-tagged proteins, 100 µl aliquot of the flow through was collected for SDS-PAGE. The column was washed with 5 ml of wash buffers each containing increasing concentrations of imidazole (20 mM to 150 mM) to remove unspecific bound proteins. Finally, the protein was eluted from the column with elution buffer containing 200-250 mM imidazole in 300-500 µl fractions. Nickel was removed from the column by washing with 10 mM EDTA and the column was loaded with 0.02% NaN_3 and stored at 4°C.

3.6.4 Cleaving of Histag for antibody production

The $GPXL3_{\Delta 1-34}$ cloned into expression vector pETG41A was purified and the protein solution was diluted with dialysis buffer (25mM Tris-HCl (pH 8.0), 500 mM NaCl and 14 mM β-mercaptoethanol) to the concentration of 1 mg mL^{-1}. GPXL3 was cleaved from the His-tag by using TEV protease (1 mg mL^{-1}) in a protease: target protein ratio of 1:50 (w/w) for eight hours. Afterwards the cleaved protein solution was loaded on two 5 mL Spectra/Por® Float-A-Lyzer® G2 dialysis devices according to the manufacturer's instructions to remove the His-tag. The sample was dialyzed at 4°C overnight with 2 complete buffer changes (~ 800 mL dialysis buffer after 2 hours and 600 ml buffer after 12 hours). The cleaved and dialyzed protein solution was loaded again over a 1 ml Ni^{2+} loaded HisTrap ™ HP affinity column (GE Healthcare) which had been equilibrated with dialysis buffer. The flow-through should mostly contain His-Tag free GPXL3. This was checked by SDS-PAGE on a 16% acrylamide gel.

3.6.5 Determination of protein concentration

The protein concentration of recombinant protein or plant protein extracts was determined according to Bradford (Bradford, 1976). The standard curve was prepared using 0.1 mg ml^{-1}, 0.2 mg ml^{-1}, 0.4 mg ml^{-1} of bovine serum albumin (BSA). 10 µl of adequately diluted protein solution were mixed with 250 µl Bradford reagent in 96-well plates and incubated for 5 min at room temperature. Absorbance was measured at 595 nm with the POLARstar Omega microplate reader.

3.6.6 SDS-PAGE

Proteins were separated on discontinuous polyacrylamide gels consisting of resolving and stacking gel. Gels were prepared and run in a BioRad Mini-PROTEAN® Tetra Cell gel system. Composition of resolving and stacking gels are shown in table 12.

Table 12: Composition of discontinuous polyacrylamide gel with 16% resolving gel

Component	Resolving gel (16%)	Stacking gel (4%)
Deionized water	0.06 ml	2.76 ml
Resolving gel buffer (1.5 M Tris-HCl pH 8.8)	2.5 ml	--
Stacking gel buffer (0.5 M Tris-HCl pH 6.8)	-	1.25 ml
30% acrylamide	5.2 ml	0.65 ml
2% bisacrylamide	2.08 ml	0.26 ml
10% SDS	0.1 ml	0.05 ml
TEMED	0.01 ml	0.005 ml
10% APS	0.05 ml	0.025 ml

Before loading, protein samples were diluted to the appropriate concentration, mixed with 5x SDS protein loading buffer (100 mM Tris-HCl pH 7, 10% SDS, 20% glycerol, 25% β-mercaptoethanol, 0.1% bromophenolblue) and heated for 5-10 min at 95°C. PageRuler Unstained Protein Ladder or the PageRuler Prestained Protein Ladder were loaded onto the gel as molecular mass standard. Gels were run at constant voltage in SDS-electrophoresis buffer (25 mM Tris-HCl pH 8.3, 192 mM glycine, 0.1% SDS), first for 10 min at 120 V, then the current was increased to 180 V and applied for approximately 30 min until the bromophenol running front reached the bottom of the gel.

Proteins were visualized by incubation in Coomassie staining solution (50% ethanol, 1% acetic acid, 0.1% Coomassie Brilliant Blue G-250) for 30 min and Coomassie destaining solution (20% ethanol, 10% acetic acid) for several hours. Gels were scanned for documentation.

3.6.7 Western blot analysis

For western blot analysis proteins were separated by discontinuous SDS-PAGE. The wet blot sandwich was assembled in blotting buffer (1.44% glycine, 0.5% Tris, 0.1% SDS, 20% methanol). Proteins were transferred to PVDF membrane using the Criterion™

Blotter (40 mA, overnight, 4°C). Subsequently, the membrane was blocked for 1 hour at room temperature with 5% milk powder in TBS (20 mM Tris-HCl pH 7.6, 137 mM NaCl) supplemented with 0.1% Tween 20 (TBS-T). The membrane was washed three times with TBS-T and incubated with 1:5,000 (for α-GPXL3), diluted primary antiserum overnight at 4°C. The membrane was washed three times for 5 min with TBS-T. ImmunoPure goat α-rabbit IgG HRP-conjugated antibody was used at a dilution of 1:20,000 in 0.5% milk powder in TBS-T and incubated on the membrane for 45 min to 1 hour. After washing the membrane six times for 5 min with TBS-T, protein-antibody complexes were visualized by using the Pierce ECL Western Blotting or SuperSignal West Dura or Femto Substrate (www.piercenet.com/cat/western-blotting-substrates). Chemiluminescence was detected with the MF-ChemiBIS 2.0 imaging system.

3.7 Microscopy methods

3.7.1 Fluorescence screen of transgenic plants

Transgenic seeds transformed with constructs encoding fluorescent proteins were sterilized and placed on nutrient medium solidified with 0.8% micro agar. Seven days after vertical growth under long-day conditions in a growth cabinet, the seedlings were screened for fluorescence with a Leica M165FC stereomicroscope equipped with a Leica DCF425C camera for imaging. For screening of roGFP2 fluorescence a GFP filter for 470 ± 40 nm excitation and emission at 525 ± 50 nm was used. Transgenic seedlings were put on soil and grown for seed harvesting.

3.7.2 CLSM analysis

3.7.2.1 Localization and expression analysis

The roGFP2 tagged fluorescent constructs were tested for localization by transient expression in tobacco epidermis cells or in stably transformed T_2 Arabidopsis seedlings. Images were collected on an inverted Zeiss confocal microscope LSM780 using a C-Apochromat 40x/1.2 W Corr M27 objective. roGFP2 fluorescence was excited at 488 nm and collected at 505-530 nm. Chloroplast autofluorescence was excited at 488 nm or 543 nm and recorded above 650 nm. RFP was excited at 543 nm and emission detected between 560 and 640 nm. TMRM fluorescence was excited with 543 nm and collected

from 560 to 620 nm. FM4-64 in root tissues was excited at 488 nm while emission was detected between 620 and 680 nm. For stacks, optical sections were collected and projected as maximum projections using the ZEN 2011 software.

3.7.2.2 Redox based topology analysis

For topology analysis of GPXL3 in *N. benthamiana,* the respective Agrobacteria were leaf infiltrated with an OD_{600} of 1.0. After 3 days leaf pieces were cut out and mounted on a Zeiss confocal microscope LSM780. Images were collected with a C-Apochromat 40x/1.2 W Corr M27 in multi-track mode with line switching between 488 nm excitation and 405 nm excitation and taking an average of two readings. The roGFP2 fluorescence was collected with a 505-530 nm emission band-pass filter. Autofluorescence excited at 405 nm was collected from 430 to 470 nm. Laser settings were adjusted according to SEC22 control constructs. Therefore roGFP2-SEC22 with roGFP2 facing the cytosolic site of the ER was defined as maximum sensor reduction. SEC22-roGFP2 with roGFP2 facing the luminal site of the ER was defined as maximum sensor oxidation (Brach *et al.*, 2009). For topology analysis of GPXL3 stably expressed in *A. thaliana,* seedlings grown for 8 days on agar plates were mounted on a Zeiss confocal microscope LSM780. Images were collected with a C-Apochromat 40x/1.2 W Corr M27 in multi-track mode with line switching between 488 nm excitation and 405 nm excitation and taking one read. The roGFP2 fluorescence was collected with a 505-530 nm emission band-pass filter.

3.7.2.3 Image processing

Images were exported as tiff files with the ZEN 2011 software and compiled using Adobe Photoshop CS5.1. For ratiometric analysis the images were imported into a custom written MatLab analysis suite (M.D. Fricker, Dept. Plant Sciences, Oxford) and analysed. The ratio analysis was performed on a pixel-by-pixel basis as $I405/I488$ following spatial averaging in (x,y) using a 3 × 3 kernel, correction of the $I405$ for autofluorescence bleeding into the 405 nm channel and subtraction of background signals for each channel measured from the vacuole of one of the cells. Pixels with intensities within 10% saturation or with less than 2 standard deviation units above background were ignored for the analysis.

4 Results

4.1 Characterization of GPXL3 deficient mutant

The identification of null mutants is the first step towards describing the function of a gene. With a confirmed mutant in hand, the next step is to determine the consequences of the mutation on growth and development relative to the wild type. Reverse genetics is a strategy to determine a particular gene function by studying the phenotypes of individuals with alterations in the gene of interest (Sessions *et al.*, 2002). However, it has become apparent that many null mutants have no readily identifiable phenotype. (Krysan *et al.*, 1999).

GPXL3 in Arabidopsis is encoded on the second chromosome. The gene structure of *GPXL3* (AT2G43350.1) is composed of six exons (Figure 4.1)

Figure 4.1: Exon-Intron structure of *GPXL3*. Exon structures are indicated as grey boxes, while introns are represented as black lines

4.1.1 Identification of homozygous T-DNA insertion lines for *GPXL3*

To investigate the role of *GPXL3* in the detoxification of H_2O_2, a T-DNA line for *GPXL3* i.e. *gpxl3-1* was selected and characterized. The *gpxl3-1* line was obtained from the SALK collection (SALK_071176). According to TAIR, the T-DNA insertion is located in the first exon of the genomic sequence of *GPXL3* (Figure 4.2(I)). The T-DNA insertion was confirmed by PCR with a T-DNA left border specific primer and an appropriate gene-specific primer. The respective primer combinations and calculated fragment sizes are shown in section 3.2.9 (Table 5). gDNA of four-week-old Arabidopsis plants was used in PCR reactions as template. On the basis of the PCR products the plants could be identified as wild-type plants (only genomic fragment, G) and as plants heterozygous (genomic and T-DNA fragment) or homozygous (only T-DNA fragment, T) for the T-DNA insertion (Figure 4.2(II))

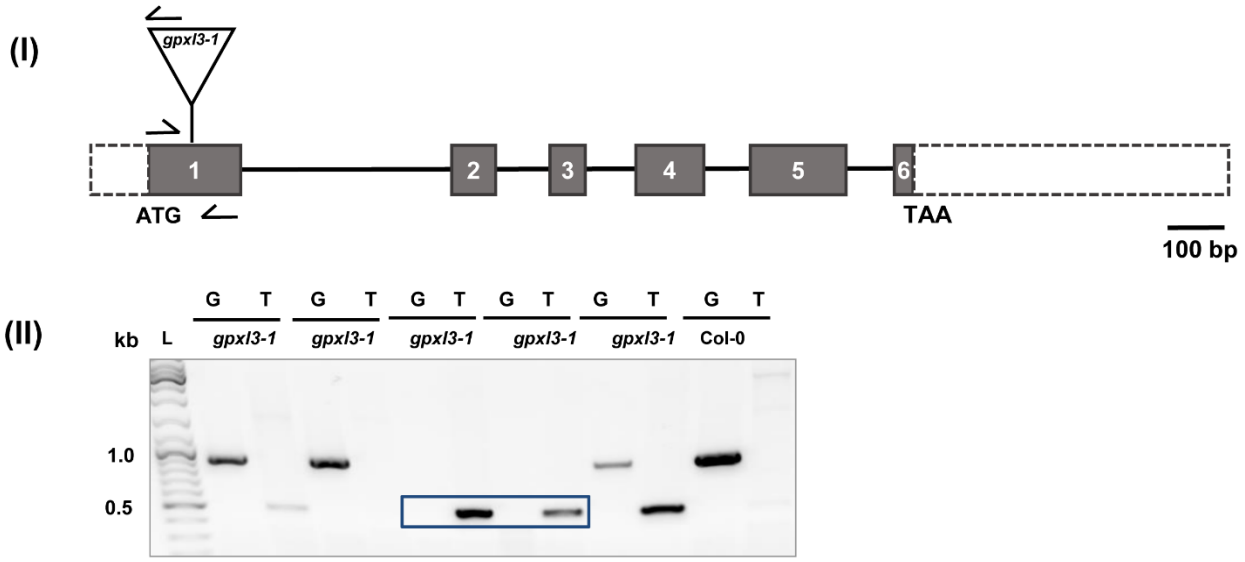

Figure 4.2: Representation of T-DNA insertion line gene model and genotyping of the mutant (I) Physical map of *gpxl3-1* with a T-DNA insertion in Exon 1. Exons and introns are represented by grey boxes and black lines respectively. Primers used for genotyping are represent by small arrows. **(II) Genotyping of *gpxl3* mutants.** gDNA was extracted from several plants (1 up to 8) and checked for the genomic wild-type allele (indicated by G) and the T-DNA insertion (indicated by T), with gene and T-DNA specific primers, respectively. "L" represents DNA marker, size is indicated in base pairs (bp).

4.1.2 Semi-quantitative RT-PCR and western blot reveals that *gpxl3-1* is a null mutant

Expression level of *GPXL3* in *gpxl3* homozygous mutants was analysed by semi-quantitative RT-PCR. Semi-quantitaive RT-PCR revealed that *gpxl3-1* with a T-DNA insertion in the first exon is a knock out. Template cDNA was generated from total RNA isolated of leaf tissue of 6-week-old homozygous *gpxl3* T-DNA insertion lines. cDNA of Col-0 wild-type of the same age was used as a control. As forward primer, a sequence annealing to the start region of the coding sequence was selected. To avoid amplification from genomic DNA contamination in the cDNA sample, exon-exon spanning sequences between the 5th and 6th exon were selected as reverse primer (Figure 4.3(I)). PCR with the indicated primers should result in a PCR fragment of 601bp. cDNA of *AtActin7* (AT5g09810) was used as a loading control and PCR amplified in the same way as *GPXL3*. RT-PCR on *gpxl3-1* with the T-DNA insertion in the first exon produced no

transcript, indicating a null mutant (Figure. 4.3(II)). Protein gel blot analysis with antiserum against GPXL3 also confirmed the absence of GPXL3 protein in *gpxl3* mutants (Figure 4.3 (III)).

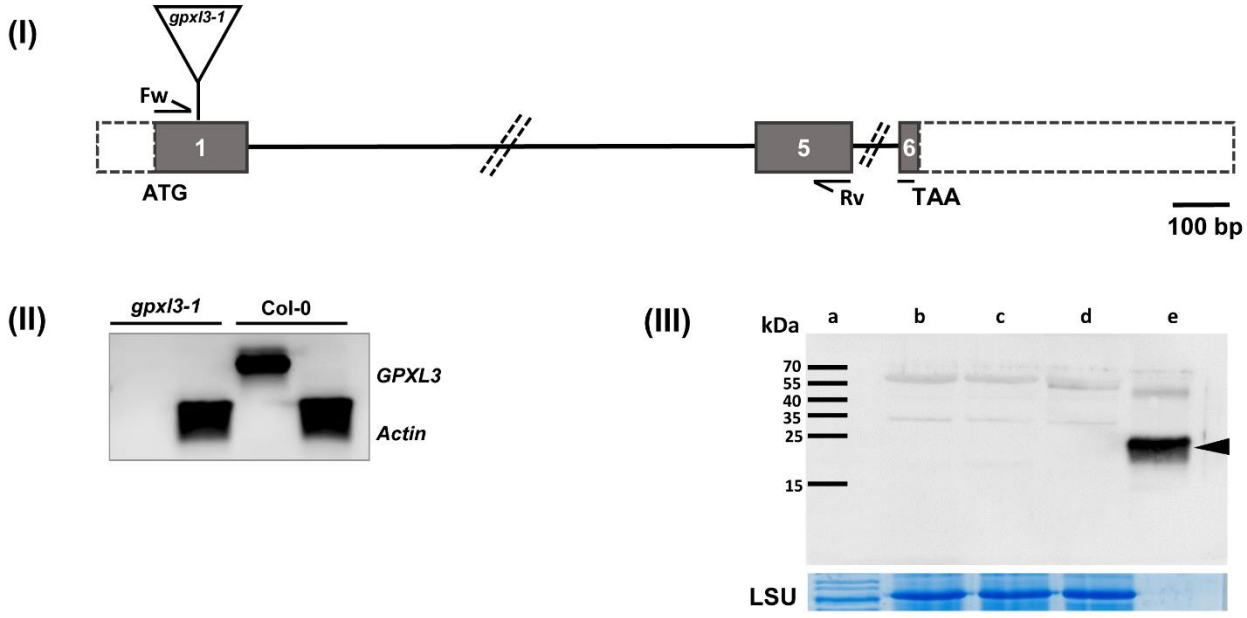

Figure 4.3: Semi-quantitative RT-PCR analysis of *GPXL3* transcript level of T-DNA insertion mutant. (I) For PCR forward primers (arrow) annealing to the start of the coding region and exon-exon spanning reverse primers (arrow) annealing to exon five (Ex.5) and exon six (Ex.6) in the coding region of *GPXL3* were used. **(II)** PCR was carried out on cDNA of homozygous *gpxl3-1* lines and Col-0 with gene-specific primers for At*GPXL3* and At*Actin7*). **(III)** Protein gel blot analysis of *gpxl3-1* (lane b,c,d) and GPXL3 recombinant protein (lane e) with GPXL3 antibody. Lane a represent molecular weight standard. 20 µg of desalted protein extract was separated by SDS PAGE. 200 ng of recombinant GPXL3 protein was used as a positive control. Protein detected with GPXL3 antiserum in recombinant GPXL3 protein had the size of ~23 kDa (black arrow). Equal loading in all lines was confirmed by staining of the large subunit (LSU) of 1,5 bisphosphate carboxylase/oxygenase (Rubisco).

4.1.3 The *gpxl3* mutant shows no obvious phenotype

As a first step in the characterization of the *gpxl3* mutant, different root, shoot and leaf traits were studied in the mutant compared to Col-0. Various root parameters such as primary, lateral and total root length along with number of lateral roots were compared with Col-0 under short (8 h) photoperiod after seven and twenty days by growing them on vertical MS plates. There was almost no difference in the root traits between *gpxl3-1* and Col-0 on day seven. On day twenty, *gpxl3* mutants showed a slight decrease in the primary, lateral, total root length and number of lateral roots compared to Col-0 (Figure 4.4 A-D). However, these differences were not significant. There was no significant difference in the branching angles of roots.also(Figure 4.4 E). While in case of shoot traits, there was no difference in shoot compactness (No. of leaves per shoot) on day seven but a slight increase was observed on day twenty for *gpxl3 mutants* compared to Col-0 but it was not significant (Figure 4.4 F). There was no significant difference fresh and dry weight of *gpxl3* and Col-0 (Figure 4.4 G). Similar observations were recorded for leaf traits in which no difference was observed for leaf area and leaf green value of the mutant and Col-0 after seven and twenty days (Figure 4.4 H-I). To conclude, no significant differences were observed in the root, shoot and leaf traits of *gpxl3-1* compared to Col-0.

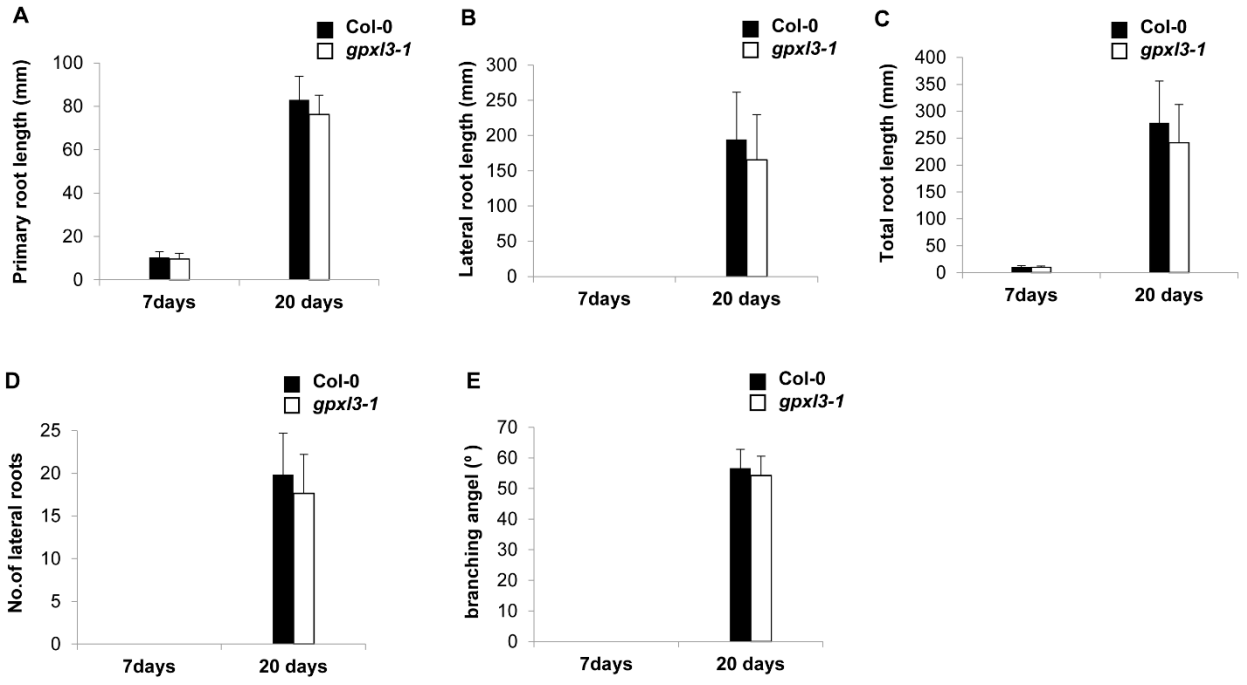

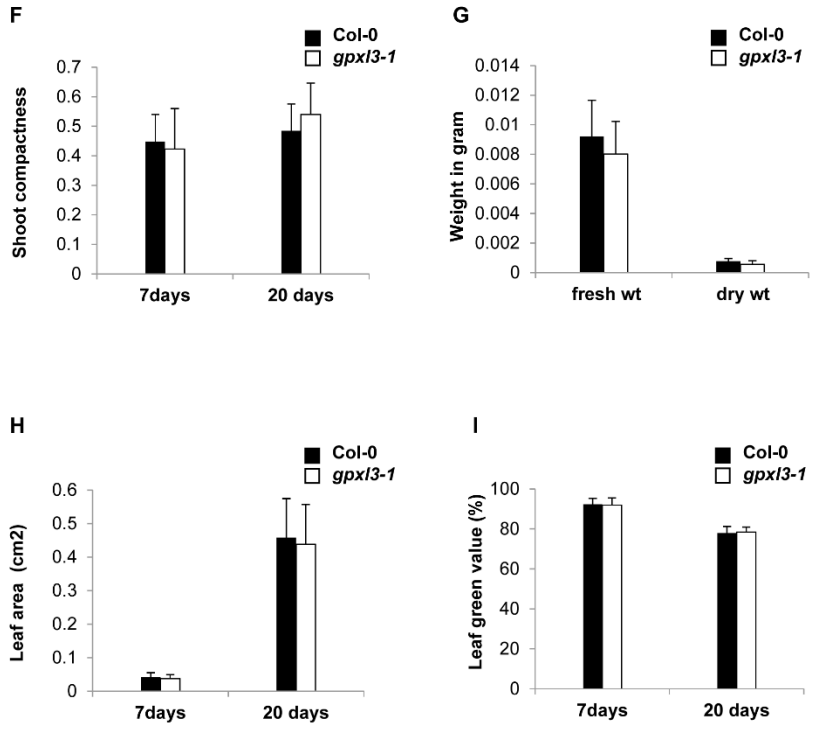

Figure 4.4: Phenotyping of roots, shoots and leaves of *gpxl3-1.* Root, shoot and leaf parameters were measured at two time points, after 7 and 20 days, on MS medium in short day conditions. Plants were grown on germination medium plates placed in a vertical position under white light. The measurements were done with 16 seedlings for each trait.in four separate plates. Graphs A-E show mean values with standard errors of root parameters, F-G show shoot parameters while H and I show leaf traits of *gpxl3-1* compared to Col-0.

4.1.4 *gpxl3* complemented with *GPXL3* or Col-0 overexpressing *GPXL3* have different phenotypes compared to Col-0

Arabidopsis plants constitutively expressing *GPXL3* were generated by floral dip transformation of *gpxl3-1* and Col-0. Transgenic *gpxl3* plants complemented (cpl) with wild type *GPXL3* and Col-0 plants overexpressing (OE) *GPXL3* were obtained by screening with Basta in the F_1 progeny. Five T_3 homozygous transgenic plants were obtained for *gpxl3-1* cpl *GPXL3* while ten overexpression lines were obtained for Col-0. One representative line each from *gpxl3-1* cpl GPXL3 and Col-0 OE *GPXL3* confirmed by SQ-RT PCR were used for further phenotyping experiments (Figure 4.5 (I) ii and iv). Phenotyping of these transgenic plants complemented with/overexpressing wild type

GPXL3 was done by growing them on MS medium and soil along with the *gpxl3* mutant and Col-0 (Figure 4.5(II)). The *gpxl3* mutant has shorter hypocotyl compared to Col-0. Transgenic plants overexpressing *GPXL3* and *gpxl3-1* cpl *GPXL3* grown on MS media showed a growth phenotype with a longer hypocotyl compared to Col-0. This phenotype was significantly more pronounced in the OE *GPXL3* line.

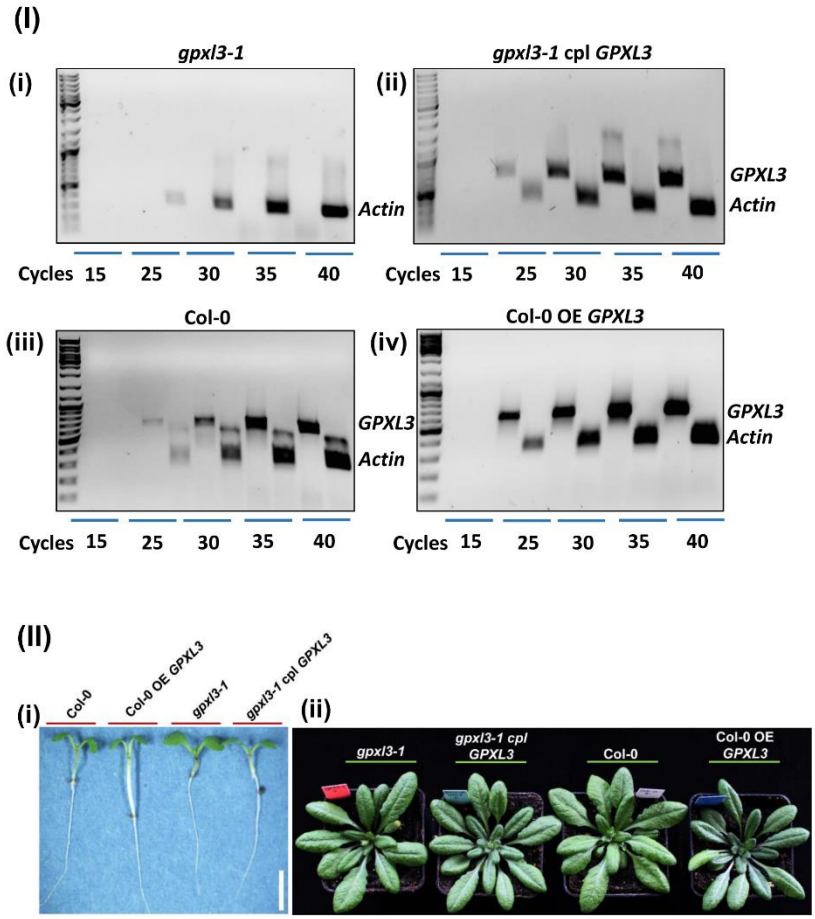

Figure 4.5: (I) Conformation of *gpxl3-1* cpl GPXL3 and Col-0 OE GPXL3 transgenic plants through SQ-RT PCR. Panel (i) represents SQ-RT PCR results of *gpxl3-1* mutant, (ii) represents *gpxl3-1* cpl *GPXL3,* (iii) represents Col-0, and (iv) represents Col-0 OE *GPXL3* **(II) Phenotyping of the *gpxl3* mutant, and transgenic plants** (i) phenotyping on MS medium (ii) phenotyping on soil. *gpxl3* mutant has shorter hypocotyl compared to Col-0. *gpxl3*-1 cpl *GPXL3* and Col-0 OE *GPXL3* has a longer hypoctyl compared to Col-0 on MS medium. In panel (I)(i) scale bar = 5 mm.

4.1.5 *gpxl3* mutants are not more sensitive to mannitol and NaCl stress

To shed light on *GPXL3* involvement in response to hyperosmolar stresses, the germination rate of *gpxl3* mutants and transgenic plants expressing *GPXL3* were assayed on media supplemented with mannitol, a sugar alcohol that is well known as an osmotic stress-imposing agent, and NaCl. Seeds of *gpxl3-1, gpxl3-1 cpl GPXL3,* Col-0 OE *GPXL3* and Col-0 were grown on MS media supplemented with mannitol concentrations ranging from 0 mM-400 mM for seven days. NaCl stress was carried out with increasing concentrations of salt, from 0-250 mM representing mild, moderate and severe salt stress. The lowest mannitol and salt concentration tested, 100 mM and 50 mM respectively, had no significant effects on the germination rate of all plants. As expected, higher mannitol and salt concentrations imposed more severe osmotic stress and led to more profound effects with no germination at all at 400 mM mannitol and 250 mM NaCl. However, no significant differences were observed in the germination rate between Col-0 and the *gpxl3* mutants. And surprisingly, *gpxl3* mutants cpl with *GPXL3* had the lowest germination rate followed by Col-0 plants OE *GPXL3* (Figure 4.6 (I) and (II)).

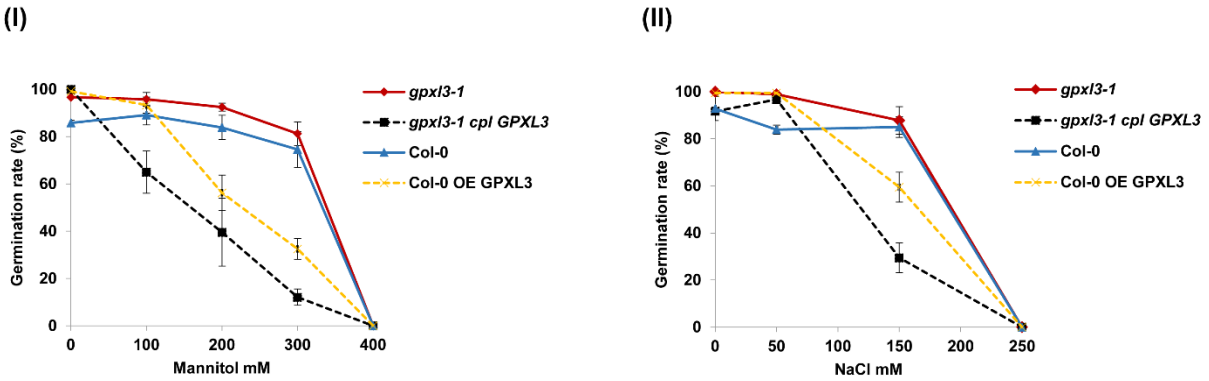

Figure 4.6: Germination rate of *gpxl3* mutants and transgenic plants during mannitol and NaCl stress. The *gpxl3* mutants, Col-0 and transgenic plants cpl with *GPXL3* or OE *GPXL3* were grown for 7 days on plates supplemented with various concentrations of mannitol and NaCl. There was no significant diffrence in the germination rate of *gpxl3* mutants compared to Col-0. However the *gpxl3* cpl *GPXL3* line was more sensitive to the stress inducing agents relative to the mutant. The same trend was observed in the other transgenic line i.e. Col-0 OE *GPXL3*.

4.1.6 *gpxl3* mutants show no correlation with drought stress

To look further into the role of *GPXL3* in abiotic stress responses, the response of the *gpxl3* mutants compared to Col-0 was tested during water deficit conditions. Drought is another form of osmotic stress. Since both salt and water deficit make it difficult for plants to take up water from soil, plants developed several common mechanisms to respond and deal with these stresses, with the phytohormone abscisic acid (ABA) being the central node of convergence between these two pathways (Terry *et al.*, 2015).

Water was withheld from 17 days old soil grown plants and the drought stress was build up over the next 15 days. After withholding water for 5 days, no visible phenotypes for *gpxl3* mutants were observed compared to Col-0 (Figure 4.7(I)). By day 10 after withholding water, all the plants began to display symptoms of dehydration, and on day 16 plants started to wilt. After the completion of drought period, all plants displayed symptoms of dehydration, such as wilting and various degrees of chlorotic leaf discoloration. All plants restored the normal phenotype after rewatering. Similar results were observed for *gpxl3-1* cpl *GPXL3* and Col-0 OE *GPXL3* (Figure 4.7(II)). Taken together these results imply that the *gpxl3* mutants were not significantly more sensitive to drought stress than Col-0. And transgenic plants overexpressing *GPXL3* were not more tolerant to drought stress compared to Col-0. So it can be concluded that *GPXL3* has no apparent role in drought stress.

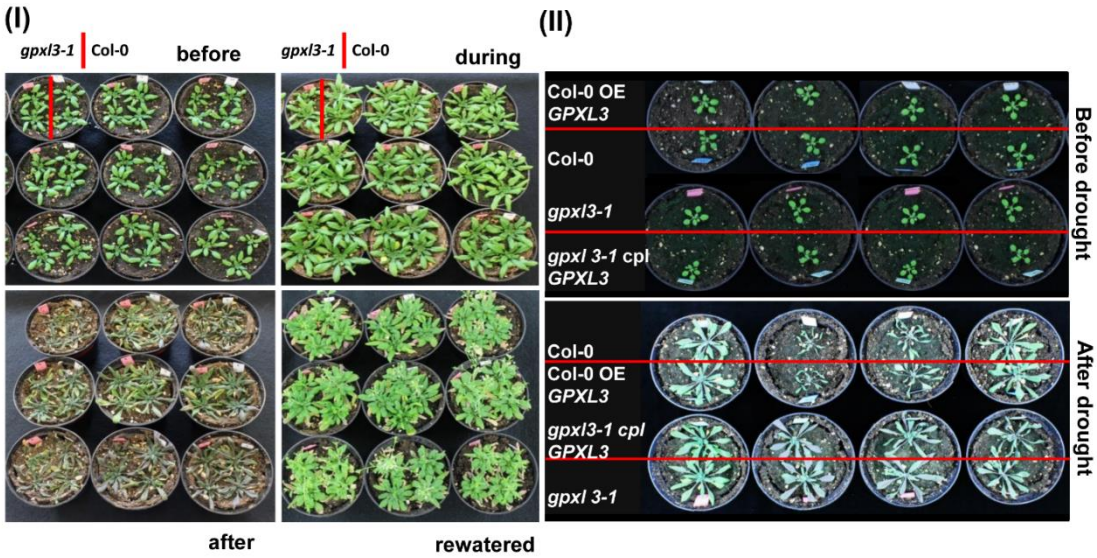

Figure 4.7: *gpxl3* mutants and transgenic plants expressing *GPXL3* compared to Col-0 before and after drought stress. No obvious differences were observed between the *gpxl3* mutants, and transgenic lines expressing *GPXL3* compared to Col-0 after drought stress. (I) Red line drawn in a pot represent the left and right sides of the pot. Where the left side contain the two *gpxl3* mutants and the right side contain two Col-0 plants grown in the same pot.(II) Red lines represent two plants with different genotypes grown in the same pot

4.2 Subcellular localization of C- and N- terminal roGFP2 fused to glutathione peroxidase-like enzymes (GPXLs)

Sequence analysis and predicted subcellular localization of GPXLs

The Arabidopsis genome encodes eight GPXL isoforms, which have been predicted to be localized in different subcellular compartments. Different bioinformatics algorithms, however, lead to different predictions and, where available, experimental evidence is frequently inconsistent with predictions (Figure. 2.5). The amino acid alignment suggests the presence of N-terminal targeting signals for GPXL1, GPXL6, and GPXL7 (Figure 2.4). While the sequences of GPXL1 and 7 have been associated with a strong probability of plastid targeting, the situation is more ambiguous for GPXL6. The highest scoring prediction is mitochondria, but some algorithms also predict the plasma membrane, the plastids and the nucleus as putative targets (Figure 2.5). GPXL3 contains a short 39 amino acids long N-terminal extension compared to GPXL2 and GPXL8 (Figure 2.4). Most bioinformatics algorithms interpret the first 12 amino acids of this extension as a mitochondrial targeting signal to guide the mature protein to the mitochondrial import machinery (Figure 2.5). This, however, contrasts with experimental evidence for the cytosol, the Golgi, and plastids (Helm *et al.*, 2014; Miao *et al.*, 2006; Nikolovski *et al.*, 2012). All other GPXLs are predicted to be localized at the plasma membrane or the cytosol, but again experimental evidence from proteome analyses and protein-protein interaction studies is not always consistent with the predictions (Figure 2.5).

To investigate the subcellular targeting of GPXLs, fusion proteins with roGFP2 were generated and initially expressed transiently in tobacco leaves. roGFP2 can be imaged as a conventional GFP but it has the additional feature of self-indicating reducing and

oxidizing subcellular compartments, which can allow fine-determination of membrane protein topology (Brach *et al.*, 2009).

4.2.1 GPXL1 and GPXL7 are targeted to plastids

In order to study the distribution of GPXL1 and GPXL7 experimentally, C- terminal roGFP2 fusions of the proteins were analysed in two expression systems separately i.e tobacco for transient expression and Arabidopsis for stable transformation by using CLSM. The fusion proteins were first tested by expressing them transiently in tobacco. The plastidic localization of GPXL1 and GPXL7 was confirmed by visualizing chlorophyll autofluorescence. Both the green fluorescence and the red chlorophyll autofluorescence were found to co-localize in the chloroplast in tobacco (Figure 4.8 (I)). Furthermore, green fluorescent thin tubular extensions (stromules) emanating from plastids were observed in some cells which indicated the localization of GPXL1-roGFP2 and GPXL7-roGFP2 fusion proteins specifically in the stroma of plastids. Since stromules lack detectable chlorophpyll, co-localization with chlorophyll autoflourescence is impossible (Kohler & Hanson, 2000).

For stable transformation the same fusion proteins were constitutively expressed in Arabidopsis. In case of non-transformed plants used as control, no green fluorescence was seen in the chloroplasts. Overlay of GFP fluorescence and chloroplast autofluoresence images confirmed that no GFP is detected in the chloroplasts of non-transformed plants (Figure 4.8 (I) A-D). However the transformed plants carrying GPXL1-roGFP2 or GPXL7-roGFP2 co- localized with chlorophyll autofluorescence (Figure 4.8 (II) E-L).

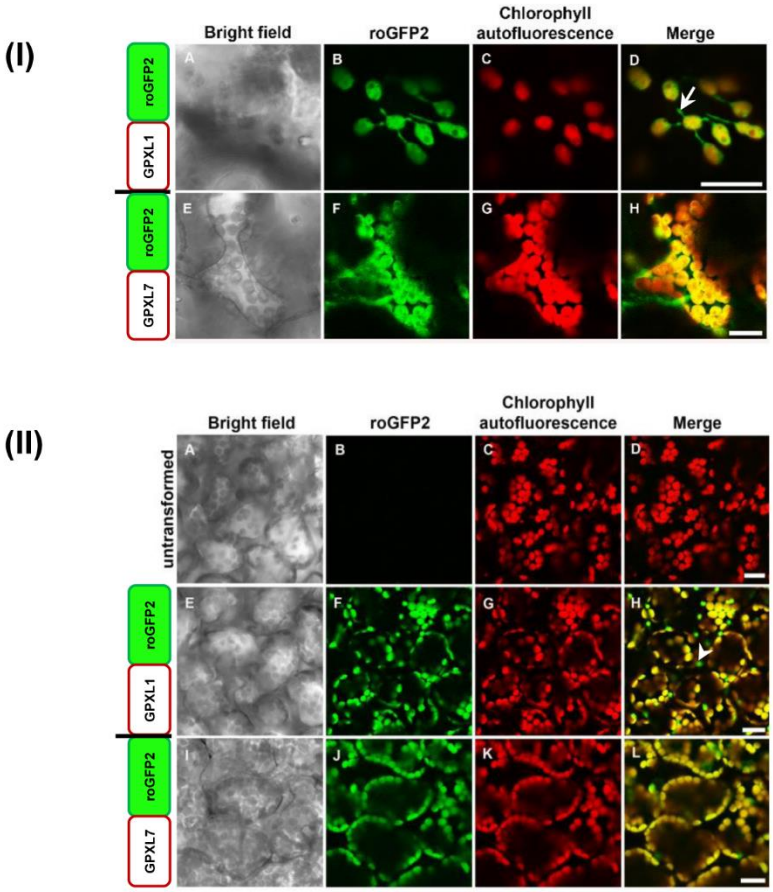

Figure 4.8: (I) GPXL1- roGFP2 (A-D) and GPXL7- roGFP2 (E-H) fusion proteins are co-localize with chlorophyll autofluorescence in tobacco. The arrow indicates stromule of the chloroplast. Scale bars = 20 µm. **(II) Stable expression of GPXL1-roGFP2 (E-H) and GPXL7-roGFP2 (I-L) fusion proteins show co-localization with chrophyll autofluorecence.** Confocal images (A-D) represent control un-transformed plants lacking GFP fusion protein and show no co-localization with chlorophyll autofluorescence. The arrowhead indicates small round green fluorescent particles, which are likely to be proplastids and do not show red chlorophyll autofluorescence. Scale bars = 20 µm.

4.2.2 GPXL2 and GPXL8 are soluble cytosolic proteins

The subcellular localization of GPXL2 and GPXL8 enzymes was examined by generating C- and N- terminal fusions of these proteins and transiently expressing them in tobacco. In cells expressing C- and N- terminal fusion proteins of GPXL2 and GPXL8, fluorescence was localized in the cytosol and nucleus (Figure 4.10 (I)) in a pattern similar to GRX1-

roGFP2 (Figure. 4.9). Fluorescence in nuclei was observed in all fluorescent plants and was not unexpected as size of free roGFP2 (~ 27 kDa) and GPXL2 and GPXL8 (18 and 19 kDa respectively) is below the exclusion limit of the nuclear pore complex (Grebenok *et al.*, 1997; Hanson & Köhler, 2001). For stable transformation, the C- terminal fusion proteins were expressed in Arabidopsis and the results were consistent with the C-terminal fusions in tobacco (Figure 4.10 (II)). Ratiometric analysis of the 405/488 nm ratio showed a low fluorescence ratio indicating complete reduction of the roGFP2 for both C- and N- terminal fusions in tobacco and C- terminal fusion in Arabidopsis expression systems (Figure 4.10 (III)). The redox-sensitive GFP (roGFP2) can be imaged as a conventional GFP but it has the additional feature of self-indicating reducing and oxidizing subcellular compartments (Figure 4.9 (I and II)).

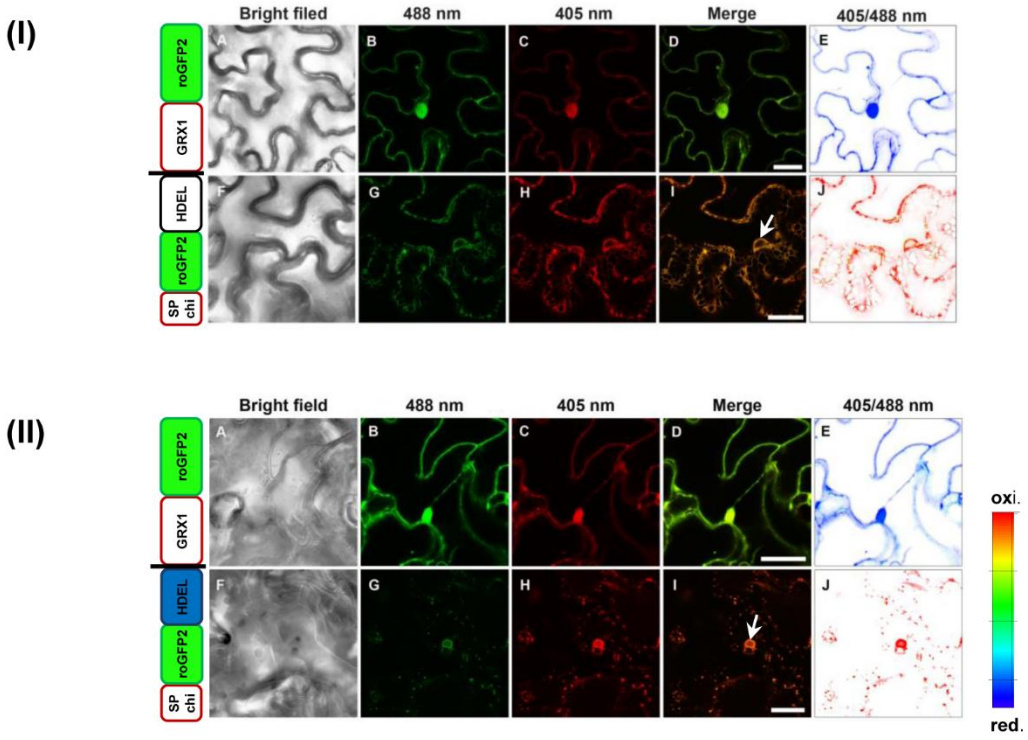

Figure 4.9: (I).and (II) Transient and stable expression of GRX1- roGFP2 (A-E)and SPchi- roGFP2- HDEL (F-J) in tobacco and Arabidopsis, respectively. (A-E) GRX1-roGFP2 targeted to the cytosol used as a reduced roGFP2 control. (F-J) Expression of Chi_{SP}- roGFP2-HDEL in the ER used as a control for oxidized roGFP2. 405/488 nm ratio showed that in case of cytosolic localization roGFP2 is reduced indicated by a blue false

colour image while in case of ER localization roGFP2 is oxidized indicated by a red false colour image. Scale bars = 20 µm.

(I)

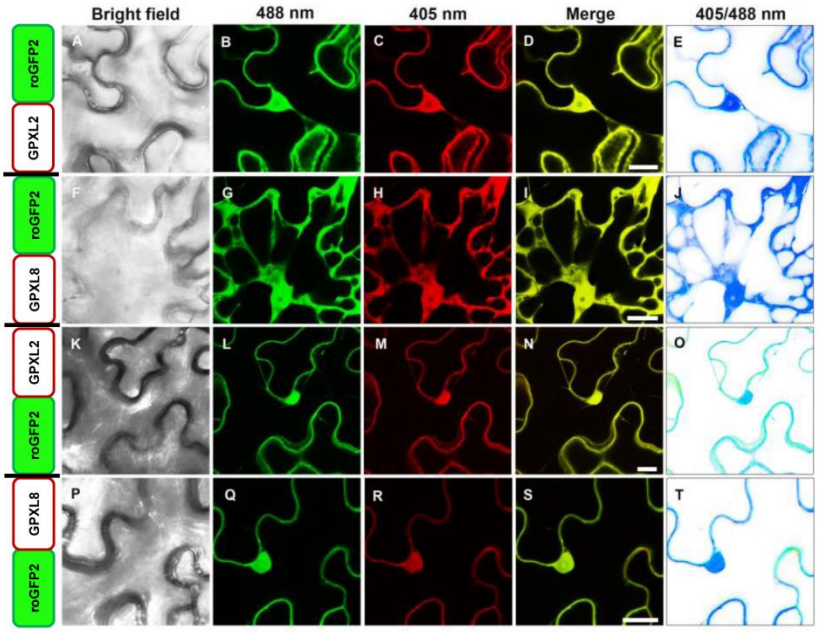

(II)

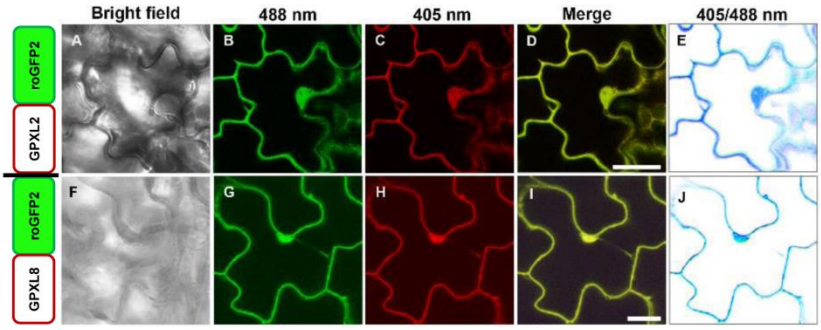

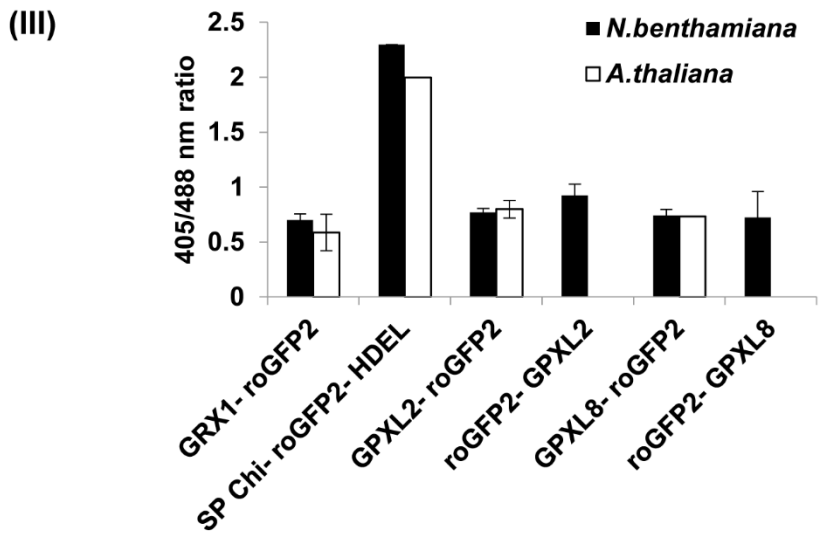

Figure 4.10: (I) Transient expression of C- and N- terminal roGFP2 fused to GPXL2/GPXL8 fusion proteins in tobacco. C- terminal fusions ,GPXL2- roGFP2 (A-E), GPXL8- roGFP2 (F-J) and N- terminal fusions, roGFP2- GPXL2 (K-L) and roGFP2- GPXL8 (P-T), result in cytosolic localization of the fusion proteins in tobacco. The ratio images showed that in both C- and N- terminal fusions the roGFP2 is reduced indicated by a blue or greenish false colour. Scale bars = 20 µm. **(II) Stable expression of C- terminal fusion of roGFP2 to GPXL2/GPXL8 in *Arabidopsis*.** After stable transformation of *Arabidopsis* GPXL2- roGFP2 (A-E) and GPXL8- roGFP2 (F-J)) stay in the cytosol. The ratio images showed that in both C- and N- terminal fusions the roGFP2 is reduced indicated by blue false colour. Scale bars = 20 µm. **(III) Quantitative ratiometric analysis of GPXL2 and GPXL8 fusion proteins.** 405/488 nm ratios of roGFP2 control constructs, GRX1- roGFP2, SP_{chi}- roGFP2- HDEL and N- and C- terminal roGFP2 fusions of GPXL2 and GPXL8 from heterologous and stable expression in tobacco and Arabidopsis, respectively (mean ± SD; *n=5*). High fluorescence ratio values indicate a large proportion of the roGFP2 to be present in the oxidised form while low ratios indicate reduction.

4.2.3 GPXL6 is targeted to mitochondria

The protein sequence of GPXL6 indicates an N-terminal 65 amino acid stretch that is interpreted as a MTS (mitochondrial targeting signal) by most bioinformatics algorithms (Figure 2.4). To explore the subcellular localization of GPXL6 protein, roGFP2 was fused

to the C- and N- terminus of GPXL6 and the respective fusion proteins were transiently expressed in tobacco and observed by confocal microscopy. In case of the C- terminal roGFP2 fusion the fluorescence was found in the cytosol (Figure 4.11 (I) A-E) whereas the N-terminal fusion was targeted to the surface of the ER represented by typical nuclear ring (Figure 4.11(I) F-J). Transgenic Arabidopsis plants were also generated by stable expression of the C- terminal roGFP2 fusion. Fluorescence analyses of the expression of GPXL6- roGFP2 revealed three distribution patterns: the fusion protein was found in the cytosol, in small punctate structures which appeared to be mitochondria and reticulate structures typical for ER in the leaf cells of the transgenic plants (Figure 4.11 (II)). The mitochondrial localization of GPXL6-roGFP2 was confirmed by co-localization with a mitochondrial-marker TMRM (Figure 4.11 (II) A-E). After ratiometric analysis roGFP2 seemed to be reduced in all the three compartments which means that in the case of ER localization the protein is attached to the surface of the ER (Figure 4.13).

It is noteworthy that there is an uneven distribution of GPXL6-roGFP2 fusion protein in these compartments. GPXL6-roGFP2 was predominantly observed in the cytosol, whereas mitochondrial labelling is comparatively much lower than the cytosolic labelling. This phenomenon is termed as ‘eclipsed distribution’ in which the relatively large amount of an isoprotein in one subcellular compartment obscures the detection of the small amount of the other isoprotein in the second location In this case the cytosol, which can be regarded as a default location of non-targeted isoproteins, occupies a several fold larger volume than other compartments thus diluting a significant amount of a dual targeted protein, so that it is easily missed. Furthermore the same protein can be imported poorly into mitochondria, probably due to its inefficient interaction with mitochondrial translocase proteins making its detection very difficult (Regev-Rudzki & Pines, 2007).

(I)

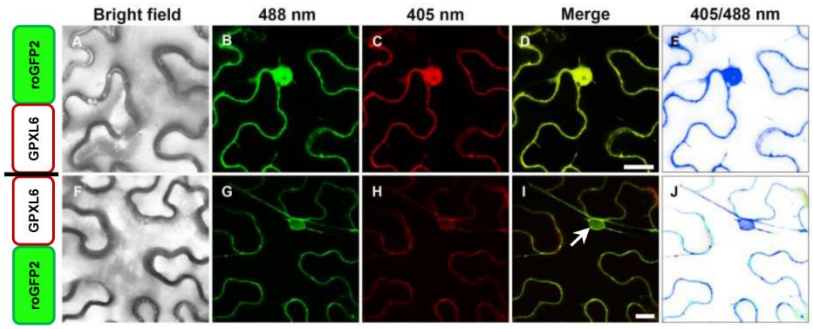

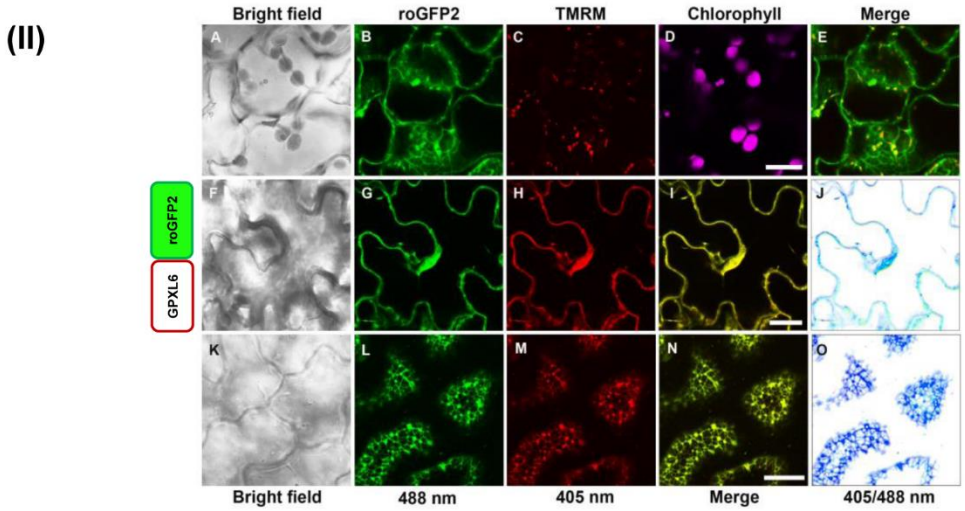

Figure 4.11: (I) Transient expression of C- and N- terminal fusion of roGFP2 to GPXL6 targets the fusion proteins into the cytosol and at the surface of ER respectively in tobacco. Panels (A-D) represent confocal images of C- terminal fusion of roGFP2 to GPX6, while (F-J) represent confocal images of N- terminal fusion of roGFP2 to GPXL6 i.e roGFP2- GPXL6. The ratiometric analysis showed that roGFP2 is reduced in both cases. Scale bars = 20 µm. **(II) GPXL6-roGFP2 is multiply distributed in mitochondria, cytosol and endoplasmic reticulum after stable transformation in Arabidopsis.** (A-E) Confocal images of GPXL6-roGFP2 infiltrated with 0.5 µM TMRM. The second compartment of GPXL6-roGFP2 distribution was cytosol which is characterized by the distribution of roGFP2 in the nucleoplasm and cytosolic rims (F-J). Panels (K-O) represent distribution of GPXL6 on the surface of ER.The blue colour of the ratio images show that roGFP2 is reduced in all the three destination compartments. Scale bars = 20 µm.

4.2.3.1 The first 65 amino acids of GPXL6 fused to roGFP2 are sufficient to target roGFP2 to mitochondria

The MTS of GPXL6 was fused to roGFP2 to assess if the N- terminal 1-65 aa residues of GPXL6 were able to target roGFP2 to mitochondria. The truncated fusion protein was expressed in tobacco and *Arabidopsis* and examined by CLSM. GPXL6$_{1-65}$-roGFP2 showed dual localization with punctate staining pattern like mitochondria and diffused roGFP2 in the cytosol in tobacco (Figure 4.12 (I)). Stable expression of GPXL6$_{1-65}$-

roGFP2 in Arabidopsis resulted in pronounced mitochondrial localization with additional cytosolic and plastidic distribution (Figure 4.12 (II)). Mitochondrial localization was confirmed by co-localization with TMRM (Figure 4.12 (II) A-E). Hence, the N- terminal 65 aa of GPXL6 are sufficient to localize the reporter protein to mitochondria.

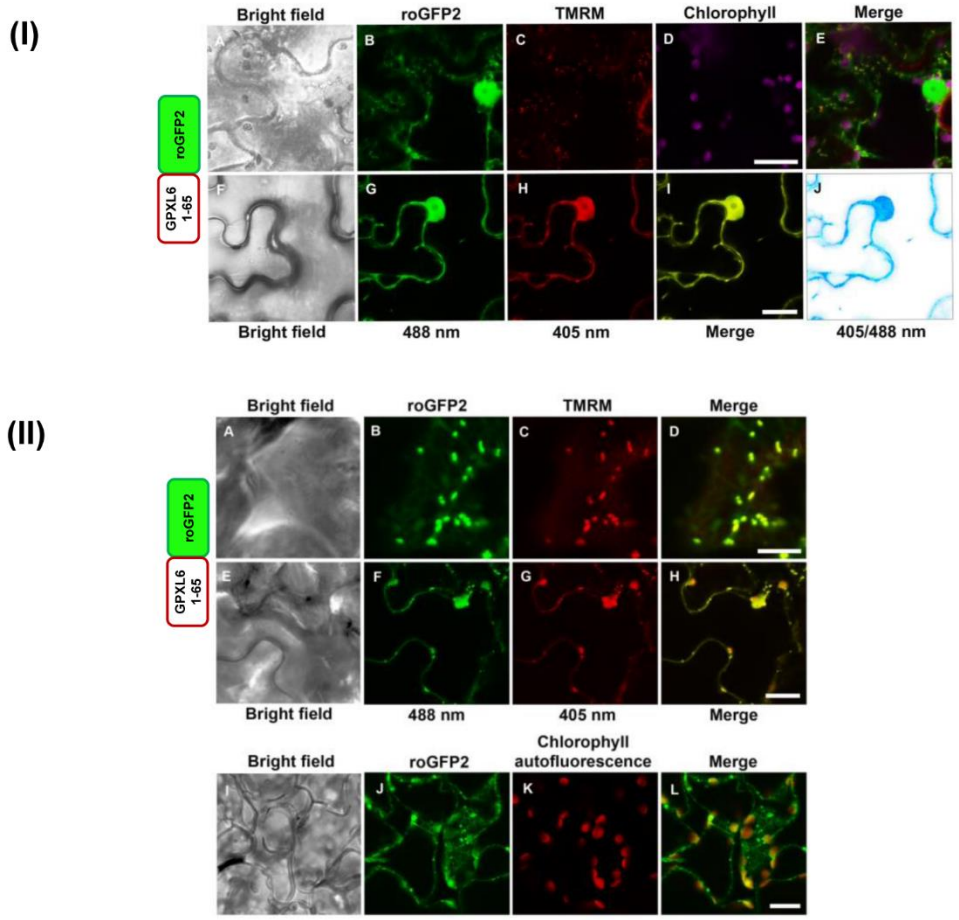

Figure 4.12: (I) The N- terminal first 65 aa of GPXL6 fused to roGFP2 mediate dual targeting to mitochondria and cytosol after transient expression in tobacco. (A-E) represent confocal images of GPXL6$_{1-65}$-roGFP2 co-localization with TMRM, a mitochondrial staining marker. Scale bar =10 µm. (F-J) represent GPXL6$_{1-65}$-roGFP2 expression in Cytosol. Scale bar = 20 µm. **(II) Stable expression of GPXL6$_{1-65}$-roGFP2 in Arabidopsis shows mitochondrial cytosolic and plastidic localization.** Panel (A-E) represent confocal images of GPXL6$_{1-65}$-roGFP2 infiltrated with 0.5 µM TMRM, for co-localization analyses. (F-J) represent GPXL6$_{1-65}$-roGFP2 expressed in cytosol which is

characterized by the distribution of roGFP2 in the nucleoplasm. Panels (I-L) represent distribution of GPXL6$_{1-65}$-roGFP2 in plastids. Scale bar = 20 µm.

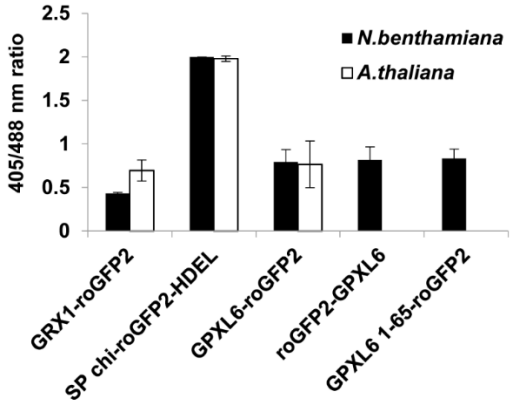

Figure 4.13: Ratiometric analysis of GPXL6-roGFP2, roGFP2-GPXL6, GPXL6$_{1-65}$-roGFP2 expressed in tobacco and Arabidopsis (mean ± SD; n = 5). High fluorescence values indicate oxidised state of roGFP2 and low fluorescence values indicate reduction of roGFP2.

4.2.4 GPXL4 and GPXL5- roGFP2 fusion proteins are anchored at the plasma membrane

The intracellular distribution of GPXL4 and GPXL5 was investigated by fusion of roGFP2 at the C- and N- terminus of these proteins. The infiltrated leaf tissue was viewed by confocal microscopy and fluorescence was observed in the cytosol and nucleus for the C- terminal fusions and the roGFP2 was in the reduced state. In case of N- terminal fusions both fusion proteins labelled endomembranes including the nuclear envelope but roGFP2 was in the reduced state (Figure. 4.14 (I)). To get stable expression, transgenic *Arabidopsis* plants expressing C- and N- terminal roGFP2 fused to GPXL4 and GPXL5 were generated. Surprisingly, GPXL4-roGFP2 and GPXL5-roGFP2 appeared to be anchored to the plasma membrane, as roGFP2 labelling was always confined exclusively to the plasma membrane and roGFP2 was in the reduced state indicating localization on the cytosolic face of the membrane. (Figure 4.14 (II) A-J). Membrane localization of the two fusion proteins was further confirmed by co-localization with plasma membrane marker FM4-64 (Figure 4.14 (III)). When the N- terminal fusion constructs were stably expressed in Arabidopsis, the expression of the fusion proteins was very low but still they

appeared predominantly on endomembranes including the nuclear envelope with roGFP2 facing the cytosol indicated by the blue/greenish false colour of the ratio images (Figure 4.14 (II) K-T).

(I)

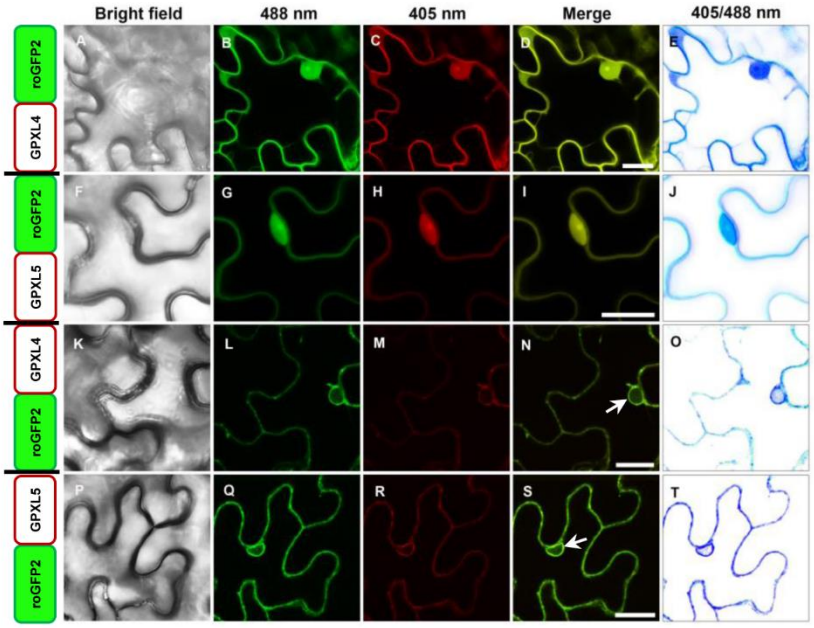

(II)

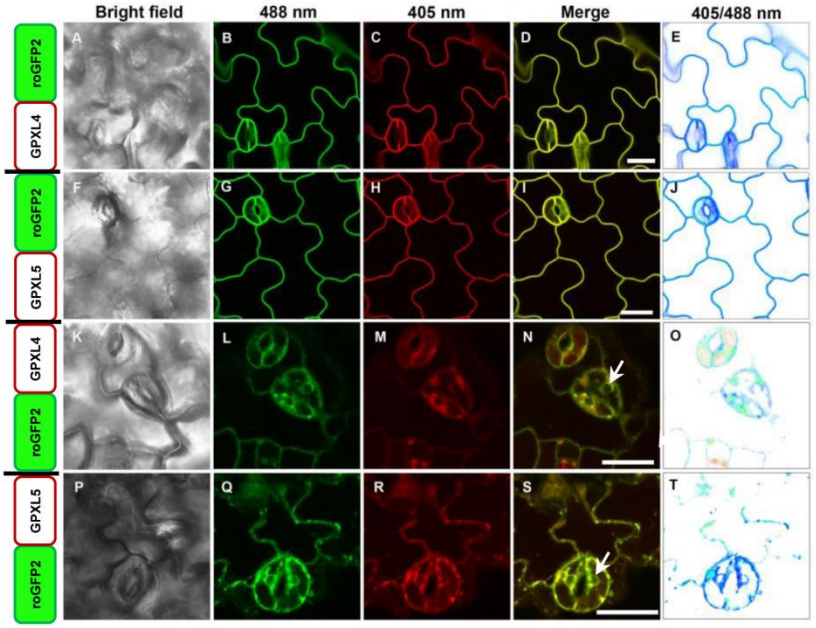

(III)

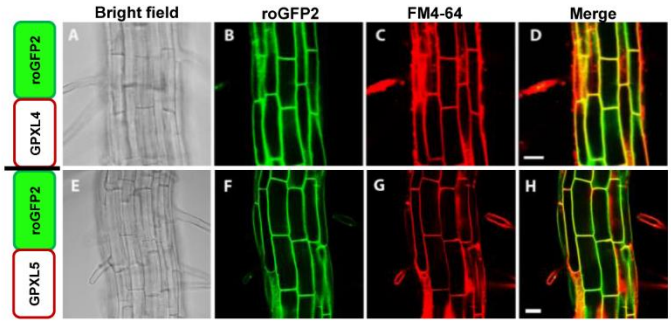

Figure 4.14: (I) C and N- terminal fusion of roGFP2 to GPXL4 and GPXL5 proteins expressed in tobacco. GPXL4-roGFP2 (A-E) and GPXL5- roGFP2 (F-J) fusion proteins results in cytosolic localization in tobacco. roGFP2-GPXL4 (K-O) and roGFP2-GPXL5 (P-T) fusion proteins results in attachment of the proteins to the endomembrane system in tobacco. The nuclear ring typical for ER can be seen for both fusion proteins indicated by arrows. Scale bars = 20 µm. **(II) Stable expression of C- and N- terminal roGFP2 fused to GPXL4 and GPXL5 in Arabidopsis.** GPXL4-roGFP2 (A-E) and GPXL5-roGFP2 fusion proteins (F-J) results in anchoring of the proteins to the plasma membrane evident by the absence of roGFP2 in the nucleoplasm. roGFP2-GPXL4 (K-O)and roGFP2-GPXL5 (P-T) fusion proteins results in attachment of the proteins to the Endoplasmic reticulum. 405 /488 nm ratio showed that in all cases roGFP2 is reduced, indicated by a blue false colour. Scale bars = 20 µm. **(III) Co-localization of GPXL4-roGFP2 (A-D)and GPXL5-roGFP2 (E-H) with plasma membrane staining dye FM4-64 in *Arabidopsis*.** Scale bars = 20 µm.

4.2.4.1 Myristoylation of GPXL4 and GPXL5 is required for association with plasma membrane

Although both proteins are membrane anchored, they do not contain recognizable TMDs. Membrane binding of these two GPXL isoforms seemed to be mediated by myristoylation of the amino terminal domain. The N- termini of both GPXL4 and GPXL5 resemble the classical myristoylation motif MGxxxSxx (Resh, 2016). To address the role of myristoylation in membrane association of GPXL4 and GPXL5, myristoylation was prevented by substituting Gly at the proposed myristoylation site to Ala (G2A). This mutation abolished membrane association of GPXL4 and GPXL5-roGFP2 indicating that

myristoylation is essential for membrane binding. The GPXL4$_{G2A}$-roGFP2 fusion protein was found attached to the surface of the ER indicated by the typical nuclear ring (Figure 4.15: (I) A-E) whereas GPXL5$_{G2A}$-roGFP2 was found in the cytosol and nucleus (Figure 4.15: (I) F-J) after transient expression in tobacco. On the other hand, after stable transformation of Arabidopsis, the GPXL4$_{G2A}$-roGFP2 (Figure 4.15: (I) A-E) and GPXL5$_{G2A}$-roGFP2 proteins were localized in the cytosol and nucleus and the roGFP2 was in the reduced state (Figure.4.15: (II) F-J).

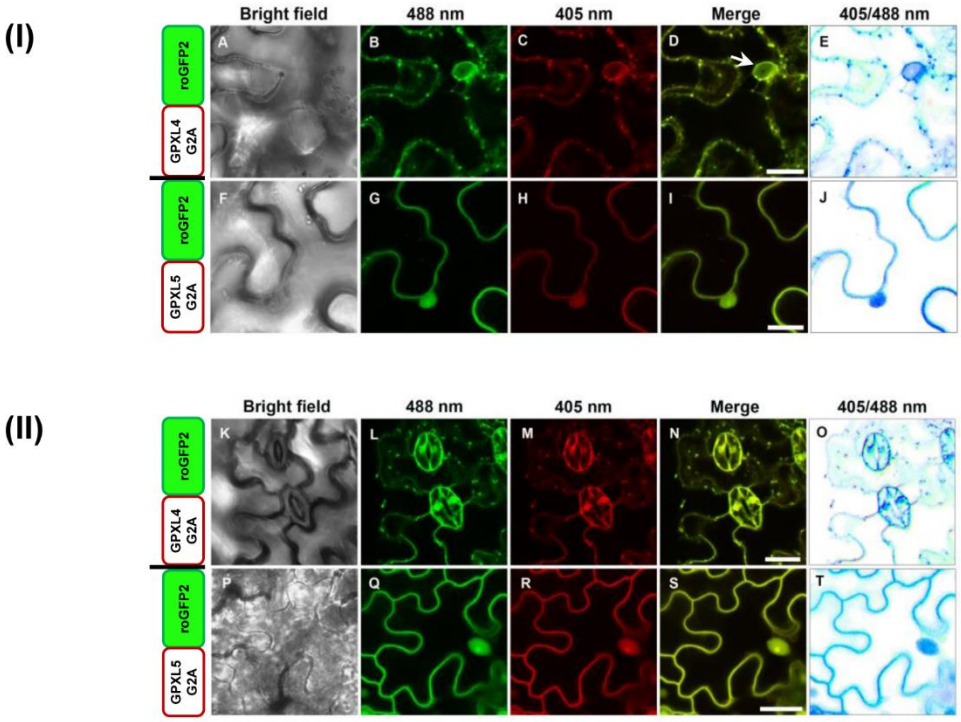

Figure 4.15 (I) Transient expression of GPXL4 $_{G2A}$-roGFP2 and GPXL5 $_{G2A}$-roGFP2 in tobacco. (A-E) G2A mutation of GPXL4 with C- terminal fusion of roGFP2 results in endomembrane localization while (F-J) GPXL5$_{G2A}$-roGFP2 leads to cytosolic and nuclear localization. **(II) Stable expression of the mutated version of GPXL4-roGFP2 (K-O) and GPXL5-roGFP2 (P-T) in Arabidopsis.** G2A mutation of GPXL4 and GPXL5 with C-

terminal fusion of roGFP2 results in cytosolic localization characterized by labelling of nucleoplasm by roGFP2. In case of GPXL4$_{G2A}$-roGFP2 fluorescence can also be seen in the punctate structures. The 405 /488 nm ratio showed that in both cases the roGFP2 is completely reduced indicated by a blue false colour. Scale bars = 20 µm.

4.2.4.2 The first 18 N-terminal amino acids of GPXL4 and GPXL5 are not sufficient to target roGFP2 to the plasma membrane

To further address the localization of GPXL4 and GPXL5, the role of N-termini of GPXL4 and GPXL5 was analysed by fusion of the the first 18 amino acids to roGFP2 and these constructs were expressed in tobacco. After transient transformation in tobacco with GPXL4$_{1-18}$-roGFP2 the fluorescence was localized to the endomembranes including nuclear envelope and the roGFP2 was reduced. GPXL5$_{1-18}$-roGFP2 fusion protein labelled the endomembrane system and nucleoplasm, again with a reduced roGFP2. (Figure 4.16 (I)). Transgenic Arabidopsis lines were also generated that stably expressed GPXL4$_{1-18}$-roGFP2, GPXL5$_{1-18}$-roGFP2. Both GPXL4$_{1-18}$-roGFP2 and GPXL5$_{1-18}$-roGFP2 were localized at the surface of the ER with roGFP2 in the reduced state. (Figure 4.16(II)).

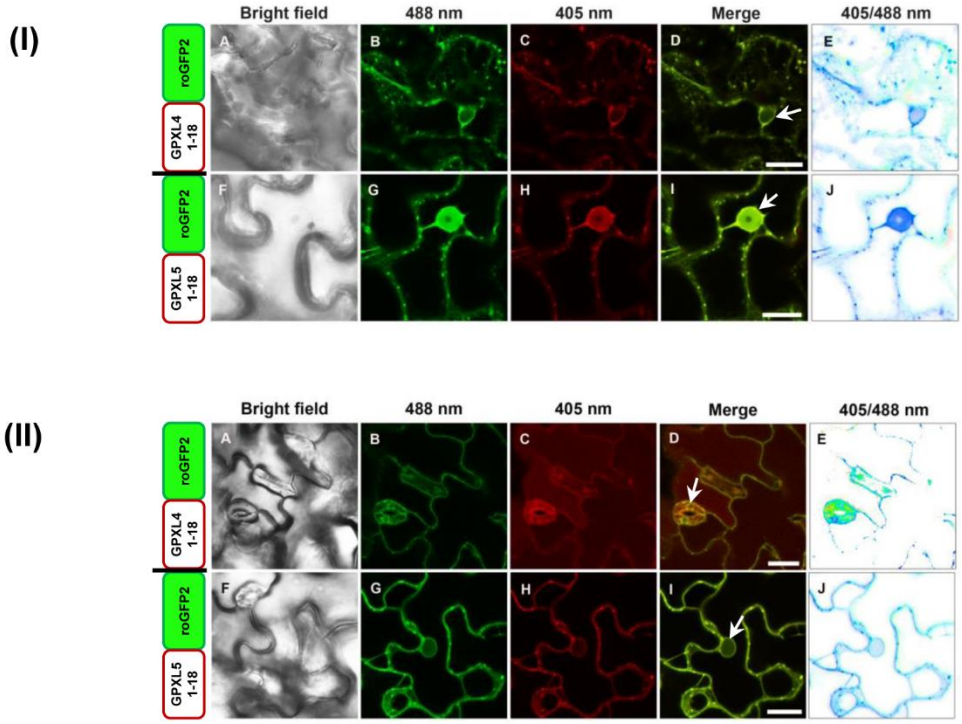

Figure 4.16: (I) Tobacco leaf epidermal cells expressing the constructs GPXL4$_{1-18}$-roGFP2 and GPXL5$_{1-18}$-roGFP2. Panel (A-E) represent GPXL4$_{1-18}$-roGFP2 while (F-J) represent GPXL5$_{1-18}$-roGFP2. Both of the fusion proteins seem to be attached to the surface of the ER. Ratio images showed that the roGFP2 is reduced in both cases indicated by a false blue colour image. Scale bars = 20 µm. **(II) Arabidopsis leaf epidermal cells expressing the constructs GPXL4$_{1-18}$-roGFP2 and GPXL5$_{1-18}$-roGFP2.** Panel (A-E) corresponds to GPXL4$_{1-18}$-roGFP2 which is present on the surface of the ER while (F-J) represents GPXL5$_{1-18}$ -roGFP2 which seems to be attached to the surface of the ER with some labelling in the punctate structures. Ratiometric analysis showed that the roGFP2 is reduced in both cases indicated by a false blue/green colour image. Scale bars = 20 µm.

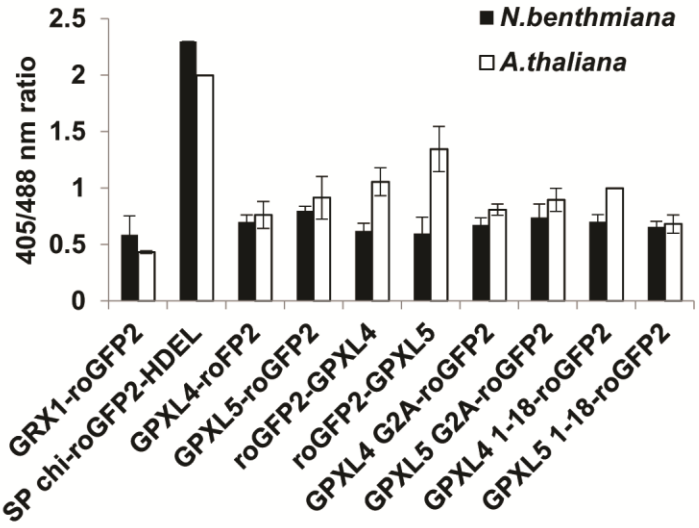

Figure 4.17: Ratiometric analysis of C- and N- terminal roGFP2 fusions of GPXL4 and GPXL5 and their truncated constructs. GPXL4-roGFP2, GPXL5-roGFP2, roGFP2-GPXL4, roGFP2-GPXL5, GPXL4$_{G2A}$-roGFP2, GPXL5$_{G2A}$-roGFP2, GPXL4$_{1-18}$-roGFP2, GPXL5$_{1-18}$-roGFP2, along with roGFP2 controls GRX1-roGFP2 and SP$_{chi}$-roGFP2-HDEL expressed in tobacco *and* Arabidopsis (mean ± SD; n = 5). High fluorescence ratio values indicate oxidized state of roGFP2 while low fluorescence ratio values indicate roGFP2 in a reduced state.

4.2.5 GPXL3 resides in the secretory pathway, predominantly in the Golgi apparatus

The subcellular localization of GPXL3 was investigated by transient expression of C- and N- terminal roGFP2 fusions to GPXL3 (GPXL3-roGFP2 and roGFP2-GPXL3) under the control of 35S promoter in tobacco. Despite prediction of GPXL3 as a mitochondrial protein (Fig. 2.5) no co-localization with the mitochondrial marker TMRM could be found (Figure 4.19 (II) (i)). Confocal microscopy of the C- terminal fusion, i.e. GPXL3-roGFP2, revealed labelling of the motile punctate structures and the nuclear ring, the latter of which is characteristic for the ER (Figure 4.19 (I) A-E). The punctate structures were present near the plasma membrane and were seen also deeper in the cytoplasm. In case of GPXL3-roGFP2 a merge of GFP images collected after excitation with 405 and 488 nm, respectively, resulted in a reddish colour, indicating oxidation of roGFP2 already. Ratiometric analysis showed that the roGFP2 is fully oxidized in case of C- terminal roGFP2 fusion, designating localization of the GPXL3-roGFP2 in the secretory pathway. Transiently expressed roGFP2-GPXL3 in tobacco leaf cells was visualized as dense patches within lobes of the epidermal pavement cells and again a characteristic nuclear ring typical for ER was observed. The ratiometric analysis showed that roGFP2 is indeed reduced in case of N-terminal fusion. Localization of GPXL3 fusion proteins was confirmed by co-localization with Golgi marker ManI-RFP (Figure 4.19 (II) (ii)). Stable expression of GPXL3-roGFP2 (Figure 4.19 (III) A-E) and roGFP2-GPXL3 (Figure 4.19 (III) F-J) in Arabidopsis revealed consistent results similar to the transient expression of the respective constructs in tobacco. To identify appropriate microscope settings allowing maximum resolution between fully oxidised and fully reduced roGFP2, C- and N-terminal fusion constructs of roGFP2 and AtSEC22, a vesicle-SNARE transmembrane protein (TMP) were used (Figure 4.18), as these constructs have been tested by Brach *et* al. (2009) for topology assays.

Taken together the ratiometric analysis of N- and C-terminal fusions of GPXL3 with roGFP2 strongly suggest that GPXL3 is targeted to the ER and/or the Golgi and that the protein contains a TMD which anchors the protein to the membrane. Indeed the peptide sequence of GPXL3 contains an N-terminal extension of 39 amino acids which includes a highly hydrophobic domain between amino acid 19 and 32. Together with few

neighbouring amino acids this domain may constitute a TMD that anchors GPXL3 to the ER membrane (Figure 4.19 (III) (K)). A single-spanning TMD would be consistent with the binary response of N- terminally fused roGFP2 being reduced and C- terminally fused roGFP2 being oxidized (Figure 4.19 (III) (L)).

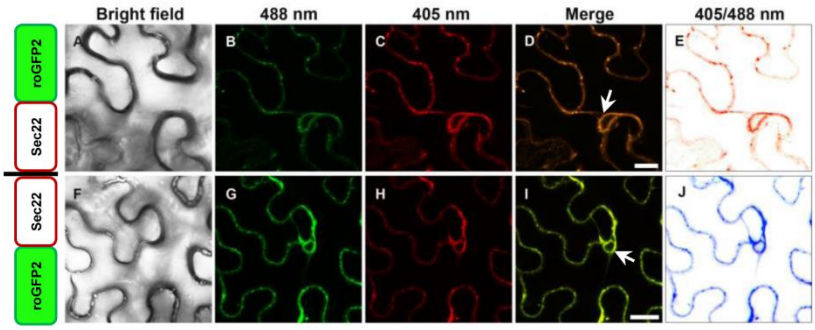

Figure 4.18: Tobacco leaf epidermal cells transiently expressing SEC22-roGFP2 or roGFP2-SEC22. C- and N- terminal roGFP2 fused to SEC22 were used as controls for fluorescence ratio readouts. Scale bars = 20 µm.

(I)

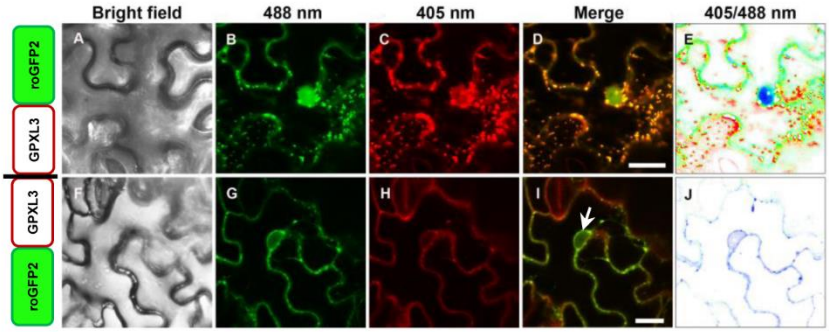

(II)(i)

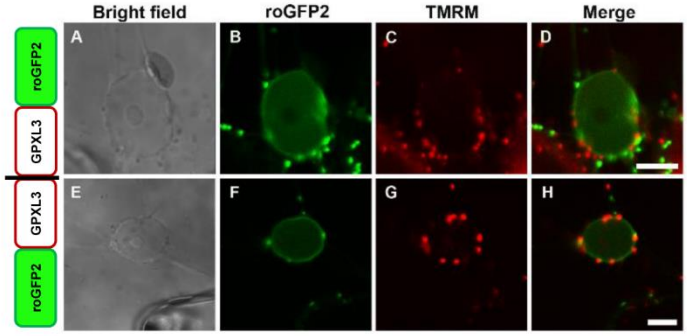

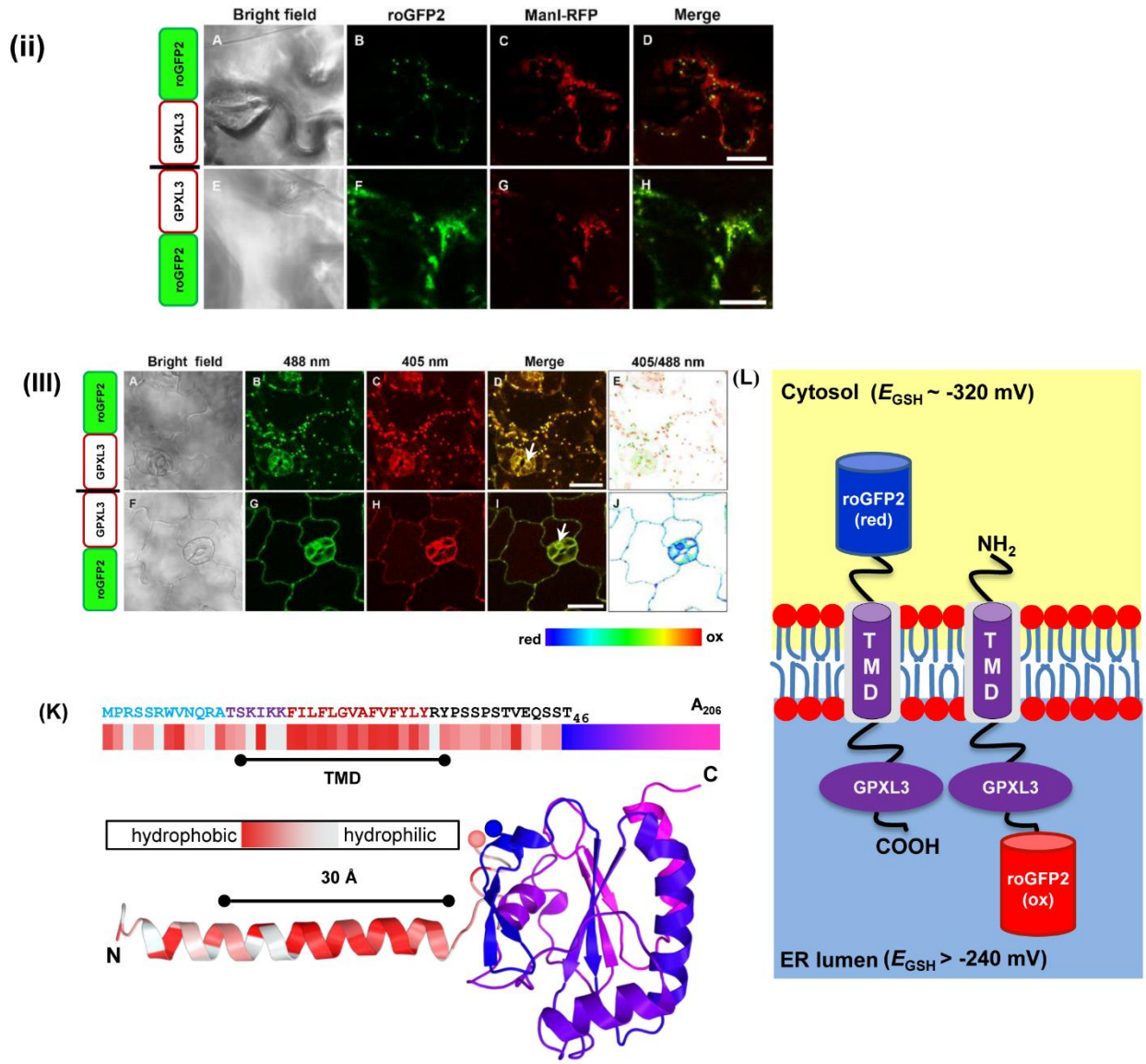

Figure 4.19: (I) Transient expressions of GPXL3-roGFP2 and roGFP2-GPXL3 in tobacco. Panel A-E represents GPXL3-roGFP2 fusion protein which is localized in the secretory pathway predominantly in the punctate structures. The red false colour of the ratiometric image indicates that the roGFP2 reporter was fully oxidised. roGFP2-GPXL3 (F-J) the fusion protein is anchored to the ER membrane and facing the cytosolic side shown by the reduced state of the roGFP2. Arrows represent the characteristic nuclear ring for the ER. Scale bars = 20 µm. **(II) Co-localization of GPXL3-roGFP2 (A-D) and roGFP2-GPXL3 (E-H) with ManI-RFP. (III) Stable expression of GPXL3-roGFP2 and roGFP2-GPXL3 in *Arabidopsis.*** Panels A-E represent GPXL3-roGFP2 fusion protein

which is localized in the secretory pathway, predominantly in Golgi. Ratiometric analysis showed that GPXL3-roGFP2 is oxidised. roGFP2-GPXL3 (F-J) is anchored to the ER membrane and facing the cytosolic side shown by the reduced state of the roGFP2. The reduced state of roGFP2-GPXL3 is indicated by a blue false colour image. Arrows represent the characteristic nuclear ring for the ER. Scale bars = 20 µm. **(K) The AtGPXL3 protein core (residues 46-206) was homologously modelled using the MODELLER tool and oxidized GPXL5 from poplar (PDB code 2P5R) as a template.** The unordered N-terminal extension was added manually to the model hydrophobicity of amino acids is indicated by different shades of red colour. The indicated TMD is the consensus TMD predicted by ARAMEMNON (Schwacke *et al.*, 2003). **(L) Cartoon displaying the topology to GPXL3 fused either N- or C- terminally with roGFP2.**

4.2.5.1 The N- terminal 1-34 amino acids of GPXL3 are capable of localizing the fusion protein in the secretory pathway

The localization of GPXL3 suggests that GPXL3 is a type-II membrane protein with a short N-terminal cytoplasmic tail (CT), a TMD, and a lumenal domain. To determine the role of the N- terminal region of GPXL3 in anchoring to ER membrane, two truncated fusion proteins were generated. First, the N- terminal 34 amino acids (aa1-34) comprising the CT and TMD of GPXL3 were fused to roGFP2 whereas in the second case these domains were deleted from GPXL3. The corresponding truncated proteins were fused to roGFP2 and named as GPXL3$_{1\text{-}34}$-roGFP2 and GPXL3$_{\Delta 1\text{-}34}$-roGFP2-HDEL, respectively. An HDEL motif which is supposed to retrieve ER proteins was also added along with roGFP2 in case of GPXL3$_{\Delta 1\text{-}34}$-roGFP2. These fusion proteins were transiently expressed in tobacco leaf epidermal cells and stably expressed in Arabidopsis. GPXL3$_{1\text{-}34}$-roGFP2 was observed in the punctate structures and nuclear ring typical for ER in both expression systems (Figure. 4.20 (I) and (III) A-E). It is noteworthy that when this truncated construct was expressed in both systems, strong ER labelling was observed unlike the full length GPXL3-roGFP2 in which Golgi labelling was predominant. Further evidence for the localization of GPXL3$_{1\text{-}34}$-roGFP2 was obtained by co-expression with ManI-RFP, where GPXL3$_{1\text{-}34}$-roGFP2 co-localized with ManI-RFP (Figure 4.20 (II) F-I). On the other hand, by removing these two domains, the truncated protein GPXL3$_{\Delta 1\text{-}34}$-roGFP2-HDEL stayed in the cytosol (Figure 4.20 (II) and (III) F-J). After co-expression, the truncated protein

GPXL3$_{\Delta 1\text{-}34}$-roGFP2-HDEL did not co-localize with ManI-RFP and stays in the cytosol. (Figure 4.20 (III) F-I).

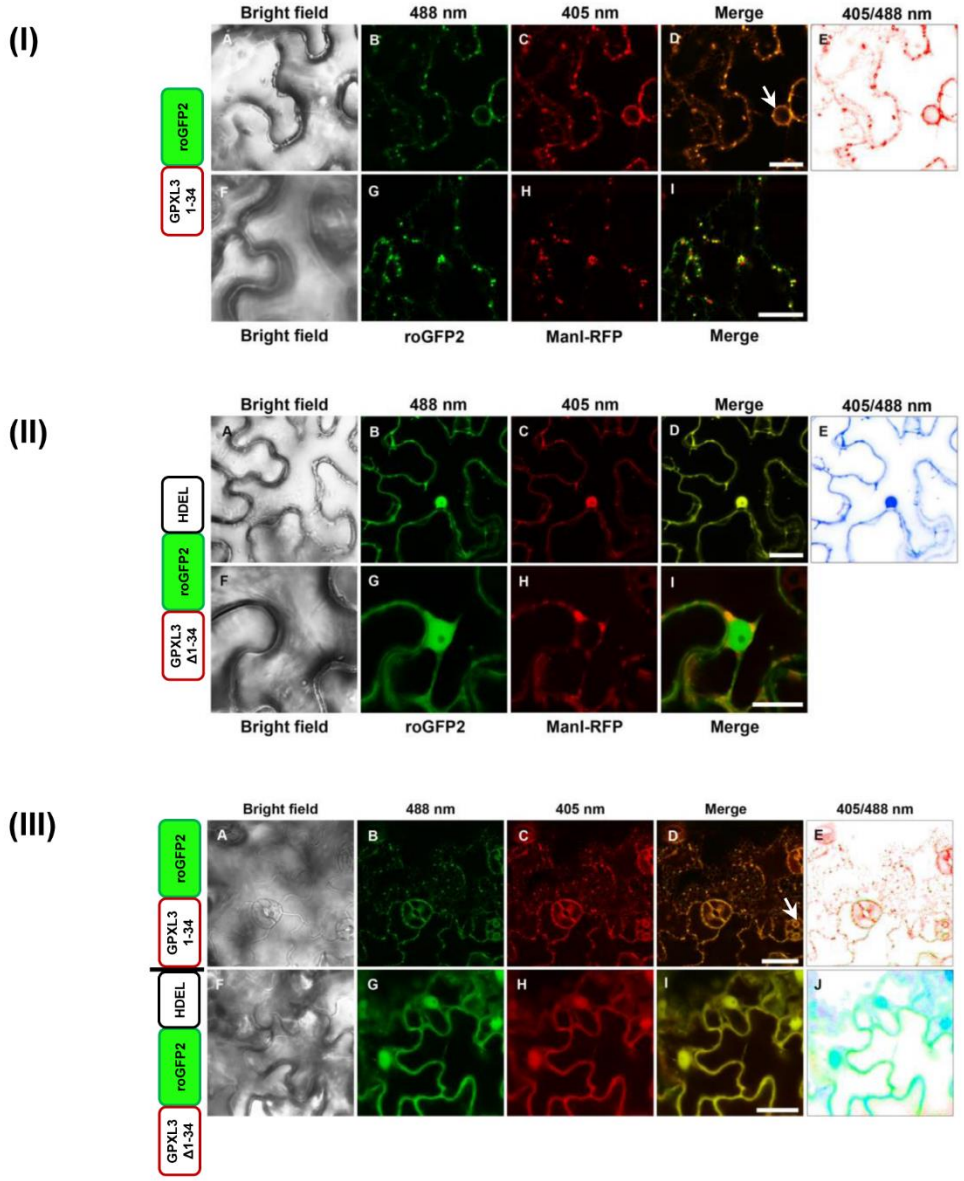

Figure 4.20: (I) Tobacco leaf epidermal cells expressing the construct GPXL3$_{1\text{-}34}$-roGFP2 shows Golgi and ER localization. Images A-E represent the ratiometric imaging of GPXL3$_{1\text{-}34}$-roGFP2. Confocal images F-I represent co-localization of GPXL3$_{1\text{-}34}$-roGFP2 with Golgi marker. Scale bars = 20 µm. **(II) Tobacco leaf epidermal cells expressing the construct GPXL3$_{\Delta 1\text{-}34}$-roGFP2-HDEL stays in the cytosol.** Images A-E represent ratiometric imaging of GPXL3$_{\Delta 1\text{-}34}$-roGFP2-HDEL**.** Confocal images F-I represent co-expression of GPXL3$_{\Delta 1\text{-}34}$-roGFP2-HDEL with ManI-RFP. Scale bars = 20

µm. **(III) Arabidopsis leaf epidermal cells expressing the truncated constructs GPXL3$_{1-34}$-roGFP2 and GPXL3$_{\Delta 1-34}$-roGFP2-HDEL.** A-E represent ratiometric imaging of the construct GPXL3$_{1-34}$-roGFP2 which leads to Golgi and ER localization, the arrow head indicates the characteristic nuclear ring for the ER. (F-J) represent GPXL3$_{\Delta 1-34}$-roGFP2-HDEL which resulted in cytosolic localization. Scale bars = 20 µm.

4.2.5.2 The GPXL3 TMD might be responsible for the retention of GPXL3 in the secretory pathway

Sequence analysis of GPXL3 using the plant membrane protein database ARAMEMNON (http://aramemnon.botanik.uni-koeln.de/) shows the presence of highly hydrophobic 20aa residues (GPXL3$_{14-34}$) at the N- terminal end of the protein. These 20aa are predicted by ARAMEMNON to serve as TMD. To examine the role of the N- terminal region in the retention of GPXL3 in the secretory pathway, the contribution of TMD was investigated specifically if it is responsible for the retention of GPXL3 in the ER and Golgi. A chimeric construct having GPXL3$_{13-34}$ fused to roGFP2 was transiently expressed in tobacco and stably transformed into Arabidopsis. Fluorescence of the truncated construct, GPXL3$_{13-34}$–roGFP2 was detected in small fluorescent spots, that moved through the cytoplasm, and in the nuclear ring and a reticulate network throughout the cytoplasm, in tobacco (Figure 4.21 (I) A-E) and in Arabidopsis (Figure 4.21 (II) A-E). To confirm that the fluorescent spots were Golgi, GPXL3$_{13-34}$ was co-expressed with ManI-RFP in tobacco. Using CLSM, both GPXL3$_{13-34}$ and ManI-RFP co-localized in the merge channel (Figure 4.21 (I) F-I). These results suggest that the 20 amino acid TMD is sufficient to retain GPXL3 in the secretory pathway.

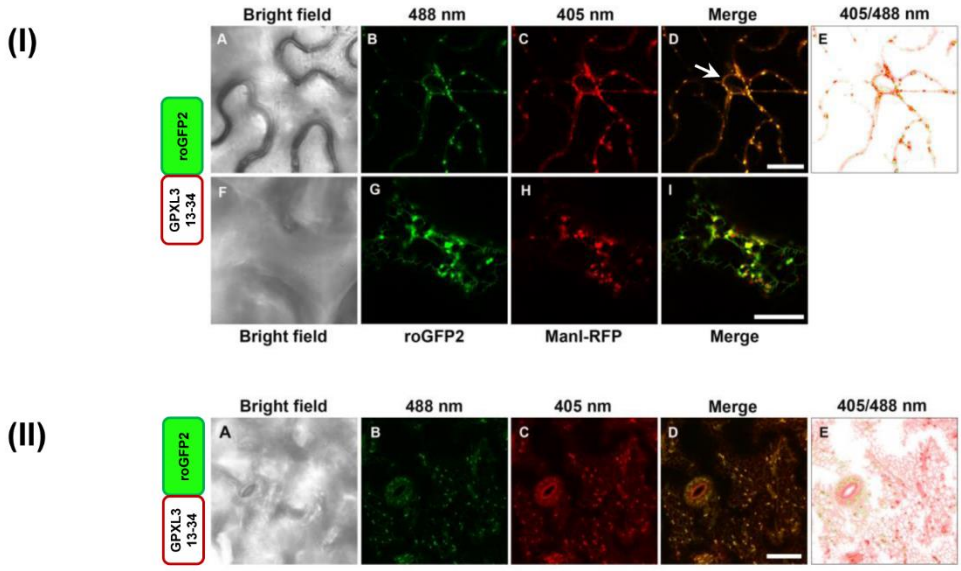

Figure 4.21: (I) Tobacco leaf epidermal cells expressing the construct GPXL3$_{13-34}$-roGFP2 (A-E) shows Golgi and ER localization. Ratiometric analysis showed that the roGFP2 is oxidised indicated by a red false colour image. Panel F-I shows co-localization of GPXL3$_{13-34}$-roGFP2 with ManI-RFP. Scale bars = 20 µm. **(II) Arabidopsis leaf epidermal cells expressing the truncated fusion protein GPXL3$_{13-34}$-roGFP2 (A-E) is targeted to Golgi and ER.** Ratiometric analysis showed that the roGFP2 is oxidised. The arrow represent the nuclear ring, typical for the ER. Scale bar = 20 µm.

4.2.5.3 The CT is not necessary for the retention of GPXL3 in the secretory pathway

To define more precisely the targeting of GPXL3 and to investigate the role of the cytoplasmic domain, CT (i.e aa1-12) was fused to roGFP2 and transiently expressed in tobacco and transformed into Arabidopsis for stable expression. An ER retrieval motif, HDEL, was added to avoid secretion of the protein. When this fusion protein was expressed in tobacco and Arabidopsis, the nuclear ring representing ER and some fluorescent punctate structures were observed. (Figure 4.22 (II) (i) and (ii)). The punctate structures were confirmed as Golgi by co-localization with, ManI-RFP (Figure 4.22 (II) i) (F-I)). Complete removal of CT was carried out by deleting the aa1-12 i.e. GPXL3 $_{\Delta 1-12}$. The truncated protein was fused to roGFP2 and transiently expressed in tobacco. This

truncation resulted in very poor expression but still the Golgi labelling seemed to be predominant with no ER labelling (Figure 4.22 (III)).

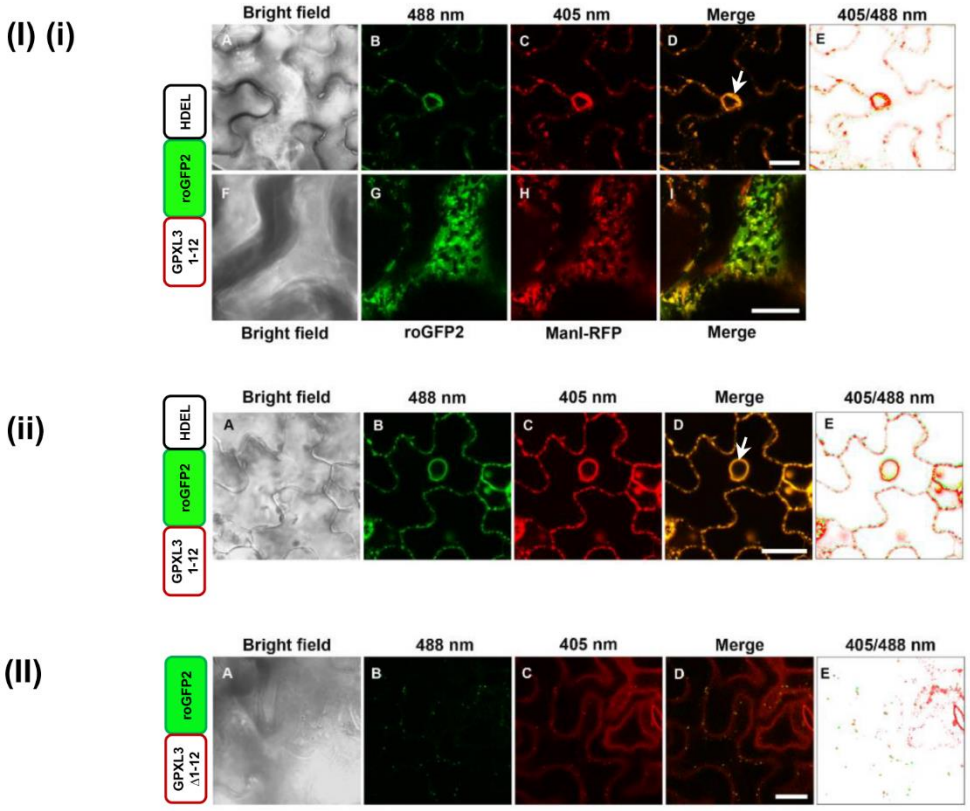

Figure 4.22: (I) (i) Tobacco leaf epidermal cells expressing the construct GPXL3$_{1-12}$-roGFP2-HDEL (A-E) shows ER localization predominantly with some Golgi labelling. Confocal images F-I represent co-expression of GPXL3$_{1-12}$-roGFP2-HDEL with ManI-RFP. Scale bar = 20 µm. **(ii) Images A-E represent GPXL3$_{1-12}$-roGFP2-HDEL in Arabidopsis. (II) Tobacco leaf epidermal cells expressing the construct GPXL3 $_{\Delta 1-12}$-roGFP2 (A-E) shows Golgi staining**. Ratiometric imaging showed that the roGFP2 is oxidised, indicated by a red false colour image. Scale bar = 20 µm.

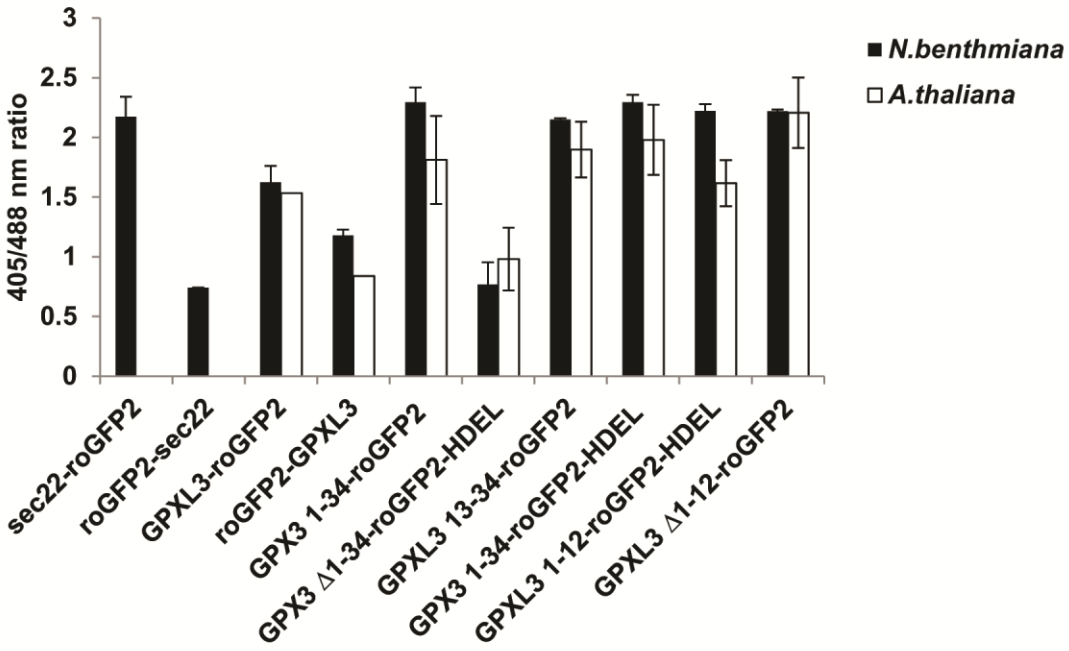

Figure 4.23: Ratiometric analysis of GPXL3 fusion proteins, along with calibration controls SP_{chi}-roGFP2-HDEL and GRX1-roGFP2 expressed in tobacco and Arabidopsis (mean ± SD). High fluorescence ratio values indicate oxidised state of the sensor while low ratio values indicate a reduced sensor.

5 Discussion

5.1 GPXL3 has no obvious role in drought stress responses

Various isoforms of GPXLs have been implicated to have a key role in different biotic and abiotic stress responses in Arabidopsis. However, each isoform seems to respond in a different way and all the enzymes may not be necessarily responsible to act in stress situations (Milla *et al.*, 2003). GPXL enzymes have been reported to play an important role in root architecture and the loss of any of the GPXL isoforms exerted an influence on lateral root density (Passaia *et al.*, 2014).

The results presented in this thesis demonstrate that *gpxl3* mutants exhibit no visible phenotypic differences compared to Col-0 under standard growth conditions, either in soil or on solid MS medium. Furthermore, deletion of GPXL3 has no adverse effects on the number of lateral roots nor on the length of primary and lateral roots, total root length and root branching angles. Similarly, there were no significant differences in the shoot weight and compactness. The leaf area and leaf green value were almost similar for *gpxl3* mutants and Col-0. Similar results have been reported for most of the GPXL isoforms where null mutation in *GPXL*s did not have adverse effects on shoot phenotypes (Passaia *et al.*, 2014). *gpxl5* is an exception to the other mutants as it has been reported to have a defect in female gametophyte development (Pagnussat et al., 2005).

gpxl3 mutants have been shown to be more sensitive to mannitol and drought stress and over expression lines of *GPXL3* have been shown to be more tolerant (Miao *et al.*, 2006). Based on this observation osmotic and NaCl stress was imposed by germination of *gpxl3* mutants, overexpressor lines and compared to Col-0 on mannitol in the course of this work. Surprisingly, *gpxl3* mutants exhibited an almost similar germination rate like Col-0 when exposed to mannitol and salt. On the other hand *GPXL3* overexpression lines had lower germination rates than *gpxl3* mutants during mannitol and salt stress.Likewise, no differences were observed between the *gpxl3* mutants and Col-0 when plants were subjected to drought stress by completely restricting water. Taken together, *GPXL3* does not seem to play a role in osmotic, NaCl and drought stress responses.

5.2 Determining the subcellular localization of GPXLs using roGFFP2 as a reporter

GPXLs are proposed to act as scavengers of H_2O_2 and lipid hydroperoxides and thus may be considered as vital players in the antioxidant defence system of plants. Most available biochemical evidence for plant GPX homologues indicates that the reducing power necessary for these enzymes is provided by the TRX system rather than GSH (Iqbal *et al.*, 2006; Navrot *et al.*, 2006). Different bioinformatics algorithms lead to different predictions regarding subcellular localization of GPXLs in Arabidopsis and experimental evidence available from proteomics data for some isoforms is frequently inconsistent with predictions. The assigning of GPXL proteins to native subcellular locations is an important aspect of defining their function.

Knowing the precise location of a particular protein within a cell can lead to a better understanding of its function, or at the very least, lead to suggested experiments to test function. Information of the subcellular location of proteins can be helpful in different aspects. It can provide useful insights about their functions and may be particularly important for the study of protein-protein interaction. The compartmentation of a protein can help us to better understand complex cellular pathways that regulate biological processes. Studying the subcellular localization of proteins is also helpful in understanding disease mechanisms and for developing novel drugs (Chou *et al.*, 2011).

Genetically encoded tags, are a unique tool that allow direct visualization of cell structures in living organisms. The localization, transport, turnover and aging of proteins can be detected by using FPs fused to proteins of interest (Chudakov *et al.*, 2010). A fluorescence tagging approach was developed to assess the subcellular localization of GPXLs gene family in Arabidopsis through C- and N-terminal roGFP2 fusions. The redox-sensitive roGFP2 can be imaged as a conventional GFP but it has the additional feature of self-indicating reducing and oxidizing subcellular compartments (Brach *et al.*, 2009).

5.2.1 GPXL1 and GPXL7 are plastidic proteins

According to the predictions by SUBAcon, GPXL1 and GPXL7 are localized in the plastids (Hooper *et al.*, 2014). The predicted transit peptide for GPXL1 and GPXL7 consists of 72 and 69 amino acids, respectively (Emanuelsson *et al.*, 2000). As the transit peptide for plastidic targeting is present at the N-terminus, only C-terminal

fusions of these two proteins were generated because they were strongly and consistently predicted for plastids by various subcellular localization prediction algorithms. The confirmation of GPXL1/GPXL7-roGFP2 fusions as plastidic proteins is in agreement with previous evidence for the presence of GPXL1 and GPXL7 in chloroplasts of Arabidopsis (Chang *et al.*, 2009). The proteomic data also revealed the abundance of GPXL1 in the stroma of chloroplasts (Zybailov *et al.*, 2008), at chloroplast envelop (Ferro *et al.*, 2003) and on thylakoid membrane (Peltier *et al.*, 2004). The results presented in this thesis evidently support the predictions from computer algorithm for the localization of GPXL1 and GPXL7 in plastids.

The major sources of H_2O_2 in chloroplasts are the Mehler reaction and plastid terminal oxidase (PTOX)-dependent generation of superoxide (Dietz, 2016). Since the rate of accumulation of H_2O_2 is quite high in chloroplasts of higher plants under normal conditions, the immediate scavenging of H_2O_2 is indispensable to maintain the photosynthetic activity of chloroplasts. The AsA-GSH cycle in chloroplasts is the major defence system for detoxifying H_2O_2 into H_2O and O_2. This cycle involves several enzymes (APX, MDA and DHA reductase, GR), ascorbate and glutathione as reductants (Edreva, 2005). Thiol peroxidases of the PRXs and GPX type, and APXs are the other main peroxide detoxifying enzymes of the chloroplast (Dietz, 2016). Chloroplastic APX isoenzymes have been shown to be sufficient to remove the H_2O_2 generated in the electron transport system in leaf cells under normal conditions. However, under photo-oxidative stress conditions, APX activity is rapidly lost in the absence of AsA, *in vitro* (Yabuta *et al.*, 2002). H_2O_2 entering the chloroplast from the cytosol undergoes stromal scavenging. H_2O_2 that has escaped from thylakoids also can be rapidly detoxified by stromal reactions (Edreva, 2005; Noctor *et al.*, 2004). In addition to H_2O_2 production phosholipid peroxides are also generated by the chloroplast envelope during oxidative stress (La Camera *et al.*, 2004).

The plastidic localization of GPXL1 and GPXL7 point towards a key role of these antioxidant enzymes in the scavenging of H_2O_2 or lipid hydroperoxides in chloroplasts. This putative role of GPXL1 and GPXL7 is supported by a study showing that depletion of these two isoforms compromised the plants ability to tolerate photooxidative stress and enhanced its resistance to virulent bacteria (Chang *et al.*, 2009). As TRXs have been shown to reduce GPXLs by acting as electron donors, TRXy1 is supposed to be the favoured electron donor to GPXL1 *in vivo* (Navrot *et al.*, 2006). To sum up GPXL1

and GPXL7 localized in plastids seem to be potential key players in the detoxification of H_2O_2 and lipid peroxides.

5.2.2 GPXL2 and GPXL8 are soluble cytosolic proteins

The predicted subcellular localization of GPXL2 and GPXL8 indicated that these two isoforms stay in the cytosol but both proteins have been proposed to be secretory as well (Emanuelsson *et al.*, 2000; Margis *et al.*, 2008). Our results showed that C-terminal fusion of GPXL2 and GPXL8 are cytosolic and nuclear proteins. The localization of GPXL8 in the cytosol is in agreement with a previous study which reported GPXL8 in the cytosolic and nuclear fractions of Arabidopsis leaves using a GPXL8 antibody (Gaber *et al.*, 2012).

The main source of H_2O_2 in cytoplasm is the ETC associated with the ER. The reduced forms of cytochrome P450 and cytochrome P450 reductase that catalyse various oxidation reactions, as well as cytochrome b5 and cytochrome b5 reductase that are involved in fatty acid desaturation, transfer electrons to O_2 which leads to the formation of superoxide (Werck-Reichhart & Feyereisen, 2000). A cytosolic form of SOD can convert O_2^- to H_2O_2. However, the cytosol cannot be considered as a major source of H_2O_2 in plant cells, but it may rather act as a sink for H_2O_2 leaking from other cellular compartments (Slesak *et al.*, 2007). H_2O_2 from various other sources such as chloroplasts, mitochondria, ER and peroxisomes can leak into the cytosol (Neill *et al.*, 2002). H_2O_2 being a neutral solute can be transported through specific membrane aquaporin homologues of the tonoplast intrinsic protein (TIP) and plasma membrane intrinsic protein (PIP) families (Bienert *et al.*, 2007). H_2O_2 and other ROS that leak out in the cytoplasm are easily removed by the activity of ROS-scavenging systems such as AsA-GSH cycle, PRXs and TRXs (Petrov & Van Breusegem, 2012). GPXL2 has been shown to be linked to cytosolic SOD1 via the linker protein DJ-1 (Xu *et al.*, 2010). Based on this interaction a function in channelling H_2O_2 generated by SOD1 to GPXL2 for further reduction has been proposed. Eight isoforms of TRXh have been reported in the cytosol of *A. thaliana* (Meyer *et al.*, 2001). Potentially these TRXs can act as hydrogen donors to reduce GPXL2 and GPXL8.

5.2.3 The target peptide of GPXL6 seems to be sufficient to target roGFP2 to mitochondria

The exact localization of GPXL6 has been unclear due to contradicting results from MS-based proteome analysis experiments. Published results include localization at the

plasma membrane (Marmagne *et al.*, 2007; Marmagne *et al.*, 2004), in the cytosol (Ito *et al.*, 2011; Zargar *et al.*, 2015), and in mitochondria (Brugiere *et al.*, 2004; Yoshida *et al.*, 2013). Expression of GPXL6-roGFP2 revealed that this protein is distributed in mitochondria, cytosol along with some ER membrane labelling. Targeting of GPXL6-roGFP2 to membranes of the secretory pathway most likely resulted from artificial interaction of the protein with unknown components of the endomembrane system Partial targeting of GPXL6-roGFP2 to mitochondria indicated the presence of a mitochondrial targeting peptide. Indeed, the target peptide $GPXL6_{1-65}$ on its own was found sufficient for targeting roGFP2 to the mitochondrial matrix.

The distribution between subcellular compartments can be achieved by one of several routes: (1) through utilization of alternative transcription or translation start sites (Figure 5.1) (2) by an ambiguous targeting signal directing a protein to two locations, (3) via two different targeting signals within one polypeptide, (4) accessibility of targeting signals (5) via retrograde translocation (6) and finally, fully translocated proteins may be redistributed as a result of leakage out of an organelle that has lost its membrane integrity (Carrie *et al.*, 2009; Yogev & Pines, 2011). GPXL6 possesses two in frame start codons and thus alternative translation in this case may lead to the synthesis of two translation products: a long one (from ATG1) harbouring a mitochondrial-targeting signal, and a short one (from ATG64) that lacks the functional signal. Accordingly, each of the translation products will be localized differently; the full-length polypeptide will be found predominantly in mitochondria while the short translation product, which lacks the mitochondrial targeting signal, would then be found most likely in the cytosol. Such an example of alternative translation initiation is found in mice Gpx4, which is synthesized as a long form (23 kDa) and a short form (20kDa). The long form of Gpx4 is targeted to the mitochondria because it has a mitochondrial signal peptide. The short form of Gpx4 has been found in the cytosol, nucleus, and ER (Liang *et al.*, 2009)

The putative localization of GPXL6 in mitochondria and the cytosol has been reported in Arabidopsis (Milla *et al.*, 2003) and explained by an assumption that it may encode mitochondrial and cytosolic enzymes by alternative initiation. The mitochondrial localization of GPXL6 is also in agreement with the identification of GPXL6 in the proteome of mitochondria in Arabidopsis (Yoshida *et al.*, 2013).

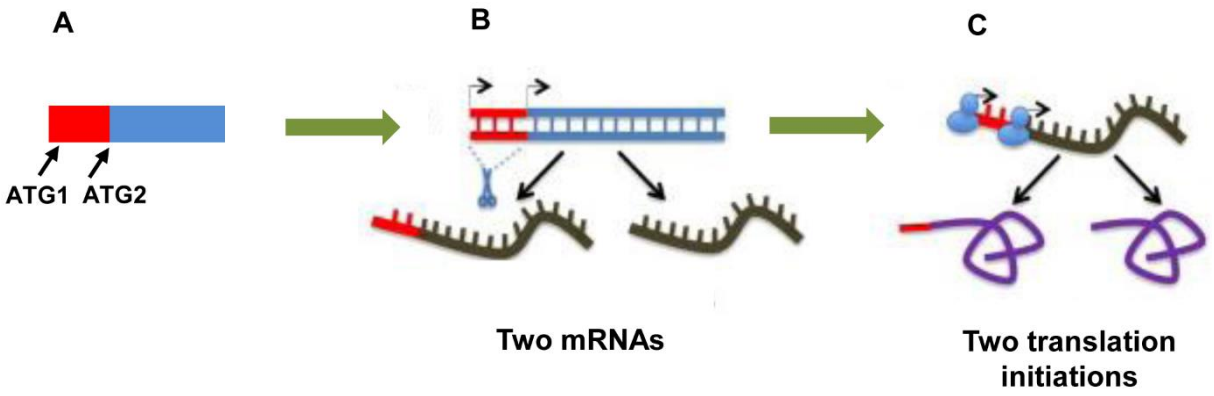

Figure 5.1 Dual targeting mechanisms based on two translation products. (A) Two genes, of which only one encodes a mitochondrial-targeting signal (MTS). (B) Two mRNAs from a single gene of which only one encodes an MTS; obtained either by alternative transcription initiation (arrows) or by splicing (scissors). (C) Two proteins from a single mRNA of which only one harbours the MTS; obtained by alternative translation initiation (ribosomes attached at initiation codons). The DNA, RNA and polypeptide specifying the MTS are coloured in red. Figure adopted from (Yogev & Pines, 2011)

About 1% of mitochondrial O_2 consumption leads to H_2O_2 production in plants (Møller, 2001). The alternative oxidase (AOX) competes with the cytochrome bc1 complex for electrons acting as a first line of defence and thus may help to reduce ROS production in mitochondria. To counteract oxidative stress in mitochondria, mitochondrial AOX and mitochondrial SOD (Mn-SOD) are very crucial (Das & Roychoudhury, 2014). Furthermore, plant mitochondria contain enzymes of the AsA-GSH cycle, PRXs and TRXs for additional possible defence strategies. The cytosol, peroxisomes or even chloroplasts can potentially facilitate scavenging of plant mitochondrial synthesized H_2O_2. However, plant mitochondria need their own defences against H_2O_2 in plants (Chew *et al.*, 2003). Gpx4 in mammalian mitochondria, has been found as the main enzyme for removing phospholipid hydroperoxides (Imai & Nakagawa, 2003). Beside AsA-GSH cycle, PRX-IIF and APX the most suitable candidate for direct detoxification of H_2O_2 or preventing lipid peroxidation in mitochondria would be GPXL6 using TRX as an electron donor system. The mitochondrial potato homologue of AtGPXL6 has been found to be a potential target of TRX (Balmer *et al.*, 2004). In Arabidopsis, two TRX proteins (TRXo1 and TRXo2) have been reported in mitochondria (Laloi *et al.*, 2001) that can potentially act as physiological electron donor for GPXL6.

5.2.4 GPXL4 and GPXL5 are anchored to the plasma membrane

The predicted subcellular location of GPXL4 is cytosol while GPXL5 is expected to be localized at the plasma membrane (Emanuelsson *et al.*, 2000). However, both of the GPXL4/GPXL5-roGFP2 fusions turned out to be associated with the plasma membrane in Arabidopsis. The differential expression patterns for GPXL4-roGFP2 and GPXL5-roGFP2 in tobacco and Arabidopsis may suggest that this second signal is based on a specific protein-protein interaction for which the second interaction partner may be available only in the homologous expression system. The mislocalization of GPXL4/GPXL5 fusion proteins to endomembrane system in case of N-terminal fusion may be due to the presence of an N-terminal tag that could possibly hinder the targeting signals (Hanson & Köhler, 2001). A G2A mutation abolished membrane association of both proteins indicating that myristoylation was essential for plasma membrane binding. The distribution of GPXL4$_{1-18}$-roGFP2 and GPXL5$_{1-18}$-roGFP2 fusion proteins on the endomembranes may be due to the weak interaction of the myristate that allow the modified protein to cycle between multiple intracellular membranes (Resh, 2016). To sum up, plasma membrane targeting of GPXL4 and GPXL5 proteins seems to be conferred by myristoylation at their N-termini.

Formation of phospholipid hydroperoxides occurs frequently in the plasma membrane, particularly under stress situations leading to increased activity of superoxide generating NADPH oxidases (Gupta *et al.*, 2016). The subcellular localization of GPXL4 and GPXL5 raises a possibility for a role of these two peroxidases as scavengers of lipid hydroperoxides which are produced in the plasma membrane. Thus, TRXh9 which is also supposed to be anchored to the plasma membrane through myristoylation (Meng *et al.*, 2010) and cytosolic TRXs can potentially serve as a reductant for GPXL4 and GPXL5 in the detoxification of lipid hydroperoxides.

5.2.5 GPXL3 is a resident of secretory pathway

Analysis of GPXL3 by several bioinformatics algorithms lead to contradictory results about its localization. Most of these tools showed strong prediction of GPXL3 for mitochondria. C- and N-terminal roGFP2 fusions of GPXL3 revealed that this isoform resides in the secretory pathway. These results indicated that the N-terminus of GPXL3 faces the cytosolic side of the ER membrane. This result is in contrast with reports of GPXL3 in the plastid proteome (Helm *et al.*, 2014) and localization of GPXL3-GFP fusions in the cytosol after transient expression in Arabidopsis protoplasts (Miao *et al.*,

2006). The orientation of GPXL3 in the secretory pathway suggested that GPXL3 is a type II membrane protein having a TMD. Type II integral membrane proteins are the proteins that consist of a short cytoplasmically orientated N-terminus (typically between 5-20 amino acids in length) and a single TMD (Banfield, 2011).

The localization of the N-terminal region of GPXL3 ($GPXL3_{1-34}$-roGFP2) in the ER and Golgi revealed that the first 34aa are sufficient for targeting GPXL3 to the secretory pathway. Furthermore, deletion of the N-terminal 34aa inhibited the targeting of the fusion protein to the secretory pathway and the protein stayed in the cytosol. Localization of the TMD ($GPXL3_{13-34}$) fused to roGFP2 illustrated that the TMD ($GPXL3_{13-34}$) alone was sufficient for the retention of GPXL3 in the secretory pathway. However the expression of the chimeric protein ($GPXL3_{13-34}$) lead to equal ER and Golgi staining in tobacco and Arabidopsis. This result differs from full length GPXL3-roGFP2 for which predominant labelling of Golgi was observed. To conclude, these results suggest that GPXL3 contains a TMD that is sufficient to prevent the protein from leaving the secretory pathway behind the Golgi.

Secretory and membrane proteins synthesized in the rough ER need to undergo proper folding and modification, such as carbohydrate addition and disulfide bond formation, in the ER before they are transferred to their final destinations (Ozgur *et al.*, 2014). The formation of disulfide bonds requires oxidizing power, the source of which has been found to be ER thiol oxidases (EROs) and quiescin sulfhydryl oxidases (QSOXs) (Aller & Meyer, 2013). Both enzymes use molecular oxygen as the terminal electron acceptor and produce H_2O_2 as a toxic by-product which needs to be detoxified to avoid possible deleterious effects. Apart from the constitutive production of ERO-derived H_2O_2, other alternative sources are also involved in the formation of ROS in the ER. For example, jamming of the ER with unfolded proteins, which results in ER stress and can lead to ROS production (Delaunay-Moisan & Appenzeller-Herzog, 2015). The H_2O_2 generated might be trapped in the ER since biomembranes are considered to be almost impermeable for H_2O_2 unless appropriate facilitators are available (Bienert *et al.*, 2007; Konno *et al.*, 2015). With the presumed inability of H_2O_2 to leave the ER lumen for cytosolic detoxification, efficient systems for decomposition of H_2O_2 are, thus, necessary within the ER.

In mammals, detoxification of H_2O_2 occurs by two types of ER peroxidases, Gpxs (Gpx7 and 8) and a Prx (Prx4). None of the PRXs encoded in Arabidopsis genome are

targeted to ER (Dietz *et al.*, 2006). However, GPXL3 in the secretory pathway can be considered as a good candidate for optimization of EROs/PDI oxidative folding pathway in Arabidopsis. GPXLs have been shown to reduce H_2O_2 or lipid hydroperoxides using TRX (Iqbal *et al.*, 2006; Navrot *et al.*, 2006) but so far, no ER-resident TRX has been identified. However, PDIs belong to the thioredoxin-family and share structural homology with TRXs (Zhang *et al.*, 2014). Thus PDIs may serve as an electron donor for GPXL3 in the secretory pathway. Taken together, GPXL3 may fulfil an important physiological role in EROs/PDI oxidative protein folding pathway by utilizing ERO-derived H_2O_2 via an EROs/GPXL3/PDI triad.

On the other hand, if GPXL3 is mainly localized in Golgi then QSOX can be considered as a potential source of H_2O_2.. The presence of a TRX- and Erv-like domains allows QSOX to efficiently oxidise proteins (Bulleid & Ellgaard, 2011). In Arabidopsis, so far no QSOX isoforms have been identified in the Golgi but the distribution of proteins of the QSOX family in ER and Golgi in humans indicate that new pathways for disulfide bond formation outside the ER remain to be investigated (Thorpe *et al.,* 2002). This assumption is supported by the presence of hQSOx1 in Golgi which is able to complement the function of Ero1 in yeast (Chakravarthi *et al.*, 2007). It is likely that QSOX are involved in the later stages of maturation and maintenance of disulfide-bridged proteins (Thorpe *et al.*, 2002). The byproduct of the reaction of QSOX with substrate proteins will be H_2O_2. Potentially GPXL3 present in Golgi can subsequently detoxify this harmful substance into H_2O.

Conclusion

Based on the results presented in this thesis, a working model summarizing the distribution of GPXLs and the putative roles speculated for each GPXL in different subcellular compartments has been proposed (Figure 5.2). Moreover, the production of H_2O_2 at different subcellular sites as well as the detoxification systems present in these compartments along with GPXLs have been presented in the working model. H_2O_2 is produced at several subcellular sites in the cell such as chloroplasts, mitochondria, ER, plasma membrane, peroxisomes, apoplast and cell wall. H_2O_2 can also leak into the cytoplasm from the ROS generating compartments. ROS above a certain threshold can cause lipid peroxidation in membranes of the cell and organelles which is damaging for cell (Sharma *et al.*, 2012). Detoxification of H_2O_2 and lipid hydroperoxides occurs by the activity of ROS-scavenging pathways in the cell that are able to scavenge it. The antioxidant system in plants comprises CAT and APX in peroxisomes, TRX, PRX, APX and the Asc-GSH cycle in cytosol, plastids and mitochondria (Petrov & Van Breusegem, 2012). To sum up, the GPXLs distributed throughout the cell except peroxisomes and vacuole, present an excellent redundant system for the scavenging of H_2O_2 and lipid hydroperoxides.

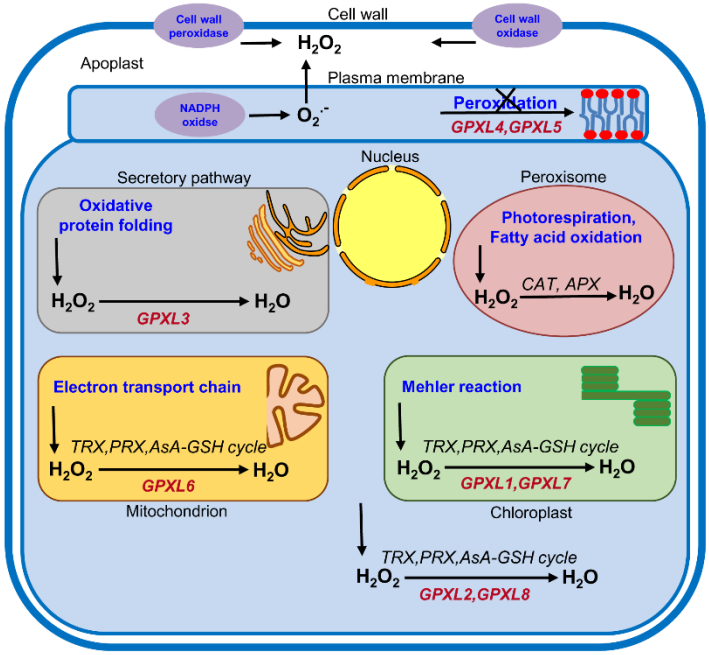

Figure 5.2: Working model for the localization and putative functions of GPXLs family in Arabidopsis. H_2O_2 is produced at several locations in the cell such as chloroplasts, mitochondria, ER, plasma membrane, peroxisomes, apoplast and cell wall. H_2O_2 and other ROS that causes cellular damage are detoxified by the activity of

ROS-scavenging systems. These systems comprises the AsA-GSH cycle, APX, CAT, TRX, PRX and GPXLs. GPXLs can also putatively protect the cell and organelle membranes from oxidative damage caused by H_2O_2 / lipid peroxidation.

6 References

Ahuja, I., de Vos, R. C., Bones, A. M., & Hall, R. D. (2010). Plant molecular stress responses face climate change. *Trends Plant Sci.,* 15(12), 664-674.

Aller, I., & Meyer, A. J. (2013). The oxidative protein folding machinery in plant cells. *Protoplasma,* 250(4), 799-816.

Ambrosone, A., Costa, A., Frusciante, A., Monti, L., Leone, A., & Grillo, S. (2008). Unravelling the molecular cues and plant adaptation or survival to water deficit. *Options Mediterranéennes A,* 84, 85-91.

Apel, K., & Hirt, H. (2004). Reactive oxygen species: metabolism, oxidative stress, and signal transduction. *Annu. Rev. Plant Biol.,* 55, 373-399.

Asada, K. (2006). Production and scavenging of reactive oxygen species in chloroplasts and their functions. *Plant Physiol.,* 141(2), 391-396.

Balmer, Y., Vensel, W. H., Tanaka, C. K., Hurkman, W. J., Gelhaye, E., Rouhier, N., Jacquot, J.-P., Manieri, W., Schürmann, P., & Droux, M. (2004). Thioredoxin links redox to the regulation of fundamental processes of plant mitochondria. *P. Natl. Acad. Sci. U.S.A.,* 101(8), 2642-2647.

Banfield, D. K. (2011). Mechanisms of protein retention in the Golgi. *Cold Spring Harb. Perspect Biol.,* 3(8), a005264.

Bayr, H. (2005). Reactive oxygen species. *Crit. Care Med.,* 33(12), S498-S501.

Bela, K., Horváth, E., Gallé, Á., Szabados, L., Tari, I., & Csiszár, J. (2015). Plant glutathione peroxidases: emerging role of the antioxidant enzymes in plant development and stress responses. *J. Plant Physiol.,* 176, 192-201.

Bhattacharjee, S. (2005). Reactive oxygen species and oxidative burst: roles in stress, senescence and signal. *Curr. Sci. India,* 89, 1113-1121.

Bienert, G. P., Møller, A. L., Kristiansen, K. A., Schulz, A., Møller, I. M., Schjoerring, J. K., & Jahn, T. P. (2007). Specific aquaporins facilitate the diffusion of hydrogen peroxide across membranes. *J. Biol. Chem.,* 282(2), 1183-1192.

Bienert, G. P., Schjoerring, J. K., & Jahn, T. P. (2006). Membrane transport of hydrogen peroxide. *BBA-Biomembranes,* 1758(8), 994-1003.

Brach, T., Soyk, S., Müller, C., Hinz, G., Hell, R., Brandizzi, F., & Meyer, A. J. (2009). Non-invasive topology analysis of membrane proteins in the secretory pathway. *Plant J.,* 57(3), 534-541.

Bradford, M. M. (1976). A rapid and sensitive method for the quantitation of microgram quantities of protein utilizing the principle of protein-dye binding. *Anal. Biochem.,* 72(1-2), 248-254.

Brandizzi, F., & Barlowe, C. (2013). Organization of the ER–Golgi interface for membrane traffic control. *Nat. Rev. Mol. Cell Biol.,* 14(6), 382-392.

Bretscher, M. S., & Munro, S. (1993). Cholesterol and the Golgi apparatus. *Science,* 261(5126), 1280-1281.

Brigelius-Flohé, R., & Maiorino, M. (2013). Glutathione peroxidases. *BBA-Gen. Subjects,* 1830(5), 3289-3303.

Brugiere, S., Kowalski, S., Ferro, M., Seigneurin-Berny, D., Miras, S., Salvi, D., Ravanel, S., d'Herin, P., Garin, J., Bourguignon, J., Joyard, J., & Rolland, N. (2004). The hydrophobic proteome of mitochondrial membranes from Arabidopsis cell suspensions. *Phytochem.*,65(12),1693-1707.

Bulleid, N. J., & Ellgaard, L. (2011). Multiple ways to make disulfides. *Trends Biochem. Sci.,* 36(9), 485-492.

Carrie, C., Kühn, K., Murcha, M. W., Duncan, O., Small, I. D., O'Toole, N., & Whelan, J. (2009). Approaches to defining dual-targeted proteins in Arabidopsis. *Plant J.,*57(6), 1128-1139.

Caverzan, A., Passaia, G., Rosa, S. B., Ribeiro, C. W., Lazzarotto, F., & Margis-Pinheiro, M. (2012). Plant responses to stresses: role of ascorbate peroxidase in the antioxidant protection. *Genet. Mol. Biol.,* 35(4), 1011-1019.

Chakravarthi, S., Jessop, C. E., Willer, M., Stirling, C. J., & Bulleid, N. J. (2007). Intracellular catalysis of disulfide bond formation by the human sulfhydryl oxidase, QSOX1. *Biochem. J.,* 404(3), 403-411.

Chang, C. C., Ślesak, I., Jordá, L., Sotnikov, A., Melzer, M., Miszalski, Z., Mullineaux, P. M., Parker, J. E., Karpińska, B., & Karpiński, S. (2009). Arabidopsis chloroplastic glutathione peroxidases play a role in cross talk between photooxidative stress and immune responses. *Plant Physiol.,* 150(2), 670-683.

Chen, M.-H., Huang, L.-F., Li, H.-m., Chen, Y.-R., & Yu, S.-M. (2004). Signal peptide-dependent targeting of a rice α-amylase and cargo proteins to plastids and extracellular compartments of plant cells. *Plant Physiol.,* 135(3), 1367-1377.

Chew, O., Whelan, J., & Millar, A. H. (2003). Molecular definition of the ascorbate-glutathione cycle in Arabidopsis mitochondria reveals dual targeting of antioxidant defenses in plants. *J. Biol. Chem.,* 278(47), 46869-46877.

Chou, K.-C., Wu, Z.-C., & Xiao, X. (2011). iLoc-Euk: a multi-label classifier for predicting the subcellular localization of singleplex and multiplex eukaryotic proteins. *PloS one,* 6(3), e18258.

Choudhury, S., Panda, P., Sahoo, L., & Panda, S. K. (2013). Reactive oxygen species signaling in plants under abiotic stress. *Plant Signal Behav.,* 8(4), e23681.

Chudakov, D. M., Matz, M. V., Lukyanov, S., & Lukyanov, K. A. (2010). Fluorescent proteins and their applications in imaging living cells and tissues. *Physiol. Rev.,* 90(3), 1103-1163.

Clough, S. J., & Bent, A. F. (1998). Floral dip: a simplified method for Agrobacterium-mediated transformation of *Arabidopsis thaliana*. *Plant J.,* 16(6), 735-743.

Corpas, F. J., Barroso, J. B., & del Río, L. A. (2001). Peroxisomes as a source of reactive oxygen species and nitric oxide signal molecules in plant cells. *Trends Plant Sci.,* 6(4), 145-150.

Criqui, M., Jamet, E., Parmentier, Y., Marbach, J., Durr, A., & Fleck, J. (1992). Isolation and characterization of a plant cDNA showing homology to animal glutathione peroxidases. *Plant Mol. Biol.,* 18(3), 623-627.

Cullis, P. M., Jones, G. D., Symons, M. C., & Lea, J. S. (1987). Electron transfer from protein to DNA in irradiated chromatin. *Nature, 330*(6150), 773-774.

Dalbey, R., & von Heijne, G. (2002). Protein targeting, transport, and translocation: Academic Press.

Das, K., & Roychoudhury, A. (2014). Reactive oxygen species (ROS) and response of antioxidants as ROS-scavengers during environmental stress in plants. *Front.Plant.Sci,* 2, 53. doi: 10.3389/fenvs.2014.00053.

Deblaere, R., Bytebier, B., De Greve, H., Deboeck, F., Schell, J., Van Montagu, M., & Leemans, J. (1985). Efficient octopine Ti plasmid-derived vectors for Agrobacterium-mediated gene transfer to plants. *Nucleic Acids Res.,* 13(13), 4777-4788.

Delaunay-Moisan, A., & Appenzeller-Herzog, C. (2015). The antioxidant machinery of the endoplasmic reticulum: Protection and signaling. *Free Radical Biol. Med.,* 83, 341-351.

Delaunay, A., Pflieger, D., Barrault, M. B., Vinh, J., & Toledano, M. B. (2002). A thiol peroxidase is an H_2O_2 receptor and redox-transducer in gene activation. *Cell,* 111(4), 471-481.

Depège, N., Drevet, J., & Boyer, N. (1998). Molecular cloning and characterization of tomato cDNAs encoding glutathione peroxidase-like proteins. *Eur. J. Biochem.,* 253(2), 445-451.

Desikan, R., Hancock, J., & Neill, S. (2005). Reactive oxygen species as signalling molecules. *Antioxidants and reactive oxygen species in plants,* Blackwell Publishing Ltd: Oxford, UK, 2007; pp. 169–196.

Desikan, R., Soheila, A.-H., Hancock, J. T., & Neill, S. J. (2001). Regulation of the Arabidopsis transcriptome by oxidative stress. *Plant Physiol.,* 127(1), 159-172.

Diao, Y., Xu, H., Li, G., Yu, A., Yu, X., Hu, W., Zheng, X., Li, S., Wang, Y., & Hu, Z. (2014). Cloning a glutathione peroxidase gene from *Nelumbo nucifera* and enhanced salt tolerance by overexpressing in rice. *Mol. Biol. Rep.,* 41(8), 4919-4927.

Dietz, K.-J. (2003). Plant peroxiredoxins. *Annu. Rev. Plant Biol*., 54(1), 93-107.

Dietz, K.-J. (2016). Thiol-based peroxidases and ascorbate peroxidases: why plants rely on multiple peroxidase systems in the photosynthesizing chloroplast? *Mol Cells,* 39(1), 20-25.

Dietz, K.-J., Jacob, S., Oelze, M.-L., Laxa, M., Tognetti, V., de Miranda, S. M. N., Baier, M., & Finkemeier, I. (2006). The function of peroxiredoxins in plant organelle redox metabolism. *J. Exp. Bot.,* 57(8), 1697-1709.

Dixon, D. P., & Edwards, R. (2010). Glutathione transferases. *The Arabidopsis Book*, e0131.

Edreva, A. (2005). Generation and scavenging of reactive oxygen species in chloroplasts: a submolecular approach. *Agric., Ecosyst. Environ.,* 106(2), 119-133.

Edwards, K., Johnstone, C., & Thompson, C. (1991). A simple and rapid method for the preparation of plant genomic DNA for PCR analysis. *Nucleic Acids Res.*, 19(6), 1349.

Edwards, R., & Dixon, D. P. (2005). Plant glutathione transferases. *Methods Enzymol.,* 401, 169-186.

Emanuelsson, O., Nielsen, H., Brunak, S., & Von Heijne, G. (2000). Predicting subcellular localization of proteins based on their N-terminal amino acid sequence. J. *Mol. Biol.,* 300(4), 1005-1016.

Eshdat, Y., Holland, D., Faltin, Z., & Ben-Hayyim, G. (1997). Plant glutathione peroxidases. *Physiol. Plant.,* 100(2), 234-240.

Ferro, M., Salvi, D., Brugière, S., Miras, S., Kowalski, S., Louwagie, M., Garin, J., Joyard, J., & Rolland, N. (2003). Proteomics of the chloroplast envelope membranes from *Arabidopsis thaliana. Mol. Cell Proteomics,* 2(5), 325-345.

Foyer, C. H., & Noctor, G. (2003). Redox sensing and signalling associated with reactive oxygen in chloroplasts, peroxisomes and mitochondria. *Physiol. Plant.,* 119(3), 355-364.

Fu, J.-Y. (2014). Cloning of a new glutathione peroxidase gene from tea plant (*Camellia sinensis*) and expression analysis under biotic and abiotic stresses. *Bot. Stud.,* 55(1), 1-6.

Gaber, A., Ogata, T., Maruta, T., Yoshimura, K., Tamoi, M., & Shigeoka, S. (2012). The involvement of Arabidopsis glutathione peroxidase 8 in the suppression of oxidative damage in the nucleus and cytosol. *Plant Cell Physiol,* 53(9), 1596-1606.

Gao, F., Chen, J., Ma, T., Li, H., Wang, N., Li, Z., Zhang, Z., & Zhou, Y. (2014). The glutathione peroxidase gene family in *Thellungiella salsuginea*: genome-wide identification, classification, and gene and protein expression analysis under stress conditions. *Int. J. Mol. Sci.,* 15(2), 3319-3335.

Gechev, T. S., & Hille, J. (2005). Hydrogen peroxide as a signal controlling plant programmed cell death. *J. Cell Biol.,* 168(1), 17-20.

Gill, S. S., Anjum, N. A., Hasanuzzaman, M., Gill, R., Trivedi, D. K., Ahmad, I., Pereira, E., & Tuteja, N. (2013). Glutathione and glutathione reductase: a boon in disguise for plant abiotic stress defense operations. *Plant Physiol. Biochem.,* 70, 204-212.

Gill, S. S., & Tuteja, N. (2010). Reactive oxygen species and antioxidant machinery in abiotic stress tolerance in crop plants. *Plant Physiol. Biochem.,* 48(12), 909-930.

Gratão, P. L., Polle, A., Lea, P. J., & Azevedo, R. A. (2005). Making the life of heavy metal-stressed plants a little easier. *Funct. Plant Biol.,* 32(6), 481-494.

Grebenok, R. J., Lambert, G. M., & Galbraith, D. W. (1997). Characterization of the targeted nuclear accumulation of GFP within the cells of transgenic plants. *Plant J,,* 12(3), 685-696.

Gupta, D. K., Pena, L. B., Romero-Puertas, M. C., Hernandez, A., Inouhe, M., & Sandalio, L. M. (2016). NADPH oxidases differentially regulate ROS metabolism and nutrient uptake under cadmium toxicity. *Plant Cell Environ.,* (in press) doi: 10.1111/pce.12711

Gutscher, M., Pauleau, A.-L., Marty, L., Brach, T., Wabnitz, G. H., Samstag, Y., Meyer, A. J., & Dick, T. P. (2008). Real-time imaging of the intracellular glutathione redox potential. *Nat. Methods*, 5(6), 553-559.

Gutscher, M., Sobotta, M. C., Wabnitz, G. H., Ballikaya, S., Meyer, A. J., Samstag, Y., & Dick, T. P. (2009). Proximity-based protein thiol oxidation by H_2O_2-scavenging peroxidases. *J. Biol. Chem.,* 284(46), 31532-31540.

Hanson, G. T., Aggeler, R., Oglesbee, D., Cannon, M., Capaldi, R. A., Tsien, R. Y., & Remington, S. J. (2004). Investigating mitochondrial redox potential with redox-sensitive green fluorescent protein indicators. J*. Biol. Chem.,* 279(13), 13044-13053.

Hanson, M. R., & Köhler, R. H. (2001). GFP imaging: methodology and application to investigate cellular compartmentation in plants. *J. Exp. Bot.,* 52(356), 529-539.

Helm, S., Dobritzsch, D., Rödiger, A., Agne, B., & Baginsky, S. (2014). Protein identification and quantification by data-independent acquisition and multi-parallel collision-induced dissociation mass spectrometry (MS E) in the chloroplast stroma proteome. *J. Proteomics,* 98, 79-89.

Herbette, S., Le Menn, A., Rousselle, P., Ameglio, T., Faltin, Z., Branlard, G., Eshdat, Y., Julien, J.-L., Drevet, J. R., & Roeckel-Drevet, P. (2005). Modification of photosynthetic regulation in tomato overexpressing glutathione peroxidase. *BBA-Gen. Subjects* 1724(1), 108-118.

Herbette, S., Roeckel-Drevet, P., & Drevet, J. R. (2007). Seleno-independent glutathione peroxidases. *FEBS J.,* 274(9), 2163-2180.

Höfer, R., Briesen, I., Beck, M., Pinot, F., Schreiber, L., & Franke, R. (2008). The Arabidopsis cytochrome P450 CYP86A1 encodes a fatty acid ω-hydroxylase involved in suberin monomer biosynthesis. *J. Exp. Bot.,* 59(9), 2347-2360.

Holland, D., Faltin, Z., Perl, A., Ben-Hayyim, G., & Eshdat, Y. (1994). A novel plant glutathione peroxidase-like protein provides tolerance to oxygen radicals generated by paraquat in *Escherichia coli*. *FEBS Lett.,* 337(1), 52-55.

Hooper, C. M., Tanz, S. K., Castleden, I. R., Vacher, M. A., Small, I. D., & Millar, A. H. (2014). SUBAcon: a consensus algorithm for unifying the subcellular localization data of the Arabidopsis proteome. *Bioinformatics,* 30(23), 3356-3364.

Hossain, M. A., Hossain, M. Z., & Fujita, M. (2009). Stress-induced changes of methylglyoxal level and glyoxalase I activity in pumpkin seedlings and cDNA cloning of glyoxalase I gene. *Aust. J. Crop Sci.,* 3(2), 53.

Imai, H., & Nakagawa, Y. (2003). Biological significance of phospholipid hydroperoxide glutathione peroxidase (PHGPx, GPx4) in mammalian cells. *Free Radical Biol. Med.,* 34(2), 145-169.

Iqbal, A., Yabuta, Y., Takeda, T., Nakano, Y., & Shigeoka, S. (2006). Hydroperoxide reduction by thioredoxin-specific glutathione peroxidase isoenzymes of *Arabidopsis thaliana*. *FEBS J.,* 273(24), 5589-5597.

Ito, J., Batth, T. S., Petzold, C. J., Redding-Johanson, A. M., Mukhopadhyay, A., Verboom, R., Meyer, E. H., Millar, A. H., & Heazlewood, J. L. (2011). Analysis of the Arabidopsis cytosolic proteome highlights subcellular partitioning of central plant metabolism. *J. Proteome Res,* 10(4), 1571-1582.

Jarvis, P. (2008). Targeting of nucleus-encoded proteins to chloroplasts in plants. *New Phytol.,* 179(2), 257-285.

Jiang, K., Schwarzer, C., Lally, E., Zhang, S., Ruzin, S., Machen, T., Remington, S. J., & Feldman, L. (2006). Expression and characterization of a redox-sensing green fluorescent protein (reduction-oxidation-sensitive green fluorescent protein) in Arabidopsis. *Plant Physiol.,* 141(2), 397-403.

Johnson, R. R., Cranston, H. J., Chaverra, M. E., & Dyer, W. E. (1995). Characterization of cDNA clones for differentially expressed genes in embryos of dormant and nondormant *Avena fatua* L. caryopses. *Plant Mol. Biol.,* 28(1), 113-122.

Karimi, M., Inzé, D., & Depicker, A. (2002). GATEWAY™ vectors for Agrobacterium-mediated plant transformation. *Trends Plant Sci.,* 7(5), 193-195.

Katoh, K., & Standley, D. M. (2013). MAFFT multiple sequence alignment software version 7: improvements in performance and usability. *Mol. Biol. Evol.,* 30(4), 772-780.

Keegstra, K., & Cline, K. (1999). Protein import and routing systems of chloroplasts. *Plant Cell,* 11(4), 557-570.

Kim, D. H., & Hwang, I. (2013). Direct targeting of proteins from the cytosol to organelles: the ER versus endosymbiotic organelles. *Traffic,* 14(6), 613-621.

Kim, Y.-J., Jang, M.-G., Noh, H.-Y., Lee, H.-J., Sukweenadhi, J., Kim, J.-H., Kim, S.-Y., Kwon, W.-S., & Yang, D.-C. (2014). Molecular characterization of two glutathione peroxidase genes of *Panax ginseng* and their expression analysis against environmental stresses. *Gene* 535(1), 33-41.

Klemm, R. W., Ejsing, C. S., Surma, M. A., Kaiser, H.-J., Gerl, M. J., Sampaio, J. L., de Robillard, Q., Ferguson, C., Proszynski, T. J., & Shevchenko, A. (2009). Segregation of sphingolipids and sterols during formation of secretory vesicles at the trans-Golgi network. *J. Cell Biol.,* 185(4), 601-612.

Klumperman, J. (2000). The growing Golgi: in search of its independence. *Nat. Cell Biol.,* 2(12), E217-E219.

Kohler, R., & Hanson, M. R. (2000). Plastid tubules of higher plants are tissue-specific and developmentally regulated. *J. Cell Sci.,* 113(1), 81-89.

Konno, T., Melo, E. P., Lopes, C., Mehmeti, I., Lenzen, S., Ron, D., & Avezov, E. (2015). ERO1-independent production of H_2O_2 within the endoplasmic reticulum fuels *Prdx4*-mediated oxidative protein folding. *J. Cell Biol.,* 211(2), 253-259.

Krysan, P. J., Young, J. C., & Sussman, M. R. (1999). T-DNA as an insertional mutagen in Arabidopsis. *Plant Cell,* 11(12), 2283-2290.

La Camera, S., Gouzerh, G., Dhondt, S., Hoffmann, L., Fritig, B., Legrand, M., & Heitz, T. (2004). Metabolic reprogramming in plant innate immunity: the contributions of phenylpropanoid and oxylipin pathways. *Immunol. Rev.,* 198(1), 267-284.

Laloi, C., Apel, K., & Danon, A. (2004). Reactive oxygen signalling: the latest news. *Curr. Opin. Plant Biol.,* 7(3), 323-328.

Laloi, C., Rayapuram, N., Chartier, Y., Grienenberger, J.-M., Bonnard, G., & Meyer, Y. (2001). Identification and characterization of a mitochondrial thioredoxin system in plants. *P. Natl. Acad. Sci. USA.* 98(24), 14144-14149.

Lazo, G. R., Stein, P. A., & Ludwig, R. A. (1991). A DNA transformation–competent Arabidopsis genomic library in Agrobacterium. *Nat. Biotechnol.,* 9(10), 963-967.

Leister, D. (2003). Chloroplast research in the genomic age. *Trends Genet.,* 19(1), 47-56.

Li, W.-J., Feng, H., Fan, J.-H., Zhang, R.-Q., Zhao, N.-M., & Liu, J.-Y. (2000). Molecular cloning and expression of a phospholipid hydroperoxide glutathione peroxidase homolog in *Oryza sativa*. *BBA-Gene Struc Expr, 1493(1), 225-230.*

Liang, H., Ran, Q., Jang, Y. C., Holstein, D., Lechleiter, J., McDonald-Marsh, T., Musatov, A., Song, W., Van Remmen, H., & Richardson, A. (2009). Glutathione peroxidase 4 differentially regulates the release of apoptogenic proteins from mitochondria. *Free Radical Biol. Med.,* 47(3), 312-320.

Lippincott-Schwartz, J., & Phair, R. D. (2010). Lipids and cholesterol as regulators of traffic in the endomembrane system. *Annu. Rev. Biophys.*, 39, 559.

Lippincott-Schwartz, J., Roberts, T. H., & Hirschberg, K. (2000). Secretory protein trafficking and organelle dynamics in living cells 1. *Annu. Rev. Cell. Dev. Biol.,* 16(1), 557-589.

Luis, A., Corpas, F. J., Sandalio, L. M., Palma, J. M., Gómez, M., & Barroso, J. B. (2002). Reactive oxygen species, antioxidant systems and nitric oxide in peroxisomes. *J. Exp. Bot.,* 53(372), 1255-1272.

Luis, A., Sandalio, L. M., Corpas, F. J., Palma, J. M., & Barroso, J. B. (2006). Reactive oxygen species and reactive nitrogen species in peroxisomes. Production, scavenging, and role in cell signaling. *Plant Physiol.,* 141(2), 330-335.

Maiorino, M., Bosello-Travain, V., Cozza, G., Miotto, G., Roveri, A., Toppo, S., Zaccarin, M., & Ursini, F. (2015). Understanding mammalian glutathione peroxidase 7 in the light of its homologs. *Free Radical Biol. Med.,* 83, 352-360.

Margis, R., Dunand, C., Teixeira, F. K., & Margis-Pinheiro, M. (2008). Glutathione peroxidase family–an evolutionary overview. *FEBS J.,* 275(15), 3959-3970.

Marino, D., Dunand, C., Puppo, A., & Pauly, N. (2012). A burst of plant NADPH oxidases. *Trends Plant Sci.,* 17(1), 9-15.

Marmagne, A., Ferro, M., Meinnel, T., Bruley, C., Kuhn, L., Garin, J., Barbier-Brygoo, H., & Ephritikhine, G. (2007). A High Content in Lipid-modified Peripheral Proteins and Integral Receptor Kinases Features in the Arabidopsis Plasma Membrane Proteome. *Mol. Cell. Proteomics,* 6(11), 1980-1996.

Marmagne, A., Rouet, M.-A., Ferro, M., Rolland, N., Alcon, C., Joyard, J., Garin, J., Barbier-Brygoo, H., & Ephritikhine, G. (2004). Identification of new intrinsic proteins in Arabidopsis plasma membrane proteome. *Mol. Cell. Proteomics,* 3(7), 675-691.

Meng, L., Wong, J. H., Feldman, L. J., Lemaux, P. G., & Buchanan, B. B. (2010). A membrane-associated thioredoxin required for plant growth moves from cell to cell, suggestive of a role in intercellular communication. *P. Natl. Acad. Sci. USA.,* 107(8), 3900-3905.

Meyer, A. J., Brach, T., Marty, L., Kreye, S., Rouhier, N., Jacquot, J. P., & Hell, R. (2007). Redox-sensitive GFP in *Arabidopsis thaliana* is a quantitative biosensor for the redox potential of the cellular glutathione redox buffer. *Plant J.,* 52(5), 973-986.

Meyer, A. J., & Dick, T. P. (2010). Fluorescent protein-based redox probes. *Antioxid Redox Signal,* 13(5), 621-650.

Meyer, Y., Siala, W., Bashandy, T., Riondet, C., Vignols, F., & Reichheld, J. P. (2008). Glutaredoxins and thioredoxins in plants. *BBA-Mol. Cell.Res.,Mol. Cell Res.* 1783(4), 589-600.

Meyer, Y., Vignols, F., & Reichheld, J. P. (2002). Classification of plant thioredoxins by sequence similarity and intron position. *Methods Enzymol.,* 347, 394-402.

Miao, Y., Lv, D., Wang, P., Wang, X.-C., Chen, J., Miao, C., & Song, C.-P. (2006). An Arabidopsis glutathione peroxidase functions as both a redox transducer and a scavenger in abscisic acid and drought stress responses. *Plant Cell,* 18(10), 2749-2766.

Michelsen, K., Yuan, H., & Schwappach, B. (2005). Hide and run. *EMBO Rep.,* 6(8), 717-722.

Milla, M. A. R., Butler, E., Huete, A. R., Wilson, C. F., Anderson, O., & Gustafson, J. P. (2002). Expressed sequence tag-based gene expression analysis under aluminum stress in rye. *Plant Physiol.,* 130(4), 1706-1716.

Milla, M. A. R., Maurer, A., Huete, A. R., & Gustafson, J. P. (2003). Glutathione peroxidase genes in Arabidopsis are ubiquitous and regulated by abiotic stresses through diverse signaling pathways. *Plant J.,* 36(5), 602-615.

Mithöfer, A., Schulze, B., & Boland, W. (2004). Biotic and heavy metal stress response in plants: evidence for common signals. *FEBS Lett.,* 566(1-3), 1-5.

Mittler, R., Vanderauwera, S., Gollery, M., & Van Breusegem, F. (2004). Reactive oxygen gene network of plants. *Trends Plant Sci.,* 9(10), 490-498.

Møller, I. M. (2001). Plant mitochondria and oxidative stress: electron transport, NADPH turnover, and metabolism of reactive oxygen species. *Annu. Rev. Plant Biol.,* 52(1), 561-591.

Mullineaux, P. M., Karpinski, S., Jiménez, A., Cleary, S. P., Robinson, C., & Creissen, G. P. (1998). Identification of cDNAs encoding plastid-targeted glutathione peroxidase. *Plant J.,* 13(3), 375-379.

Nanda, A. K., Andrio, E., Marino, D., Pauly, N., & Dunand, C. (2010). Reactive Oxygen Species during Plant-microorganism Early Interactions. *J. Integr. Plant. Biol.*, 52(2), 195-204.

Navrot, N., Collin, V., Gualberto, J., Gelhaye, E., Hirasawa, M., Rey, P., Knaff, D. B., Issakidis, E., Jacquot, J.-P., & Rouhier, N. (2006). Plant glutathione peroxidases are functional peroxiredoxins distributed in several subcellular compartments and regulated during biotic and abiotic stresses. *Plant Physiol.,* 142(4), 1364-1379.

Navrot, N., Rouhier, N., Gelhaye, E., & Jacquot, J. P. (2007). Reactive oxygen species generation and antioxidant systems in plant mitochondria. *Physiol. Plant.,* 129(1), 185-195.

Neill, S. J., Desikan, R., Clarke, A., Hurst, R. D., & Hancock, J. T. (2002). Hydrogen peroxide and nitric oxide as signalling molecules in plants. *J. Exp. Bot.,* 53(372), 1237-1247.

Nelson, B. K., Cai, X., & Nebenfuhr, A. (2007). A multicolored set of in vivo organelle markers for co-localization studies in Arabidopsis and other plants. *Plant J,* 51(6), 1126-1136.

Nikolovski, N., Rubtsov, D., Segura, M. P., Miles, G. P., Stevens, T. J., Dunkley, T. P., Munro, S., Lilley, K. S., & Dupree, P. (2012). Putative glycosyltransferases and other plant Golgi apparatus proteins are revealed by LOPIT proteomics. *Plant Physiol.,* 160(2), 1037-1051.

Nilsson, T., Hoe, M., Slusarewicz, P., Rabouille, C., Watson, R., Hunte, F., Watzele, G., Berger, E., & Warren, G. (1994). Kin recognition between medial Golgi enzymes in HeLa cells. *EMBO J.*, 13(3), 562.

Noctor, G., Dutilleul, C., De Paepe, R., & Foyer, C. H. (2004). Use of mitochondrial electron transport mutants to evaluate the effects of redox state on photosynthesis, stress tolerance and the integration of carbon/nitrogen metabolism. *J. Exp. Bot.,* 55(394), 49-57.

Noirot, E., Der, C., Lherminier, J., Robert, F., Moricova, P., Kiêu, K., Leborgne-Castel, N., Simon-Plas, F., & Bouhidel, K. (2014). Dynamic changes in the subcellular distribution of the tobacco ROS-producing enzyme RBOHD in response to the oomycete elicitor cryptogein. *J. Exp. Bot., 65: 5011–5022.*.

O'Brien, J. A., Daudi, A., Finch, P., Butt, V. S., Whitelegge, J. P., Souda, P., Ausubel, F. M., & Bolwell, G. P. (2012). A peroxidase-dependent apoplastic oxidative burst in cultured Arabidopsis cells functions in MAMP-elicited defense*. Plant Physiol.,* 158(4), 2013-2027.

Ozgur, R., Turkan, I., Uzilday, B., & Sekmen, A. H. (2014). Endoplasmic reticulum stress triggers ROS signalling, changes the redox state, and regulates the antioxidant defence of *Arabidopsis thaliana*. *J. Exp. Bot., 6*5(5), 1377-1390.

Passaia, G., Queval, G., Bai, J., Margis-Pinheiro, M., & Foyer, C. H. (2014). The effects of redox controls mediated by glutathione peroxidases on root architecture in *Arabidopsis thaliana*. *J. Exp. Bot.,* 65(5), 1403-1413

Patterson, G. H., Hirschberg, K., Polishchuk, R. S., Gerlich, D., Phair, R. D., & Lippincott-Schwartz, J. (2008). Transport through the Golgi apparatus by rapid partitioning within a two-phase membrane system. *Cell,* 133(6), 1055-1067.

Peltier, J.-B., Ytterberg, A. J., Sun, Q., & van Wijk, K. J. (2004). New functions of the thylakoid membrane proteome of *Arabidopsis thaliana* revealed by a simple, fast, and versatile fractionation strategy. *J. Biol. Chem.,* 279(47), 49367-49383.

Petrov, V. D., & Van Breusegem, F. (2012). Hydrogen peroxide-a central hub for information flow in plant cells. *AoB Plants*, 2012, in plant cells. AoB PLANTS 2012: pls014; doi:10.1093/aobpla.

Pfannschmidt, T. (2003). Chloroplast redox signals: how photosynthesis controls its own genes. *Trends Plant Sci.,* 8(1), 33-41.

Pubsley, A. (2012). Protein targeting: *Elsevier.Amstedarm,Netherlands.*

Quan, L. J., Zhang, B., Shi, W. W., & Li, H. Y. (2008). Hydrogen peroxide in plants: a versatile molecule of the reactive oxygen species network. *J Integr Plant Biol*, 50(1), 2-18.

Rabouille, C., Hui, N., Hunte, F., Kieckbusch, R., Berger, E. G., Warren, G., & Nilsson, T. (1995). Mapping the distribution of Golgi enzymes involved in the construction of complex oligosaccharides. *J. Cell Sci.,* 108(4), 1617-1627.

Racchi, M. L. (2013). Antioxidant defenses in plants with attention to prunus and citrus spp. *Antioxidants*, 2(4), 340-369.

Rapoport, T. A. (2007). Protein translocation across the eukaryotic endoplasmic reticulum and bacterial plasma membranes. *Nature,* 450(7170), 663-669.

Regev-Rudzki, N., & Pines, O. (2007). Eclipsed distribution: a phenomenon of dual targeting of protein and its significance. *Bioessays,* 29(8), 772-782.

Resh, M. D. (1999). Fatty acylation of proteins: new insights into membrane targeting of myristoylated and palmitoylated proteins. *BBA-Mol. Cell Res.,* 1451(1), 1-16.

Resh, M. D. (2013). Covalent lipid modifications of proteins. *Curr. Biol.,* 23(10), R431-R435.

Resh, M. D. (2016). Fatty acylation of proteins: The long and the short of it. *Prog Lipid Res*, 63, 120-131.

Roeckel-Drevet, P., Gagne, G., Labrouhe, D., Tourvieille, D., Dufaure, J. P., Nicolas, P., & Drevet, J. (1998). Molecular characterization, organ distribution and stress-mediated induction of two glutathione peroxidase-encoding mRNAs in sunflower (*Helianthus annuus*). *Physiol. Plant.,* 103(3), 385-394.

Ronquist, F., & Huelsenbeck, J. P. (2003). MrBayes 3: Bayesian phylogenetic inference under mixed models. *Bioinformatics,* 19(12), 1572-1574.

Rouhier, N., San Koh, C., Gelhaye, E., Corbier, C., Favier, F., Didierjean, C., & Jacquot, J.-P. (2008). Redox based anti-oxidant systems in plants: biochemical and structural analyses. *BBA-GEN SUBJECTS,* 1780(11), 1249-1260.

Sagi, M., & Fluhr, R. (2006). Production of reactive oxygen species by plant NADPH oxidases. *Plant Physiol.,* 141(2), 336-340.

Saint-Jore-Dupas, C., Nebenführ, A., Boulaflous, A., Follet-Gueye, M.-L., Plasson, C., Hawes, C., Driouich, A., Faye, L., & Gomord, V. (2006). Plant N-glycan processing enzymes employ different targeting mechanisms for their spatial arrangement along the secretory pathway. *Plant Cell,* 18(11), 3182-3200.

Schlecker, T., Schmidt, A., Dirdjaja, N., Voncken, F., Clayton, C., & Krauth-Siegel, R. L. (2005). Substrate specificity, localization, and essential role of the glutathione peroxidase-type tryparedoxin peroxidases in *Trypanosoma brucei*. *J. Biol. Chem.,* 280(15), 14385-14394.

Schürmann, P., & Jacquot, J.-P. (2000). Plant thioredoxin systems revisited. *Annu. Rev. Plant Biol.,* 51(1), 371-400.

Schwacke, R., Schneider, A., van der Graaff, E., Fischer, K., Catoni, E., Desimone, M., Frommer, W. B., Flügge, U.-I., & Kunze, R. (2003). ARAMEMNON, a novel database for Arabidopsis integral membrane proteins. *Plant Physiol.,* 131(1), 16-26.

Schwarzländer, M., Fricker, M., Müller, C., Marty, L., Brach, T., Novak, J., Sweetlove, L., Hell, R., & Meyer, A. J. (2008). Confocal imaging of glutathione redox potential in living plant cells. *J. Microsc.,* 231(2), 299-316.

Sessions, A., Burke, E., Presting, G., Aux, G., McElver, J., Patton, D., Dietrich, B., Ho, P., Bacwaden, J., & Ko, C. (2002). A high-throughput Arabidopsis reverse genetics system. *Plant Cell,* 14(12), 2985-2994.

Sharma, P., Jha, A. B., Dubey, R. S., & Pessarakli, M. (2012). Reactive oxygen species, oxidative damage, and antioxidative defense mechanism in plants under stressful conditions. *J Bot*, 2012.

Shigeoka, S., Ishikawa, T., Tamoi, M., Miyagawa, Y., Takeda, T., Yabuta, Y., & Yoshimura, K. (2002). Regulation and function of ascorbate peroxidase isoenzymes. *J. Exp. Bot.,* 53(372), 1305-1319.

Sies, H. (2014). Role of metabolic H_2O_2 generation: redox signaling and oxidative stress. *J. Biol. Chem.,* 289(13), 8735-8741.

Slesak, I., Libik, M., Karpinska, B., Karpinski, S., & Miszalski, Z. (2007). The role of hydrogen peroxide in regulation of plant metabolism and cellular signalling in response to environmental stresses. *Acta Biochim. Pol. -english edition-*, 54(1), 39.

Strompen, G., Dettmer, J., Stierhof, Y. D., Schumacher, K., Jürgens, G., & Mayer, U. (2005). Arabidopsis vacuolar H^+-ATPase subunit E isoform 1 is required for Golgi organization and vacuole function in embryogenesis. *Plant J.,* 41(1), 125-132.

Sugimoto, M., Furui, S., & Suzuki, Y. (1997). Molecular cloning and characterization of a cDNA encoding putative phospholipid hydroperoxide glutathione peroxidase from spinach. *Biosci Biotechnol Biochem,* 61(8), 1379-1381.

Sugimoto, M., & Sakamoto, W. (1997). Putative phospholipid hydroperoxide glutathione peroxidase gene from *Arabidopsis thaliana* induced by oxidative stress. *Genes Genet. Syst.,* 72(5), 311-316.

Sweetlove, L. J., & Foyer, C. H. (2004). Roles for reactive oxygen species and antioxidants in plant mitochondria. Plant mitochondria: from genome to function vol. 1, Kluwer Academic Press, Dordrecht, The Netherlands (pp. 307-320). .

Tanz, S. K., Castleden, I., Hooper, C. M., Vacher, M., Small, I., & Millar, H. A. (2012). SUBA3: a database for integrating experimentation and prediction to define the SUBcellular location of proteins in Arabidopsis. *Nucleic Acids Res.,* 41: D1185-D1191.

Terry, B. C., Liu, X., Murphy, A. M., & Pajerowska-Mukhtar, K. M. (2015). *Arabidopsis thaliana* GCN2 is Involved in Responses to Osmotic and Heat Stresses. *Plant,* 5(4), 87-95.

Thorpe, C., Hoober, K. L., Raje, S., Glynn, N. M., Burnside, J., Turi, G. K., & Coppock, D. L. (2002). Sulfhydryl oxidases: emerging catalysts of protein disulfide bond formation in eukaryotes. *Arch Biochem Biophys,* 405(1), 1-12.

Tosatto, S. C., Bosello, V., Fogolari, F., Mauri, P., Roveri, A., Toppo, S., Flohé, L., Ursini, F., & Maiorino, M. (2008). The catalytic site of glutathione peroxidases. *Antioxid. Redox Signal.,* 10(9), 1515-1526.

Triantaphylidès, C., & Havaux, M. (2009). Singlet oxygen in plants: production, detoxification and signaling. *Trends Plant Sci.,* 14(4), 219-228.

Turrens, J. F. (2003). Mitochondrial formation of reactive oxygen species. *J. Physiol*, 552(2), 335-344.

Uemura, S., Yoshida, S., Shishido, F., & Inokuchi, J.-i. (2009). The cytoplasmic tail of GM3 synthase defines its subcellular localization, stability, and in vivo activity. *Mol. Biol. Cell,* 20(13), 3088-3100.

Van Meel, E., & Klumperman, J. (2008). Imaging and imagination: understanding the endo-lysosomal system. *Histochem. Cell Biol.,* 129(3), 253-266.

Werck-Reichhart, D., & Feyereisen, R. (2000). Cytochromes P450: a success story. *Genome Biol.*, 1(6), 3001.3-3001.9

Wiedemann, N., Frazier, A. E., & Pfanner, N. (2004). The protein import machinery of mitochondria*. J. Biol. Chem.,* 279(15), 14473-14476.

Xu, X. M., Lin, H., Maple, J., Björkblom, B., Alves, G., Larsen, J. P., & Møller, S. G. (2010). The Arabidopsis DJ-1a protein confers stress protection through cytosolic SOD activation*. J Cell Sci,* 123(10), 1644-1651.

Yabuta, Y., Motoki, T., Yoshimura, K., Takeda, T., Ishikawa, T., & Shigeoka, S. (2002). Thylakoid membrane-bound ascorbate peroxidase is a limiting factor of antioxidative systems under photo-oxidative stress. *Plant J,,* 32(6), 915-925.

Yang, T., & Poovaiah, B. (2002). Hydrogen peroxide homeostasis: activation of plant catalase by calcium/calmodulin. *Proc. Natl. Acad. Sci.*, 99(6), 4097-4102.

Yogev, O., & Pines, O. (2011). Dual targeting of mitochondrial proteins: mechanism, regulation and function. *BBA-Biomembranes*, 1808(3), 1012-1020.

Yoshida, K., Noguchi, K., Motohashi, K., & Hisabori, T. (2013). Systematic exploration of thioredoxin target proteins in plant mitochondria. *Plant Cell Physiol,* 54(6), 875-892.

Zargar, S. M., Kurata, R., Inaba, S., Oikawa, A., Fukui, R., Ogata, Y., Agrawal, G. K., Rakwal, R., & Fukao, Y. (2015). Quantitative proteomics of Arabidopsis shoot microsomal proteins reveals a cross-talk between excess zinc and iron deficiency. *J. Proteomics, 15*(7), 1196-1201.

Zhai, C.-Z., Zhao, L., Yin, L.-J., Chen, M., Wang, Q.-Y., Li, L.-C., Xu, Z.-S., & Ma, Y.-Z. (2013). Two wheat glutathione peroxidase genes whose products are located in chloroplasts improve salt and H_2O_2 tolerances in Arabidopsis. *PloS one*, 8(10), p. e73989.

Zhang, L., Niu, Y., Zhu, L., Fang, J., Wang, X. e., Wang, L., & Wang, C.-c. (2014). Different interaction modes for protein-disulfide isomerase (PDI) as an efficient regulator and a specific substrate of endoplasmic reticulum oxidoreductin-1α (Ero1α). *J. Biol. Chem.,* 289(45), 31188-31199.

Zybailov, B., Rutschow, H., Friso, G., Rudella, A., Emanuelsson, O., Sun, Q., & van Wijk, K. J. (2008). Sorting signals, N-terminal modifications and abundance of the chloroplast proteome. *PloS one,* 3(4), e1994.

List of figures

Publications

Glutathione peroxidase-like enzymes cover five distinct cell compartments and membrane-surfaces in *Arabidopsis thaliana*. Attacha, S., Solbach, D., Bela, K., Moseler, A., Wagner, S., Schwarzländer, M., Aller, I., Müller, S.J & Meyer, A.J. 2017. *Plant Cell & Environment*.

General Statement

I declare that I am the sole author of this submitted dissertation and I did not make use of any sources apart from those specifically referred to experimental data or material collected from or produced by other persons is made easily identifiable. I also declare that I did not apply for permission to enter the examination procedure at another institution and that the dissertation is neither presented to any other faculty, nor used in its current any other form or any other examination.

……..... ……….....

Place, Date Safira Attacha

Acknowledgement

Firstly, I would like to express my sincere gratitude to my supervisor Prof. Dr. Andreas J Meyer for his continuous support during my Ph.D. and for his patience, motivation, and immense knowledge. His guidance helped me in all the time of research and writing of this thesis. I could not have imagined having a better supervisor for my Ph.D study.

Besides my supervisor, I would like to thank the rest of my thesis committee: Prof. Dr. Frank Hochholdinger, Prof. Dr. Michael Frei, and Prof. Dr. Claudia Knief.

My sincere thanks also goes to Dr. Isabel Aller, Anna Moseler, Sajid Ali Khan Bangash Dr. Stefanie Müller, Dr. Stephan Wagner and Dr. Daniela Bausewein for their precious support in my research. I thank Dr. Markus Schwarzländer and all my fellow labmates for the useful discussions in progress seminars. Likewise many thanks to technical assistants for their kind support in lab. Special thanks to Claudia Befort Trimborn and Stefan Hey for their moral support in any kind of lab and private issues. Thanks to Christine Jessen and Sonja Skamel for their support in administrative matters. Also I thank my colleagues and technical assistants in Crop functional genomics group.

Last but not the least, I would like to thank my family: my parents and my brother and sister and friends for supporting me spiritually throughout my Ph.D. and my life in general.